NORTHWESTERN UNIVERSITY

Synthesizing Mixed Phase Titania Nanocomposites with Enhanced Photoactivity and Redshifted Photoresponse by Reactive DC Magnetron Sputtering

A DISSERTATION

SUBMITTED TO THE GRADUATE SCHOOL

IN PARTIAL FULFILLMENT OF THE REQUIREMENTS

for the degree

DOCTOR OF PHILOSOPHY

Field of Civil and Environmental Engineering

By

Le Chen

EVANSTON, ILLINOIS

December 2008

ABSTRACT

Synthesizing Mixed Phase Titania Nanocomposites with Enhanced Photoactivity and Redshifted Photoresponse by Reactive DC Magnetron Sputtering

Le Chen

Recent work points out the importance of the solid-solid interface in explaining the high photoactivity of mixed phase TiO_2 catalysts. The goal of this research was to probe the synthesis-structure-function relationships of the solid-solid interfaces created by the reactive direct current (DC) magnetron sputtering of titanium dioxide. I hypothesize that the reactive DC magnetron sputtering is a useful method for synthesizing photocatalysts with unique structure including solid-solid interfaces and surface defects that are associated with enhanced photoreactivity as well as a photoresponse shifted to longer wavelengths of light.

I showed that sputter deposition provides excellent control of the phase and interface formation as well as the stoichiometry of the films. I explored the effects exerted by the process parameters of pressure, oxygen partial pressure, target power, substrate bias (RF), deposition incidence angle, and post annealing treatment on the structural and functional characteristics of the catalysts. I have successfully made pure and mixed phase TiO_2

films. These films were characterized with UV-Vis, XPS, AFM, SEM, TEM, XRD and EPR. to determine optical properties, elemental stoichiometry, surface morphology, phase distribution and chemical coordination. Bundles of anatase-rutile nano-columns having high densities of dual-scale of interfaces among and within the columns are fabricated. Photocatalytic performance of the sputtered films as measured by the oxidation of the pollutant, acetaldehyde, and the reduction of CO_2 for fuel (CH_4) production was compared (normalized for surface area) to that of mixed phase TiO_2 fabricated by other methods, including flame hydrolysis powders, and solgel deposited TiO_2 films. The sputtered mixed phase materials were far superior to the commercial standard (Degussa P25) and solgel TiO_2 based on gas phase reaction of acetaldehyde oxidation under UV light and CO_2 reduction under both UV and visible illuminations. The sputtered films also displayed a light response strongly shifted into the visible range. This is explained by the creation of non-stoichiometric titania films having unique features that we can tailor to the solar energy harvest. By further studying the non-stoichiometric titania, I observed an optimal non-stoichiometry for the titania films in terms of methane yield from CO_2 reduction. On one hand, the oxygen vacancies, which are mostly produced at the solid-solid interfaces, are associated with a redshift photoresponse and served as trapping sites or/and adsorption sites to increase the photocatlytic efficiency. On the other hand, excessive oxygen vacancies might also serve as recombination centers to hinder the reactivity. These two competing effects explained the fact that there is an optimum non-stoichiometry. In addition, I studied the influence of adding other reactive gases such as nitrogen and hydrogen during the sputtering as well as deposition angles (normal, low and glancing angles), on the structures and reactivities of titania based nanocomposites.

Our work illustrates the feasibility of reactive DC magnetron sputtering as both a powerful reserach tool and potentially practical technique for manufacturing highly active nanostructured TiO_2 photocatalysts tailored for solar applications.

Acknowledgements

The work presented here could not have been completed without the help of many people. I would like to record here my gratitude to those who have helped me through my study and dissertation work at Northwestern University.

First, I would like to thank my advisor, Prof. Kimberly Gray, for her continuous guidance and support in my research work. I also want to thank her for encouraging me to explore the exciting field of the renewable energy. I have learned a lot from her dedication to the academic field and will benefit from the experience of working under her guidance.

I would like to thank Prof. Michael Graham, my co-advisor for introducing me to a whole new world of material science and engineering. He was always very helpful with his strong technical background and provided many ideas and solutions to my research project.

I would like to thank Prof. Jean-Francois Gaillard and Eric Weitz for serving as committee members of my Ph.D. thesis defense. I am also indebted to my former or current lab-mates as well as rest of my officemates for help in my research and my life. I will always remember the good time we shared together and your friendship that warmed my heart.

I am particularly grateful to my parents and my boy friend, Jing Dong for their consistent encouragement and endless love. My doctoral study could not have been completed without their support. I would like to dedicate this dissertation to them.

This work was supported by Department of Energy (DE-FG02-03ER15457/A003, 5F-00546/W-31-109-ENG38).

Table of Contents

List of Tables

List of Figures

CHAPTER 1

Introduction

1.1. Problem Statement

Titanium dioxide (TiO_2) is one of the most widely studied photocatalysts for environmental applications due to its nontoxic nature, chemical stability, commercial availability at a low cost and robust, general reactivity. It has attracted much interest during the past decades due to its ability to photo-oxidize harmful chemicals in both air and water to CO_2 in the presence of UV light. In addition to its use in environmentally related treatments, it is also studied for energy applications such as water splitting [46, 119] and photochemical solar cells [56]. With increasing concern about carbon release to the atmosphere, there is growing interest in TiO_2 mediated conversion of CO_2 to storable fuels such as methane, methanol, etc.[177] which provides a potential alternative of carbon neutral energy production and consumption cycle .

Despite progress in expanding the application of TiO_2, there are still several challenges ahead if we want to expand the application of TiO_2 for both environmental treatment and energy production. These are 1) To enhance charge separation to improve TiO_2's photoactivity. 2) To extend TiO_2's photoresponse into the visible range (most of the TiO_2 based catalysts can only be excited by ultraviolet (UV) light which accounts for 3-4% of the solar spectrum.) 3) To target chemical reaction (e.g. oxidation, reduction or specific products). [97]

Previous approaches to improve TiO_2's photocatalytic efficiency have included coupling TiO_2 with other metals or metal oxides to stablize charge carriers or using metal dopants as electron sinks [4, 115, 147, 14]. Ion doping in TiO_2 (such as nitrogen)[16, 187] can give rise to a redshift of the photoresponse into the visible range by creating oxygen vacancies intermediate state between the valence band and the conduction band, and thus narrowing the band gap. However, some researchers have proposed that the doped ions may also serve as recombination centers and thus, the photoactivity could be reduced [43].

Anatase and rutile are the two most studied phases of TiO_2. Anatase, the most commonly used crystal phase for photocatalysis of TiO_2, shows good photoactivity only under UV illumination (wavelength ¡385 nm). On the other hand, rutile, the other ubiquitous crystal phase of TiO_2, displays small visible light activation (wavelength ¡400 nm), but with low photoactivity due to the very high recombination rate of its photo-generated electrons and holes. The high reactivity of the mixed phase TiO_2 (e.g. Degussa P25 with 70-80% of anatase and 20-30% of rutile) has been reported [137, 94, 58]. Based on the previous study of the mixed phase TiO_2 (Degussa P25) in our laboratory by EPR (Electron paramagnetic resonance) measurements, Hurum et al., proposed that there is a nanostructured morphology comprised of rutile crystallites interwoven with anatase crystallites creating solid-solid interfaces across which, photoexcited electrons are transferred from rutile to lower energy anatase lattice trapping sites. Such a mechanism points to the critical role of the solid-solid interfaces across which electrons are transferred and at which unique trapping sites may serve as catalytic hot spots.[66, 65].

In order to probe the nature of the solid-solid interface, there is a need to be able to synthesize it under controlled conditions in sufficient quantity to study. We believe that the reactive DC magnetron sputtering technique is a promising and controllable way to produce titania based material with high interfacial densities and structural defects which might be related to the 'hot spots'. Although the 'wet process' of dip-coating sol-gel particles is one of the dominant synthesis methods in the environmental catalysis area [105, 183, 113], it does not reliably and repeatably produce specific films with desired structures. However, reactive direct current (DC) magnetron sputtering provides more controls in the thin film deposition process, and it is increasingly employed in the synthesis of highly active environmental catalyst thin films [78, 2]. Reactive DC magnetron sputtering usually deposits metal oxide by using pure metal as the target and oxygen as the reactive gas with the assist of some special equipment to minimize surface charging, such as an arc suppression unit. In comparison to radio frequency (RF) magnetron sputtering which is used in many studies for directly sputtering metal oxide, reactive DC magnetron sputtering shows advantages in the deposition of oxides due to its high rate and range of process control. In contrast to RF magnetron sputtering, as well as other synthesis methods which rely on heat treatment[170, 12], DC magnetron sputtering provides an alternative means to control the synthesis of the non-stoichiometric metal oxides by directly controlling oxygen partial pressure during the sputtering. Furthermore, given its higher deposition rate, DC magnetron sputtering is applied in large-scale industrial production [168].

The goal of the study is to fabricate photoactive mixed phase TiO_2-based nanocomposite materials for energy applications and in doing so test the hypothesis that the

solid-solid interface is the key to tailoring highly efficient catalysts with unique activity. Specifically, the sputtered mixed phase TiO_2-based nanocomposites are compared with TiO_2 synthesized by other methods (sol-gel and commercial TiO_2), characterized by spectroscopic and microscopic tools and tested to photocatalytically oxidize a model indoor air pollutants, acetaldehyde, as an example to improve building energy efficiency by purifying the indoor air, and reduce carbon dioxide to methane and methanol, thereby producing carbon neutral, storable and energy-rich fuels.

Observations in our work and in the literature have indicated that the creation of oxygen vacancies as part of the defect structure contributes to the high photoactivity and redshifted photoresponse. In the later part of the work, the role of the oxygen vacancy in photoactivity and photoresponse as well as its relationship to the solid-solid interfaces is further studied and discussed.

1.2. Thesis Objectives

The objectives of the proposed tasks are to test the hypothesis that the solid-solid interface is the key to tailor catalysts for 1) enhanced photocatlytic efficiency, 2) targeted reactions (energy application), and 3) redshifted photoresponse. They are:

- To gain a comprehensive understanding of the relationship among the magnetron sputtering fabrication process, titania-based nanocomposite film structure and the photoactivity.
- To sputter TiO_2 with different phase compositions and structures and compare their photocatlytic activity (both oxidation and reduction) with TiO_2 based catalysts synthesized by other methods (e.g. hydrothermal method).

- To optimize sputtering deposition process and film structures to tailor the photoactivity of CO_2 reduction for energy production.
- To control and synthesize non-stoichiometric titania films by monitoring and controlling oxygen partial pressures during sputtering to explore the role of the oxygen vacancies and their effects on both reactivity and photoresponse.

1.3. Thesis Organization

Chapter 2 is a background review. In Chapter 2, the principles of TiO_2 based photocatalysis are introduced, followed by an overview of the development and application of the TiO_2 photocatalysts. Approaches to enhance photoactivity and redshift the photoresponse are also discussed in this chapter.

In Chapter 3, DC reactive magnetron sputtering, the main synthesis method used in my study, is explained and compared to the other fabrication technologies such as hydrothermal methods. The critical sputtering parameters are discussed and correlated with films' phase composition as well as surface structures.

In Chapter 4, a variety of sputtered TiO_2 films are compared to conventional TiO_2 materials relative to their performance for acetaldehyde oxidation. In addition, the structural characterization reveals a unique surface morphology of the sputtered TiO_2 associated with a high density of solid-solid interfaces that contributes to high photoactivity.

In Chapter 5, the activity test results for CO_2 reduction by the sputtered TiO_2 are presented. The attempt to carry out the activity test under visible illumination conditions is also described. Further characterization indicates the potential influence of the oxygen vacancies on the photoresponse as well as photoactivity.

In Chapter 6, the influence of the oxygen vacancies on structure-photoactivity-photoresponse are further explored and discussed. In addition, trace nitrogen was added for stabilizing sputtering process when operating on the low oxygen partial pressure end point of the transition mode. The influence of nitrogen addition on the films' structure and photoactivity is also studied.

In Chapter 7, other attempts to sputter titania based nanocomposites, aiming for high photoactivity and redshifted photoresponse, are introduced: sputtering with nitrogen (at high concentration to make doped titania) and oxygen; sputtering with hydrogen and oxygen; and the use of glancing angle deposition (GLAD). These approaches are explored in a preliminary way as there was insufficient time to pursue them in the same detail as our other work. However, we gained some basic insights into the approaches that may help future studies.

Chapter 8 concludes the overall work and summarized the fulfillment of the objectives.

CHAPTER 2

Literature Review of TiO_2-based photocatalysts

This section starts with an explanation of the basic mechanism of TiO_2 photocatalysis, followed by an overview of various approaches to improve its photo-reactivity and photo-response, and a review of the literature describing the synthesis and modification methods of TiO_2 based photocatalystsas. Finally, I discuss the application of TiO_2 photocatalysis in both environmental treatment and energy production.

2.1. History of TiO_2 photocatalysis

Photocatalysis is usually defined as the acceleration of a photon initiated reaction in the presence of a catalyst. Among many semiconductor based photocatalysts, TiO_2 is probably the most studied and commercially viable material at the present time, due to its high photo-activity and other properties such as nontoxic nature, chemical stability, low cost and robust performance.

Since ancient times, TiO_2 powders have long been used as white pigments [59]. The photo-activity of TiO_2 under sunlight (mostly UV wavelengths) was observed from the flaking of paints and the degradation of fabrics incorporating TiO_2[83] published in 1929. Since then, there have been many scientific studies on the photoactivity of TiO_2. For example, there was another report in 1938 on the photobleaching of dyes by TiO_2 both in vacuum and in oxygen[37]. It was reported that reactive oxygen species are created

by UV illumination in TiO_2 and are responsible for the bleaching of dyes, but that TiO_2 itself does not change through the reaction.

World wide attention was not drawn towards TiO_2 based photocatalysts until the 1970s when Fujishima and his colleagues studied its ability to split water to hydrogen and oxygen [46]. Single crystal, n-type rutile TiO_2 was used for anodes and a near-UV light source was applied. The discovery was made at the onset of 'oil crisis' and attracted scientists all over the world to the study of TiO_2. However, the O_2 produced by water splitting was subsequently reduced and recombined with H_2, causing very low reaction efficiency. After years of studies, the photo-efficiency of water splitting by TiO_2 was eventually improved by adding organic compounds to react with reduced oxygen species to stabilize the hydrogen production [143]. However, the restriction of TiO_2's photo-response to the near-UV range hindered the further development of TiO_2 in hydrogen production.

In the 1980s, the focus of TiO_2 shifted to the environmental treatment area. The strong photo-oxidative power of TiO_2 was utilized to degrade organic pollutants in both water and air [52, 54, 109]. TiO_2 was usually synthesized in powder form and immobilized on different supports for better handling [121]. Although there were many research studies on the purification of wastewater and polluted air, TiO_2 photocatalysis did not evolve to the stage of a real industrial technology in the 1980s due to low efficiency and relatively high cost compared to the other environmental treatment technologies.

The research and application of TiO_2 continued to grow and expand through 1990s and gradually found market success. For the past two decades, TiO_2 has not only been incorporated into commercialized products (e.g. Sunclean glass by PPG), but has also been

widely used in all kinds of areas including solar energy and medical applications, in addition to environmental treatment. This progress may be in part, due to the revolution in the technology and knowledge of nano-materials. Nanotechnology provides insight into the understanding of the relationship among TiO_2's fabrication-structure-reactivity/photo-response relationships. How this understanding benefited efforts to improve TiO_2-based photocatalysts will be discussed later of the session.

2.2. Mechanisms of TiO_2 photocatalysis

The mechanisms of TiO_2-based photocatalysis is schematically demonstrated in Figure 2.1[109]. The process is initiated by light absorption with energy equal to or greater than the TiO_2 band gap (3.2eV for anatase, the most reactive pure phase of TiO_2), which is shown in the insert of Figure 2.1. An electron (e^-) can be excited from the valence band (VB) to the conduction band (CB), leaving a charge vacancy or hole(h^+) in the valance band.

$$TiO_2 \xrightarrow{h\nu} e^- + h^+ \tag{2.1}$$

Upon excitation, the fate of the separated electron and hole can follow several pathways. Some of the h^+ from the VB and electrons from CB may recombine directly (Path B) in the bulk, or move to the surface and recombine (Path A). Recombination results in release of heat as shown.

$$e^- + h^+ \longrightarrow heat \tag{2.2}$$

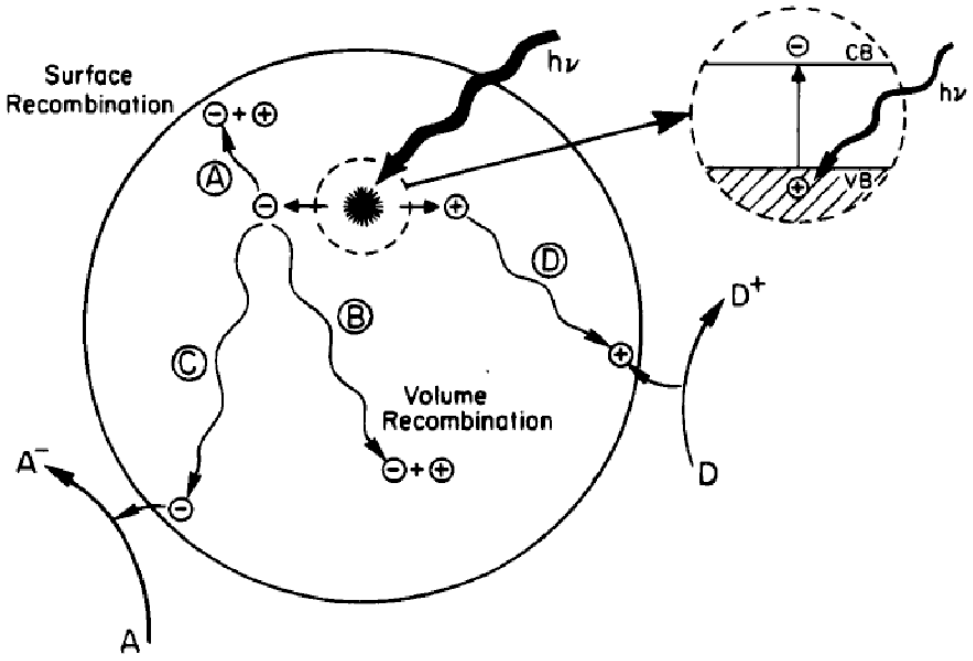

Figure 2.1. Schematic photocatalysis in a semiconductor [109]

In addition to recombination, h^+ can move to the surface, where an electron from a donor species can combine with the surface hole oxidizing the donor species (pathway D). The electron in the conduction band can also migrate to the surface and react with electron acceptors (Path C). For example, electrons can reduce absorbed O_2 to produce superoxide ions ($O_2^{\cdot -}$). The probability and rate of the charge transfer processes for electrons and holes depends upon the respective positions of the band edges for the conduction and valence bands and the redox potential levels of the adsorbate species. The formation of

hydroxy radicals and superoxide ions can be formulated as follows:

$$\mathrm{Ti^{IV}OH} + \mathrm{h^+} \longrightarrow \mathrm{Ti^{IV}{\cdot}OH^+} \tag{2.3}$$

$$\mathrm{R_{ads}} + \mathrm{h^+} \longrightarrow \mathrm{R_{ads}{\cdot}^+} \tag{2.4}$$

$$\mathrm{Ti^{IV}} + \mathrm{e^-} \longrightarrow \mathrm{Ti^{III}} \tag{2.5}$$

$$\mathrm{Ti^{III}} + \mathrm{O_2} \longrightarrow \mathrm{Ti^{IV}} + \mathrm{O_2^{\cdot -}} \tag{2.6}$$

where R represnts an organic molecule, and R_{ads} represents an adsorbed organic molecule [76, 63]. Both superoxide ions and OH are extremely reactive with organic compounds (R_{ads}) adsorbed on the catalyst surface.

Based on the analysis above, we can conclude: 1) the band gap energy determines the photocatalysts' photo-response. Narrowing the energy band gap of TiO_2 can facilitate the photo-reactions excited by the photons with lower energy (e.g. visible light); 2) the recombination of electrons and holes can largely decrease the photo-activity of TiO_2 photocatlysts. Thus, the modification of TiO_2-based photocatalysts to separate the electron and hole and hinder recombination is essential to increase their photocatalytic efficiency, and thereby, provide the separated electron and hole pair more opportunity to move to the surface.

In addition determining the band gap energy, the position of TiO_2's band edge energy relative to the redox potentials of the electron acceptors and donar species is also very critical to target a certain chemical reaction. Due to thermodynamic requirements, the relevant potential level of the electron acceptor species should be below (more positvie than) TiO_2's conduction band potential in order to accept the electron donated by TiO_2.

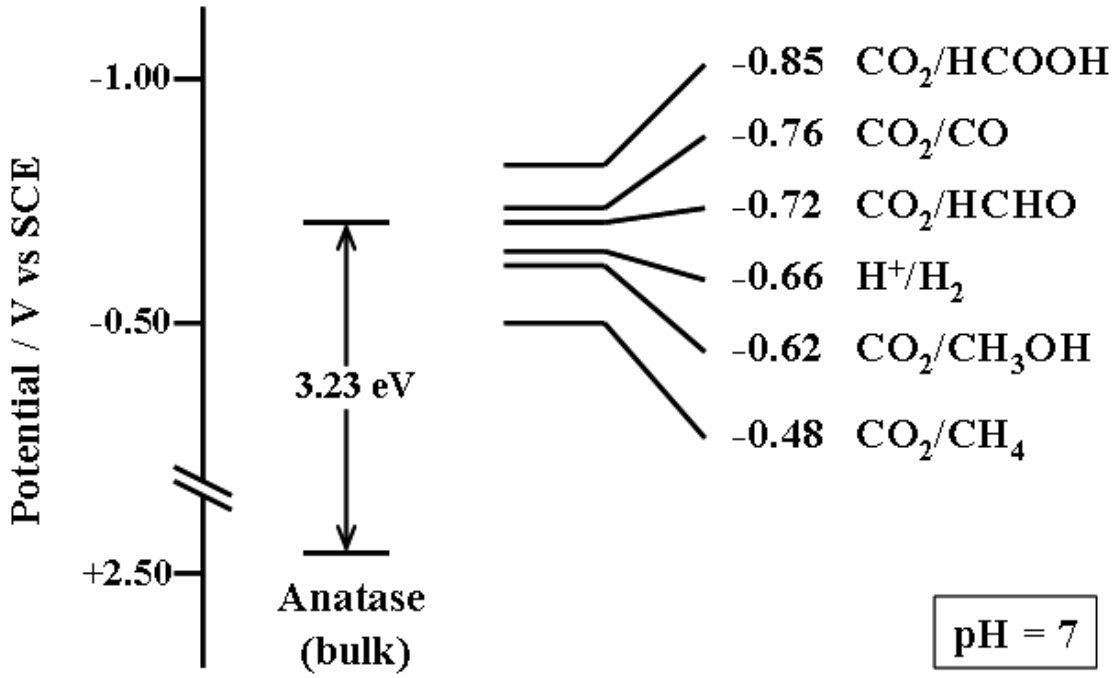

Figure 2.2. Energetic correlation of bulk anatase and reduction of CO_2 to various products in aqueous solution at pH 7.

In contrast, the potential level of the electron donor species should be above (more negative than) TiO_2's valence band position in order to donate an electron to the surface holes. Figure 2.2 shows the band edge positions of pure anatase relative to the potential levels of different band edges relative to CO_2 reduction at pH 7 [192, 72].

2.3. The synthesis of TiO_2 photocatalysts

2.3.1. The chemical methods of synthesizing TiO_2

2.3.1.1 Hydrothermal methods

As the most studied and utilized form of TiO_2, nano-sized TiO_2 powders are produced mostly by using a simple sol-gel method or/and hydrothermal process. The crystal size and crystal structure of TiO_2 nanocomposites prepared by solution-phase methods are

dependent on parameters including aging [106], solvent [113], additive [91],temperature [130, 53], and acidity [188, 101].

A typical hydrothermal method starts with hydrolyzing titanium tetra-isopropoxide or other titanium-precursors with a weak acid ethanol solution. The obtained TiO_2 gel is refluxed at higher temperature, around 373K for up to one day in the presence of varying amounts of hydrochloric acid and water. The resulting colloidal nanocrystals are collected and dried at room temperature. Further sintering at different temperatures can be applied for better crystallinity and formation of different phases [101].

Anion or metal doped TiO_2 can also be made by the hydrothermal process by adding precursors e.g. ammonia, urea, and alkylammonium salts as nitrogen precursors for nitrogen doping [182, 71, 48] and $FeCl_3$, or Fe(III)-acetyloacetonate, etc. for Fe doping [184, 156].

TiO_2 powders can be used in a suspended aqueous phase, or can be dip-coated onto supporting materials to make thin film coatings, which is also called the 'wet process'.

2.3.1.2 Flame hydrolysis method

Flame hydrolysis is another traditional chemical synthesis method for metal oxides. For example, the well-known high reactive commercial product, Degussa P25 TiO_2 powders, are produced by flame hydrolysis of $TiCl_4$.

The flame hydrolysis or the aerosil process, was originally developed by Klopfer et al [89]. and has been designed initially to make highly-dispersed silica. A group of volatizable

compounds like for example $TiCl_4$, or $SiCl_4$, react in an oxygen-hydrogen flame leads to highly dispersed oxides.

The major advantages of flame hydrolysis are the high purity of the compounds, its chemical flexibility, and the possibility to synthesize mixed oxides which are homogeneous even on a molecular scale. In addition, theoretically, powder properties like specific surface area and powder size can be easily controlled by varying the reaction conditions.[93] However, the fine nano-sized powders produced by flame hydrolysis easily aggregate into particles with sizes varying in a wide range (e.g. Degussa P25).

2.3.2. The physical methods to synthesize TiO_2 thin films

2.3.2.1 Introduction of TiO_2 thin film deposition

There are a variety of physical vapor deposition methods including evaporation [122], ion beam assisted deposition [95] and sputtering deposition [28, 29, 187] that guarantee high-quality films and provide good synthesis control to make structurally different films with nanoscale structures.

Among all the existing physical vapor deposition methods, sputtering is known to produce more uniform and mechanically durable films over larger areas without high temperature heat treatment that is required in other physical deposition methods such as evaporation[98]. The other important advantages of sputtering as a deposition technique are that the deposited films have the same composition as the source material and lower impurity incorporation into the films due to the relatively high deposition rates [81].

2.3.2.2 Mechanism of DC magnetron sputtering

Figure 2.3. illustrates the TiO_2 magnetron sputtering process. During the sputtering process, the sputtering gas (usually argon) at a relatively low pressure and low temperature (less than 200 degrees centigrade) is partially ionized and is sustained by the presence of energetic electrons. The resulting ionized gas and liberated energetic electrons which transfer the energy to the ions or atoms are attracted to opposite electrodes and produce the plasma.[151] Furthermore, for a discharge to be self-sustaining. Regeneration of the electrons by the positive ion bombardment of the cathode is required. This produces secondary electrons and enhances ionization. The ionized gas atoms have relatively little kinetic energy unless they are accelerated through an electric field. When accelerated, they bombard the surface of a target with sufficient force to dislodge an atom from the target material due to the momentum exchange. The dislodged atoms from the target material along with a reactive gas (e.g. O_2) form a thin film on a substrate. Practically any material that can be made into a solid target can be sputtered, including metals and dielectrics. In magnetron sputtering, extra magnets are placed close to the target. The magnetic field capture the escaping plasma electrons and confines them to the immediate vicinity of the target so that an effective sputtering discharge is maintained and the deposition rate is largely improved. The ion current (density of ionized argon atoms hitting the target) is increased by an order of magnitude over conventional diode sputtering systems, resulting in faster deposition rates at lower pressure. The lower pressure in the chamber helps create a cleaner film [151].

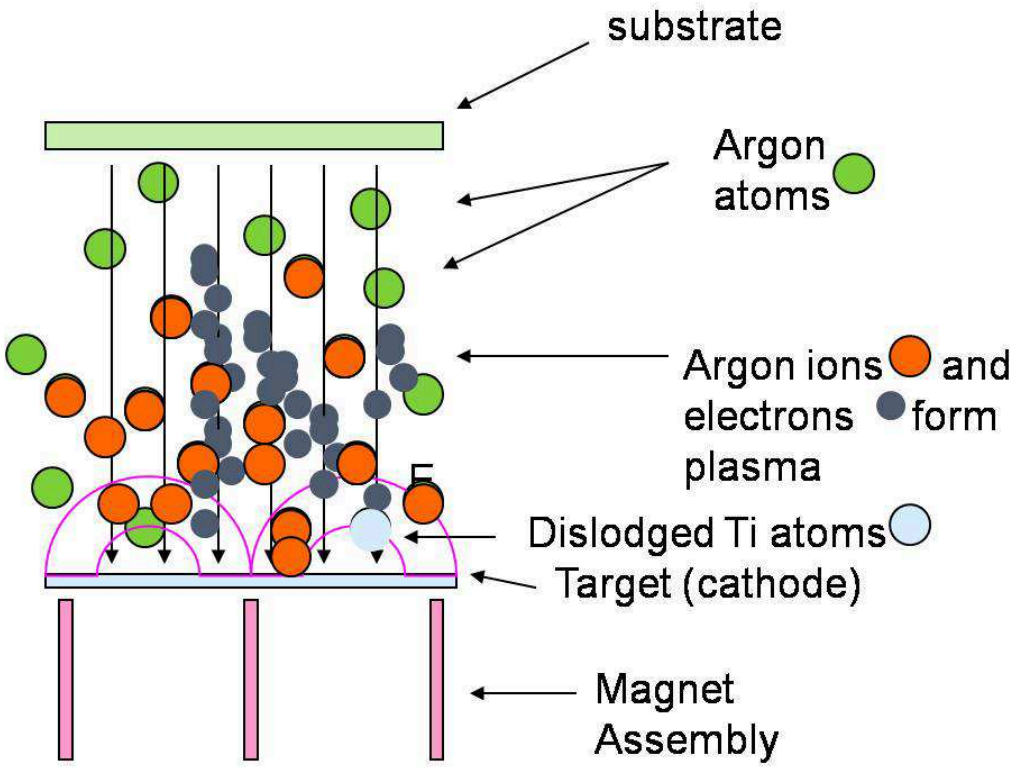

Figure 2.3. The mechanism of magnetron sputtering process

Most of the sputtered TiO_2 films reported in the research literature are prepared by Radio Frequency (RF) magnetron sputtering. RF magnetron sputtering is typically used for depositing insulating films (e.g. metal oxides) directly from insulating targets by alternating current to neutralize the charge on the target. The drawbacks of the RF magnetron technology are very low deposition rates and complicated operation (e.g. RF power supply and its matching networks), which hinders the applications on a commercial scale.

DC magnetron sputtering, which has more potential for industrial application due to much higher deposition rates and easier operation, has historically been regarded as infeasible for metal oxides like TiO_2, because during the deposition process, the target

(Ti) would become oxidized and the oxidized layer would not conduct DC power, causing charge accumulation on the surface of the target. In order to overcome this limitation, engineers developed pulsed DC power technology as a solution to high rate deposition of metal oxides[44]. However, this brought about concerns regarding high expense with existing DC power supplies. A less expensive alternative was provided by applying a device such as an arc suppression unit between the DC magnetron power supply and the sputtering target [161, 150]. Arc suppression is needed to maintain stable control over the sputtering process by eliminating arcs on the target surface due to oxide build up [150], especially in regions adjacent to the main sputtering track. Arc suppression involves the use of high frequency (20-100 kHz) positive voltage pulses that alternate the polarity of the target power from negative to positive dissipating negative charge build-up on the target. Similar issues of charge build-up arise on the substrate as well. When depositing films with low conductivity, such as oxides, charge build up on the film can shut down the ion bombardment that controls structure, so RF, pulsed DC, or high frequency AC power is applied on the substrates to sweep the charge away. The high frequency power on the substrate has an additional advantage that it also increases the ionization in the plasma, enhancing the ion currents and the reactivity between metal and oxygen.

2.4. Approaches to improve TiO_2 based photocatalytic reactivity or/and photo-response

There are several challenges associated with making TiO_2 a more commercially viable photocatalyst. These are: 1) To improve TiO_2's photoactivity by retarding the recombination of holes and electrons. 2) To extend TiO_2's photoresponse into the visible light

range to harvest abundant solar energy. 3) To target certain chemical reactions. [97] I will discuss some approaches to modify TiO_2 based photocatalysts to overcome the challenges.

2.4.1. Mixed phase TiO_2

Two crystal structures of TiO_2 are commonly used in photocatalysis: rutile and anatase. Commercially available anatase materials have a band gap of 3.2 eV, corresponding to a UV wavelength of 385 nm. The adsorptive affinity of anatase for organic compounds is often higher than that of rutile [164, 159], and anatase exhibits lower rates of recombination in comparison to rutile due to its 10-fold greater rate of hole trapping [137] and inherent surface band bending having a steeper potential compared to rutile [165, 155]. Degussa P25 (about70-80% anatase and 20-30% rutile) is a well known commercial TiO_2 powder product and serves as the model of mixed phase TiO_2 in our experiments. Our early studies found that P25 exhibited unique adsorptive affinities and sub-band gap photo-reaction associated with the formation of charge transfer complexes [6]. Further experimental results suggested that the differences between surface reactions on mixed and pure phase TiO_2 may be explained in terms of the morphology of P25, specifically the anatase-rutile interface at which unique active sites are located [67, 66]. It has been well accepted that unique catalytic chemistry occurs at the interface between two solid phases [8, 18, 194, 5, 158]. Previously researchers in our group probed the charge separation characteristics of pure and mixed phase TiO_2 by Electron Paramagnetic Resonance (EPR) spectroscopy in order to explore the role that rutile, a relatively inactive catalytic phase, plays in enhancing the photoactivity of mixed phase of TiO_2 [65, 66]. One explanation shows rutile serving as a passive electron sink hindering charge recombination in

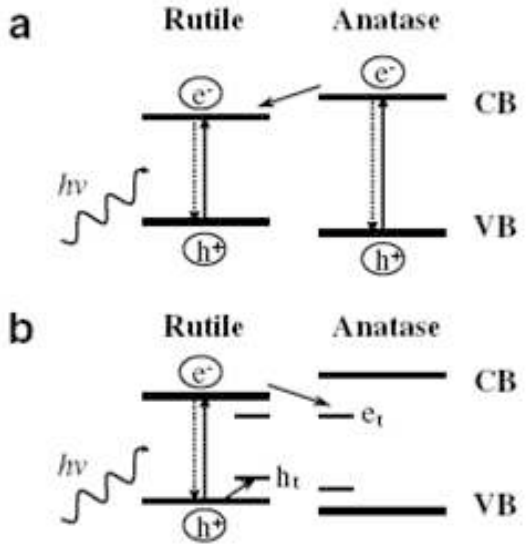

Figure 2.4. (a) The conventional model of charge transfer based on the relative energies of the conduction bands showing electron transfer from anatase to rutile. (b) Our conceptual model based on the relative energies of electron trapping sites showing electron transfer from rutile to anatase trapping sites [104].

anatase (Figure 2.4 a) [26, 82], a picture based principally on the lower energy conduction band edge of rutile relative to that of anatase. We suggest an opposite direction of electron transfer [66, 65] from rutile to anatase (Figure 2.4 b). At the interfaces of antase and rutile, charges produced on rutile are stabilized through electron transfer to lower energy anatase trapping sites, with energies 0.8 eV less than the anatase conduction band and thus, below the rutile conduction band.

Figure 2.5 [65, 103] shows a conceptual model of the solid-solid interface of mixed-phase TiO_2. The solid-solid interface (Region 4) is a third phase that is created when particles of a certain size are arranged in a certain way. EPR results illustrated that in P25 as the aggregate size increases the trapped charges remain on rutile (Region 1) and less transfer

to anatase occurs [65]. We proposed that there is a particular nanocluster morphology containing rutile crystallites intermixed with anatase crystallites creating a solid-solid interface, across which photoexcited electrons are transferred from rutile to lower energy anatase lattice trapping sites (Region 2) and anatase surface sites (Region 3). Thus, rutile acts as an antenna to extend the photoresponse of the mixed phase TiO_2 into the visible light region. Anatase, on the other hand, serves to activate rutile by stabilizing charges and retarding charge recombination. EPR results also documented that recombination reactions are dominated by surface reactions following charge migration via a random flight mechanism [68]. We identified tetrahedrally coordinated Ti trapping sites at the solid-solid interface in P25, which may contribute to the high photocatalytic activity of P25 by creating catalytic 'hot spots' or active sites (Region 4) [101].

2.4.2. Coupled metal/semiconductor-TiO_2 composites

Interfacial solid-solid interfaces can also be created between TiO_2 and other metal or semiconductor compounds. By loading noble metals or coupling with other semiconductors, the electrons transfer across the solid-solid interfaces, thus the recombination of electrons and holes is reduced for enhanced photoactivities.

For noble metal loading (such as Pt, Ag, Au et al.), it is commonly assumed that a metal such as Ag or Pt serves as a sink for photoinduced electrons and promotes interfacial charge-transfer processes[77]. Usually there is an optimal metal loading in terms of photoactivity. With excessive metal loading, electron transfer from TiO_2 particles into metal particles can deform the potential field in TiO_2 particles and draw a portion of holes near

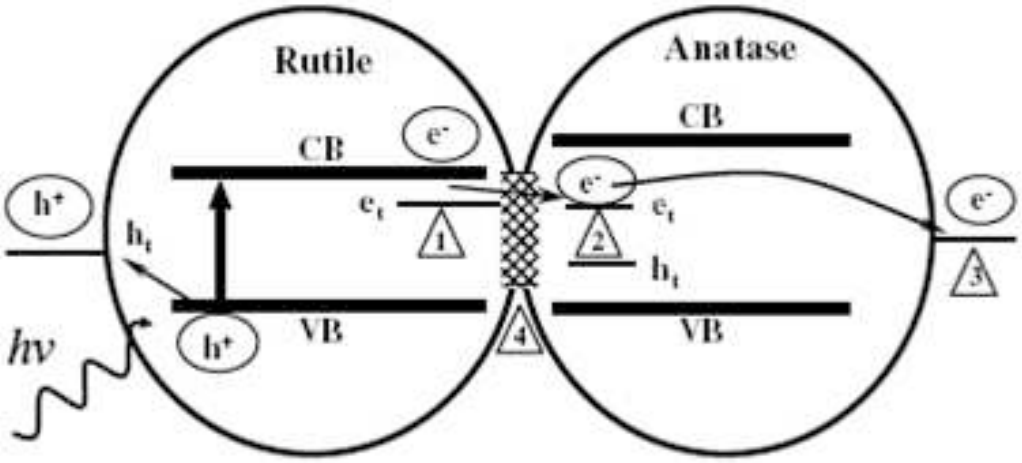

Figure 2.5. A proposed model of highly active solid-solid interface in mixed phase TiO_2 photocatalysts. The sites for electron trapping in rutile (Region 1), in anatase (Region 2), on the anatase surface (Region 3), and at the anatase-rutile interface (Region 4) are labeled [103].

the metal/TiO_2 junction, which instead, increases the electron-hole recombination rate and reduces the overall reactivity[166].

When the energies of valence and conduction bands are properly matched, nanocomposite materials consisting of TiO_2 coupled with another semiconductor also show improved photocatalytic efficiency and/or visible light response [153]. The mechanism of coupling TiO_2 with other semiconductor compounds resembles that of mixed phase TiO_2 explained above. The electrons are transferred and then trapped on the lower energy site instead of recombining with holes. Kamat et al. studied CdS-TiO_2 composites [146] and observed electrons transfer from conduction band of CdS to the conduction band of TiO_2. The electron transfer depends on the particle size of TiO_2, where charge transfer was

observed only when TiO_2 particles were at least 1.2 nm in diameter. Brahimi et al.[25] prepared coupled compounds of TiO_2 with PbS (band gap energy 0.41 eV). There is an optimal amount (up to 40 times more photo-active than pure TiO_2) of PbS coupled TiO_2 composite in terms of photo-degrading eosin (a red dye) under visible conditions. Other coupled compounds such as TiO_2-SnO_2[132], TiO_2-WO_3 [84], etc. were also fabricated and show good application potentials in visible conditions.

2.4.3. Anion/ Cation doped TiO_2

For doped TiO_2, the threshold energy for photoactivation can be reduced, potentially increasing photoactivity under solar irradiation. There has been a great deal of interest recently in the use of both nonmetal and transition metal doping.

Asahi et al. reported doping TiO_2 with nitrogen in 2001 (nitrogen atoms substitute for oxygen atoms) [16]. Results of density of states (DOS) calculations for anatase TiO_2 suggest that substitutional type doping (interstitial type doping and a mixture of both substitutional and interstitial type were both found to be ineffective) using nitrogen is effective due to the mixing of nitrogen 2p states with oxygen 2p states, thus causing a significant decrease in the width of the overall band gap. Figure 2.6 illustrates that light absorption at wavelengths above 400 nm is characteristic of the nitrogen-doped material [16]. The nitrogen doped films showed enhanced photocatalytic acetaldehyde degradation under visible illumination. However, in general, the photo-activity (especially oxidation) of nitrogen doped TiO_2 under UV condition is decreased probably due to the recombination of electrons and holes taking place via the new states in conjunction with slow hole transport in the nitrogen-created band above the valence band edge[142, 173].

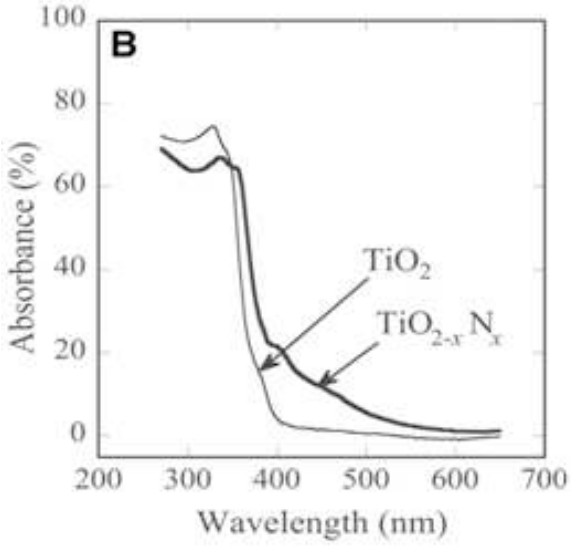

Figure 2.6. Experimental optical absorption spectra of nitrogen doped TiO_2 and undoped TiO_2 films [16].

Since the report of nitrogen-doped TiO_2 by Asahi et al., anion-doped TiO_2 soon became a hot research area and has attracted great interest. Both experiments and theoretical calculations demonstrated that anion dopants, such as carbon [73, 107], sulfur [175, 176] or fluorine[99, 190] in addition to nitrogen, can be used to extend the photocatalytic activity of TiO_2 into the visible-light region as well.

Transition metals including V[90, 64], Nb [85], Fe[125, 124] etc. may also be used for dopants (cation dopants) to extend the photo-response of doped TiO_2 composites. The order of effectiveness in the red shift was found to be as follows: V > Cr > Mn > Fe > Ni ions. Such a shift allows the metal ion-implanted titanium oxide to use solar irradiation more effectively, with photon efficiencies in the range of 20-30%[12]. The method of doping influences the properties of the catalysts significantly. For example, recent studies by Anpo and co-workers showed that the metal ion implantation technique to produce

metal-doped TiO_2 can enhance photoinduced surface redox reactions even in the visible-light region, where the wet chemical method to metal dope TiO_2 failed [12]. For different TiO_2 phases, the solubility of the doped metal differs (e.g. Nb has more solubility in anatase phase than rutle phase [140]).

Both of anion and cation doping are suspected to involve the creation of oxygen vacancies in TiO_2 [107, 136, 178, 42]. The intermediate states that the doped material introduces in TiO_2 to narrow the band gap energy are mostly oxygen vacancy states which are then, stabilized by the doped materials. However, Serpone et al. argued that doped ions introduce oxygen vacancies and do not narrow the band gap. Instead, they are merely color centers[152, 41]. Heavy doping, on the other hand, may change the chemical structures of titania and narrow the band gap for visible response.

2.4.4. Non-stoichiometric titania

Oxygen vacancies can also be directly introduced into titania without the addition of doping materials during the formation of the titania, or after annealing or plasma treatment of stoichiometric titania [170]. The non-stoichiometric titania is reported to possess a red shifted photo-response similar to most doped titanias [86, 75] as well as controversial influences on photo-reactivies. For example, Justicia et al. stated that the band of defect states existed just below and overlapping with the conduction band minimum and these states facilitated the transfer of photocarriers to the active sites on the surface [75]. Yates et al. [170] created bulk and surface oxygen vacancies on stoichiometric TiO_2 (110) and in CO_2 adsorption experiments, oxygen vacancies on the surface served as adsorption sites.

In contrast, Satoshi Takeda et al., suggested that, oxygen vacancies created energy levels around the mid-gap and served as recombination centers for electrons and holes [168].

2.5. Application of TiO_2 photocatalysts in solar energy conversion

TiO_2 is regarded as the most efficient and environmentally benign photocatalyst, and it has been most widely used for photodegradation of various pollutants in water [52, 54, 51, 10, 61] or air [45, 195]. TiO_2 photocatalysts can also be used to kill bacteria, as has been shown with E. coli suspensions [167]. The strong oxidizing power of illuminated TiO_2 can be used to kill tumor cells in cancer treatment [31]. Due to the photocatalytic and hydrophobic properties under UV illumination, TiO_2 has also been commercialized as a self-cleaning coating [131]. More recently, TiO_2 photocatalysis has been incorporated into many other novel processes and applications, including sensors, photochromic and electrochromic devices, and corrosion protection [96, 7, 123].

With the development of technologies for preparing highly active TiO_2 photocatalyst and the potential environmental and economic crisis caused by fossil fuels, more researchers are turning back to energy production applications. Solar energy is potentially the most abundant (120000 TW /year, much greater than the present annual global energy consumption of 10 TW/year [36]) and accessible alternative energy source. Thus, TiO_2 based materials can play a central role in the direct or indirect harvest, conversion, and/or storage of solar energy.

2.5.1. Hydrogen production from water splitting

As mentioned in the previous section about TiO_2's history, water splitting to produce H_2 as an energy carrier using TiO_2 based photocatalysis was initiated by Honda and Fujishima [46]. Figure 2.7 illustrates the system for water splitting used at that time, which was exposed to near-UV light, and was connected to a platinum black counter electrode through an electrical load. When UV light was irradiated on the n-TiO_2 electrode, they observed that the photocurrent flowed from the platinum counter electrode to the TiO_2 electrode through the external circuit and oxygen was produced (oxidation reaction) at the TiO_2 electrode while hydrogen was produced (reduction reaction) at the Pt electrode. The oxidation and reduction reactions both occur at the surface of TiO_2, which can be summarized as the following scheme:

$$TiO_2 \xrightarrow{h\nu} e^- + h^+ \tag{2.7}$$

$$H_2O + 4\,h^+ \longrightarrow O_2 + 4\,H^+ \qquad \text{(at the } TiO_2 \text{ electrode)} \tag{2.8}$$

$$2\,H^+ + 2\,e^- \longrightarrow H_2 \qquad \text{(at the Pt elctrode)} \tag{2.9}$$

However, The limited photoresponse within the UV range hindered the further application of hydrogen production by TiO_2. It was not until later with more advanced deposition techniques available, that researchers such as Anpo et al., were able to develop visible light responsive TiO_2 thin films prepared by RF magnetron sputtering in the application of water splitting [12, 120]. The most photocatalytically active Pt-loaded titania film under visible light conditions has a stoichiometric surface (Ti:O=2:1) and reduced bulk

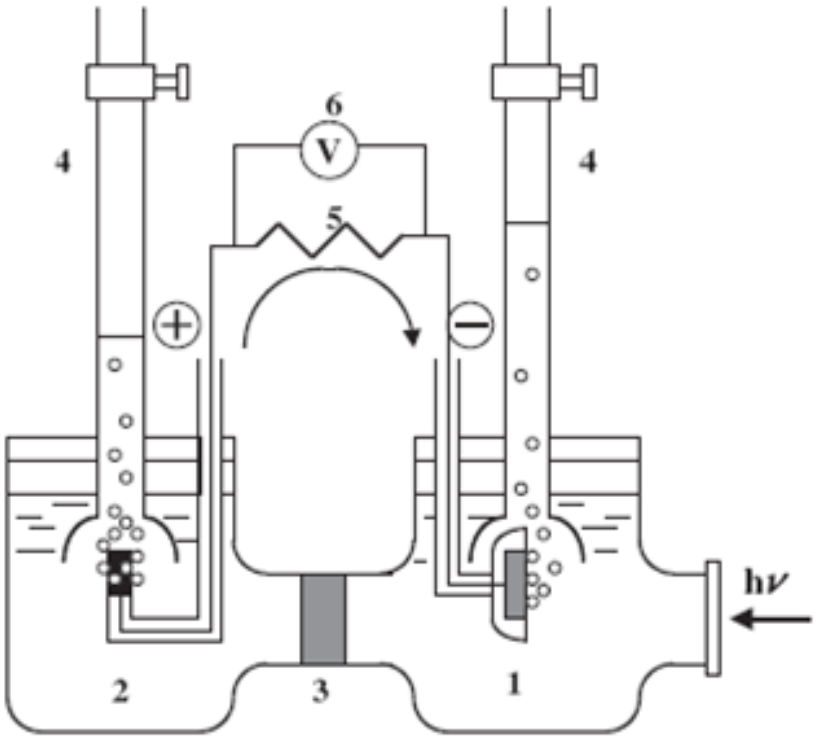

Figure 2.7. Schematic diagram of electrochemical photocell. (1) n-type TiO_2 electrode; (2) platinum black counter electrode; (3) ionically conducting separator; (4) gas buret; (5) load resistance; and (6) voltmeter.

(Ti:O=1.93:1). The authors suggested that the unique vis-TiO_2 thin films with a non-stoichiometric structure at the bottom of the films causes a significant improvement in the electronic structure of the TiO_2, enabling the absorption of visible light. The typical absorption band of vis-TiO_2 is in the range of 600-800 nm which they ascribed to Ti^{3+} induced defect centers formed by the strong attack of the high energy sputtered atoms or Ar plasma around the TiO_2 target.

2.5.2. Dye sensitized solar cells

Dye sensitized solar cells (DSC), a remarkably efficient photochemical solar cell based on the dye sensitization of mesoporous nanocrystalline titanium dioxide films, was invented by Michael Gratzel and Brian O'Regan at the Ecole Polytechnique Federale de Lausanne in 1991[129]. This type of solar cell is often called a Gratzel cell.

The photovoltaic devices are based on the concept of charge separation at an interface of two materials of different band gaps. In the liquid junction cell, the contact is between an electrolyte and the nanostructured TiO_2 film. A schematic presentation of the operating principles of the dye-sensitized nanocrystalline solar cell is given in Figure 2.7[55]. Attached to the surface of the nanocrystalline film is a monolayer of the charge transfer dye. In the TiO_2 based dye sensitized solar cells, current is generated when a photon absorbed by a dye molecule gives rise to electron injection into the conduction band of TiO_2. To complete the circuit, the dye must be regenerated by electron transfer from a redox species in solution which is then reduced at the counter electrode. TiO_2 powders are prepared by hydrothermal methods and form a colloidal solution with nanosized particles. This is used subsequently to produce a few micron-thick (1-20 m) film with good electrical conduction properties. Analysis of the porous films shows the porosity to be approximately 50% (the average pore size being 15 nm). The pores between the nanoparticles are filled with an electrolyte or a solid state organic hole conductor forming an interpenetrating heterojunction of very large contact area. Thus, the large internal surface area of this mesoporous film is very critical to determining the overall fuel cell efficiency.

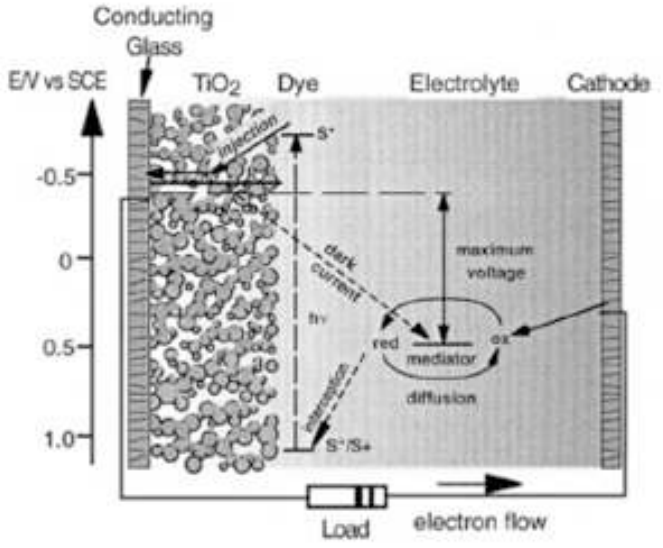

Figure 2.8. Principle of operation and energy level scheme of the dye-sensitized nanocrystalline solar cell. Photoexcitation of the sensitizer (S) is followed by electron injection into the conduction band of the mesoporous oxide semiconductor. The dye molecule is regenerated by the redox system, which itself is regenerated at the counter electrode by electrons passed through the load. Potentials are referred to the standard calomel electrode (SCE) [55].

2.5.3. CO_2 reduction to fuels

As CO_2 from fossil fuel combustion is the main source of the green house gases contributing to global warming, the reduction of CO_2 into fuel compounds such as CO, CH_4 and CH_3OH by TiO_2 provides an approach to transfer solar energy to storable chemical energy and introduces a new option of recycling CO_2 and promoting a carbon neutral process. In 1979, Inoue et al. [72] first reported the photocatalytic reduction of CO_2 in aqueous solution to produce formaldehyde (HCHO), formic acid (HCOOH), methyl alcohol (CH3OH), and trace amounts of methane (CH_4) using various semiconductors,

including TiO_2. These semiconductors were activated by both xenon- and mercury-lamp irradiation.

Nowadays, most photoreduction studies are carried out by metal-loaded titanium dioxide and dispersed nanosized photocatalysts. Anpo and his group incorporated dispersed titanium oxides in the framework of mesoporous silica. This exhibited high and unique photocatalytic reactivity for the reduction of CO_2 with H_2O to produce CH_4 and CH_3OH under UV irradiation, its reactivity being much higher than bulk TiO_2. The cationic rhenium(I) complex was encapsulated into a mesoporous AlMCM-41 material by ion-exchange method, yielding a visible light photocatalyst for photoreduction of CO_2. The incorporated titanium oxides were found to exist as tetrahedral species [69]. Cu-loaded TiO_2, studied by I-Hsiang Tseng et al. [174], obtained a maximum methanol yield of about 1000 mol/gCatal with the 25 molar %Cu of total loading located on the surfaces of TiO_2 particles. Dispersed nanosized Cu/TiO_2 and anatase TiO_2 were also studied by Yamashita, et al. [191]. According to their study, anatase TiO_2, which had a large band gap and numerous surface OH groups, showed high efficiency for CH_4 formation while Cu/TiO_2 brought about additional formation of CH_3OH. Li et al. pointed out that the Ti-O-Cu linkages created at the interfaces of TiO_2 and loaded Cu species may contributed to the improved photoactivity mentioned above [100]. The efficiency of the photoreaction depended strongly not only on the kind of catalyst but also on the ratio of H_2O to CO_2. The photoreduction of CO_2 in water is readily available and inexpensive. The CO_2 reduction reactions were suggested as follows [189, 177]. Two important species involved in CO_2 photoreduction are $\cdot H$ (hydrogen atom) and $CO_2^{-}\cdot$ (carbon dioxide anion radical) produced by electron transfer from the conduction band. After electrons and holes are

generated from TiO_2,

$$H_2O \rightleftharpoons H^+ + OH^- \tag{2.10}$$

$$H^+ + e^- \longrightarrow \cdot H \tag{2.11}$$

$$CO_2 + e^- \longrightarrow CO_2^- \cdot \tag{2.12}$$

Carbon monoxide formation

$$CO_2^- \cdot + 2\,H^+ + e^- \longrightarrow CO + H_2O \tag{2.13}$$

Or formic acid formation

$$CO_2^- \cdot + 2\,H^+ + e^- \longrightarrow HCOOH \tag{2.14}$$

Or formaldehyde formation

$$CO_2^- \cdot + 2 \cdot H + 2\,H^+ + e^- \longrightarrow H_2CO + H_2O \tag{2.15}$$

Or methanol formation

$$H_2CO + \cdot H \longrightarrow \cdot H_3CO \tag{2.16}$$

$$\cdot H_3CO + \cdot H \longrightarrow CH_3OH \tag{2.17}$$

or methane formation

$$CH_3OH + \cdot H \longrightarrow \cdot CH_3 + H_2O \tag{2.18}$$

$$\cdot CH_3 + \cdot H \longrightarrow CH_4 \tag{2.19}$$

F. Saladin proposed a tentative model to explain the photoreduction of CO_2 and H_2O at the surface of TiO_2. TiO_2 is partially reduced to $TiO_{2\text{-x}}$ with oxygen vacancies formed under UV excitation, and serves an electron pool. All the steps except for the first one are dark reactions [144].

$$2\,TiO_2 \xrightarrow{h\nu} 2\,TiO_{2-x} + xO_2 \tag{2.20}$$

$$TiO_{2-x} + xH_2O \longrightarrow TiO_2 + xH_2 \tag{2.21}$$

$$TiO_{2-x} + xCO_2 \longrightarrow TiO_2 + xCO \tag{2.22}$$

$$4\,xH_2 + xCO_2 \longrightarrow xCH_4 + 2\,xH_2O \tag{2.23}$$

For the CO_2 reduction, the conditions of the reaction such as pH values, temperatures, pressures play important roles. As for the aqueous reaction, the solubility of CO_2 in water can also be very critical to the reaction outcomes [177]. In addition, applying low-dielectric constant solvents or low-polarity solvents instead of water as hole scavengers like ethanol, 1-propanol etc. can largely increase the fuel yield by pushing $\cdot CO_2^-$ radicals out of solution to the photocatalysts [111]. However, the addition of organic solvent can interfere with the organic compounds produced from the CO_2 reduction. Thus, detailed mass balance of carbon needs to be carried out to make sure that CO_2 is the ultimate carbon source instead of added organic solvents.

2.6. Conclusions

Although TiO_2 has been widely used as a photocatalyst for almost 40 years in various fields including environemtnal treatment and energy production, there are still challenges to be solved: limited photoresponse to UV wavelenths and recombination of electrons and holes. Both of them hinder efficient application of TiO_2 to energy and environmental problems. Modified titania based nanocomposites such as coupled compounds and doped materials have been developed to solve one of these two problems. The mixed phase TiO_2 of anatase and rutile, based on the early studies from our lab, shows both high activity and redshifted photoresponse compared to the single phase TiO_2 and we attributed the enhanced photocatlytic efficiency and photoresponse to the creation of the solid-solid interfaces with reactive interfacial sites, 'hot spots'.

My work seeks to explore the relationships of synthesis-structure-activity by focusing on the synthesis technology to create the mixed phase TiO_2 based materials with high density of solid-solid interfaces and reactive sites. DC magnetron sputtering, a commercial physical vapor deposition method, shows a potential to create unique film structures and phase compositions correlated with activities in a controllable way. I will show the fabrication-structure relationship in the next chapter.

CHAPTER 3

Fabricating TiO_2 Films with Different Phase Compositions by Reactive DC Magnetron Sputtering

3.1. Equipment Setup

Titanium dioxide thin films were deposited by reactive DC magnetron sputtering, with RF bias, onto cleaned substrates. Pure titanium (99.95%) was used as the sputtering target. High-purity argon and oxygen were used as sputtering and reactive gases respectively. The sputtering system used for this work utilized a dual cathode, closed-field unbalanced magnetron configuration [161]. A schematic of the deposition system we used is shown in Figure 3.1. The essential features of the system shown are:

(1) Cryo-pumped chamber and load lock

(2) Closed-field unbalanced magnetron target arrangement (13cm x 38 cm targets)

(3) Arc suppression (pulsed power) for targets

(4) RF or DC power for substrate

(5) Mass spectrometer control of reactive gas partial pressure

(6) Rotating substrate table

We use an unbalanced magnetron reactive DC sputtering system. The unbalanced magnetron sputtering with the closed field arrangement (north poles on one side facing south poles on the other) produces a dense plasma in the vicinity of the substrate because of the strong magnetic fields there. Some electrons in the plasma are no longer confined to

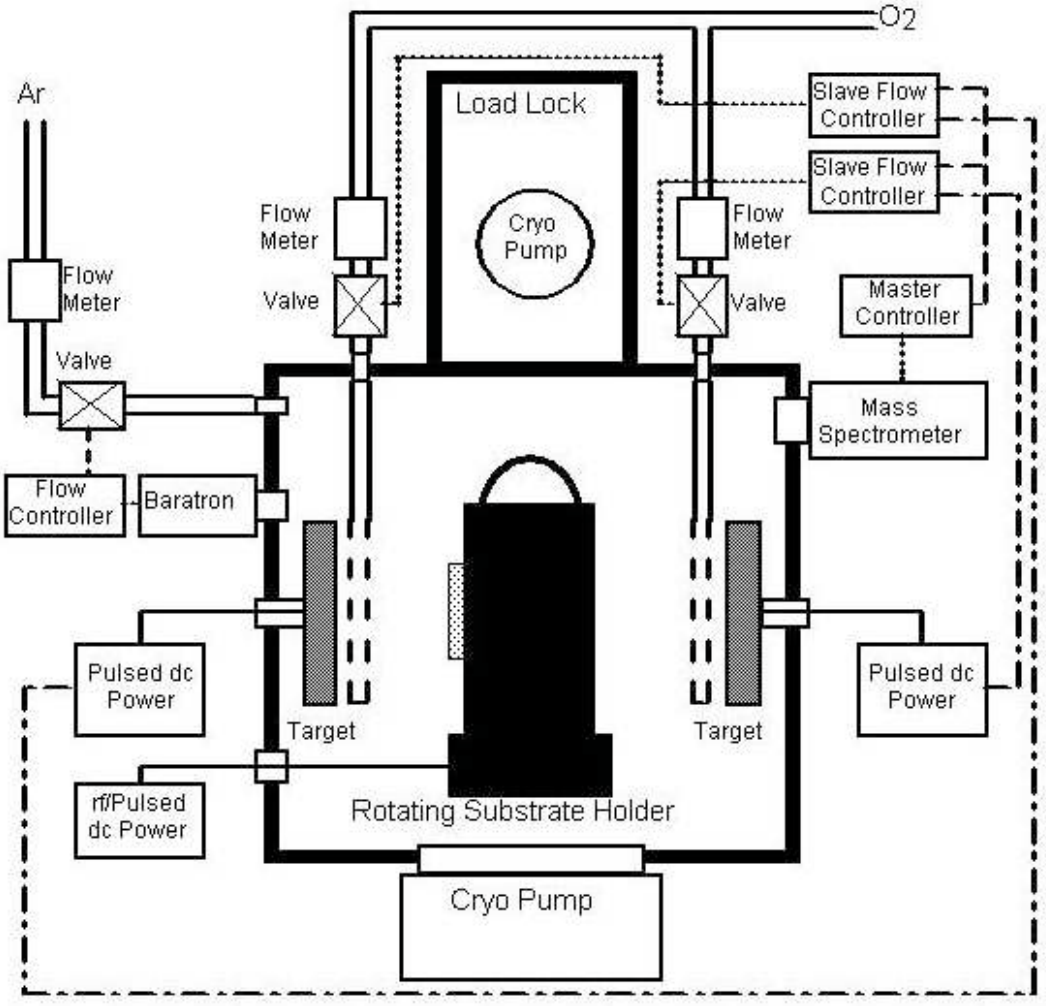

Figure 3.1. Schematic of dual-cathode unbalanced magnetron system

the target region, but are able to follow the magnetic-field lines and flow out towards the substrate. As a result, ion bombardment at the substrate is increased with a consequent improvement in the coating structure. The use of unbalanced magnetron configurations allows high ion currents to be transported to the substrate so that coatings of excellent quality can be deposited under conditions providing of crystallite growth and film density at relatively low temperature [15].

The mass spectrometer is used to monitor the partial pressure of the reactive gas (O_2) during sputtering and uses these data to compare with a set point, the difference being used to drive mass flow control valves to increase or decrease O_2 flow. This is a critical control for the process and allows direct control of Ti:O stoichiometry without resorting to post deposition annealing[170], etc.

The arc suppression is used to maintain stable control over the process by eliminating arcs on the target surface due to oxide formation[160]. High frequency (20-100kHz) positive voltage pulses dissipate localized charging on the target. Charging issues arise for the substrate and charge build up on the oxide film can stop the ion bombardment controlling structure. We typically use RF-power (13.56 MHz) to sweep the charge. The substrates were fixed by steel wires on the sides of an aluminum hexagonal prism sample holder. The sample holder with substrates then is placed on the rotating substrate table. The distance between the rotating substrate table to the target is about 15 cm. Before each run, the substrates were etched in pure Ar atmosphere at 1000 KW substrate bias for 3-5 mins in order to clean the surface of the substrates, and then O_2 gas was introduced into the chamber. The films produced by deposition are polycrystalline.

There are a number of operating parameters that individually and in combination controlling the films' phase composition and morphology. They are:

- Target power
- substrate bias
- Total pressure
- Partial pressure of oxygen
- Deposition angle

- Post-deposition annealing
- Different substrates

The effect of the each parameter is discussed below.

3.2. TiO_2 phase composition

The crystalline phase composition of the prepared samples was principally determined by X-ray Diffraction (Rigaku) using Cu-Kα radiation ($\lambda = 1.5418$Å) over a range of $20^\circ < 2\theta < 60^\circ$ operated at 40kV-200mA.

X-rays are electromagnetic radiation with the wavelength comparable to the size of atoms, they are ideally suited for probing the structural arrangement of atoms and molecules in a wide range of materials. The energetic x-rays can penetrate deep into the materials (hundreds of nanometers for sputtered TiO_2 films) and provide information about the bulk structure. In general, X-ray diffraction techniques are based on the elastic scattering of x-rays from collision with electrons of atoms. Diffracted X-rays by different atoms can interfere with each other and the resultant intensity distribution is strongly modulated by this interaction. The diffracted X-rays consist of sharp interference maxima (peaks) with the same symmetry as in the distribution of atoms. The peaks in a X-ray diffraction pattern are directly related to the atomic distances. For a given set of lattice plane with an inter-plane distance of d, the condition for a diffraction (peak) to occur can be simply written as

$$2d \sin\theta = n\lambda$$

which is known as the Bragg's law, after W.L. Bragg, who first proposed it in 1913. In the equation, λ is the wavelength of the x-ray, θ the scattering angle, and n an integer representing the order of the diffraction peak.

The ratio of peak areas of the different phases was interpreted as the weight percentage of different phases of the films by using Spurr equation [163]:

$$F_R = \left[\frac{1}{1 + 0.78(\mathrm{I}_{A(101)}/\mathrm{I}_{R(110)})}\right] 100\% \tag{3.1}$$

where, F_R is the mass fraction of rutile in the sample and $\mathrm{I}_{A(101)}$ and $\mathrm{I}_{R(110)}$ are the integrated main peak intensities of anatase and rutile, respectively. Other phases like brookite can also be calculated by using modified Spurr equation. The crystal size different phases can be calculated by using the Scherrer equation:

$$\phi = \frac{0.9\lambda}{\beta \cos\theta} \tag{3.2}$$

where ϕ = crystallite size, λ = X-ray wavelength, θ = Bragg angle, and β = full width at half-maximum.

3.3. The influence of the parameters on the phase composition of TiO_2 thin films

3.3.1. The influence of target power and substrate bias

Compared to anatase, rutile is more thermally stable. Anatase will transform to rutile under high energy input. As the target power increases, the ion bombardment enhances and resulting the phase transformation. Figure 3.2 demonstrates the influence of sputtering power (3.5-4.5 kw) and substrate RF bias (-150 V) on the phase composition of the films

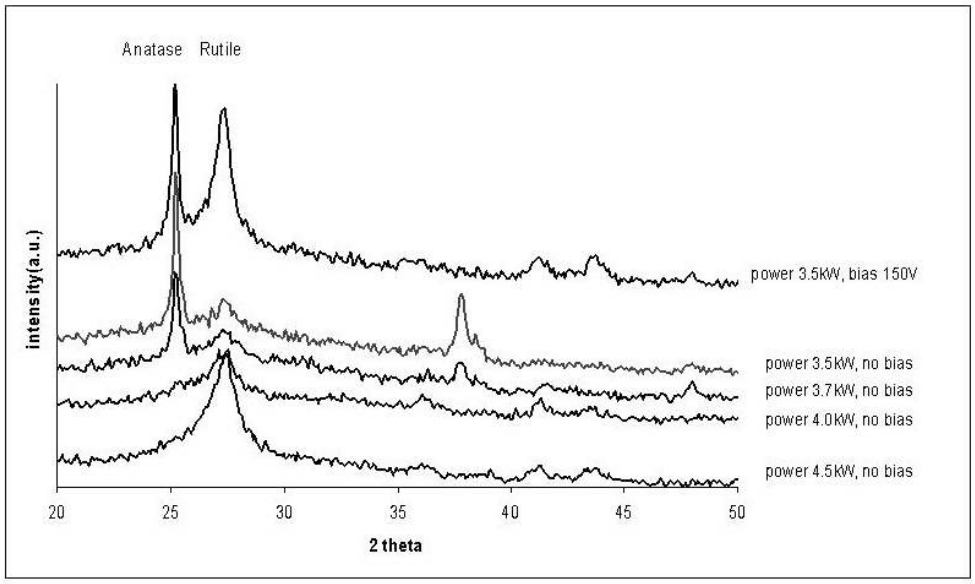

Figure 3.2. XRD intensity plots for TiO_2 films deposited at different power levels and RF bias.

prepared on the glass slides and all the other deposition parameters were kept constant. At a higher power input, more rutile crystals tended to grow, while the anatase phase was dominant with lower power input. Mixed phase films of both anatase and rutile could be made at intermediate power levels. Independent of power input level, the RF bias also contributes to the production of a high energy environment for growing rutile , since the bias voltage determines the energy of the Ar^+ ions bombarding the film during growth. A higher portion of rutile phase composition was obtained when combining RF bias with sputtering power input. For example, rutile content of the samples prepared at 3.5 kW, increased from 30% to around 60% after substrate bias was applied in Figure 3.2.

3.3.2. The influence of total pressure

The total pressure of the sputtering chamber is mostly determined by the sputtering gas (Argon). For the sputtering process, as the total pressure increases, depositing particles are less energetic due to the high chance of collision among each other on their way from the target to the substrate. However, at the low total pressure, the energetic particles also bombard the growing films causing film removal which leads to a reduced growth rate. Thus, higher total pressure will result in higher deposition rates with more porous films. As depositing particles' energy decreases with the increasing total pressure, the phase composition will be influenced as well.

Figure 3.3 shows the influence of total pressure on phase composition of sputtered TiO_2 thin films with all the other controlling parameters constant. The films were mixed phases of anatase and rutile for the different total pressures ranging from 0.35 pa to 0.55 pa. The anatase content increased from 55% to 76%, as the total pressure increased. This is can be explaned by the theory described in the previous paragraph that higher energetic depositing particles are generated under lower total pressure. This finding is also consistent with studies in the literature [193, 57].

3.3.3. The influence of oxygen partial pressure

In principle, we can make a film with any atom ratio (Ti:O) since we have independent control of both component sources (oxygen gas, Ti target). However, the target is also part of the reactive process and forms a surface oxide during sputtering, which interferes with our ability to control the process and to produce a film with any desired Ti:O ratio. The rate of Ti sputtering decreases as the surface oxide forms on the target, decreasing

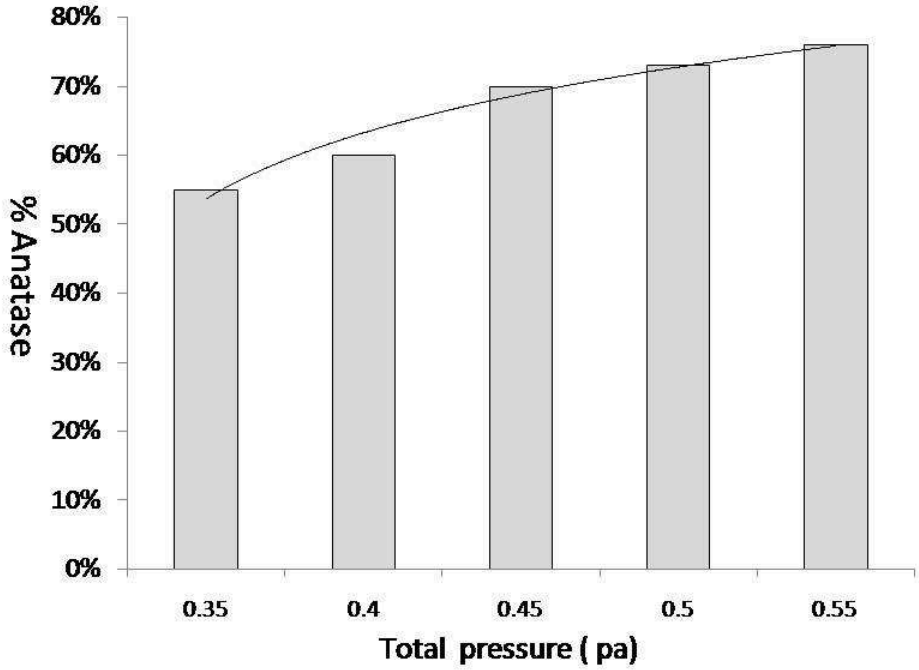

Figure 3.3. XRD intensity plots for TiO_2 films deposited at different total pressures

the demand for oxygen. A "hysteresis" could emerge as a result of two competitive processes: sputtering of the target surface and covering of this surface by the reaction product. Figure 3.4 shows the hysteresis curve for TiO_2 and hysteresis usually happens at low oxygen partial pressure. The hysteresis curve shows the system response when the partial pressure signal of O_2 is used as the control variable. The flow response to increasing O_2 pressure is represented by solid squares and to decreasing pressure (with time) by solid triangles. In addition, this also demonstrates the advantage of using partial pressure instead of flow to control the oxygen input. Since the system response shows

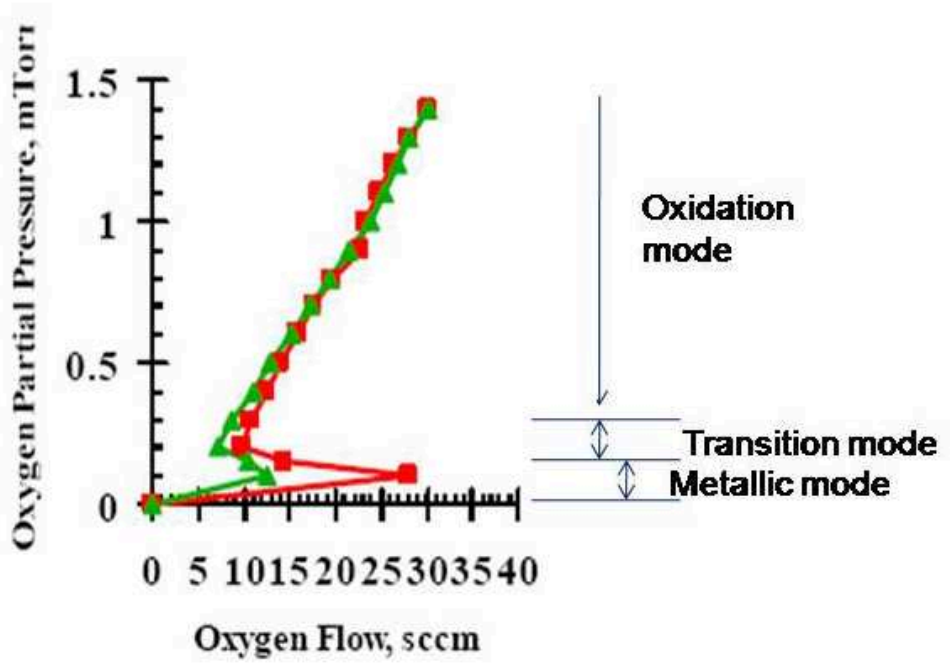

Figure 3.4. Partial pressure vs. flow hysteresis curve for TiO_2[162]

both positive and negative sloped regions, the flow value is not unique and cannot be used to obtain a single value of partial pressure. The hysteresis effect is undesirable because it can prevent the formation of a compound film of a required stoichiometry (Ti:O ratio in our case).

There are three deposition modes based on the oxidation states of the target which are also illustrated on Figure 3.4: the oxidation mode, the transition mode and the metal mode. In the metal mode, the process is operated at low oxygen partial pressure. The rate of oxide growth at the target is low, so that the etching process predominates by the sputtering removal of the oxide layer. The target surface therefore remains metallic. However, insufficient oxygen is introduced to form the oxide (TiO_2) in this mode. In the

oxidation mode, the oxygen partial pressure is much higher and stoichiometric titania film can be deposited, but with the trade off that an oxide layer also grows on the target surface. The deposition of Ti is hindered and deposition rates are slowed due to the covered oxide layer on the target. the target regions covered with reaction products are described as "poisoned target regions". In the transition mode, the process is operated between the metallic mode and oxidation mode and thus, relatively high deposition rates and near stoichiometric titania can be achieved.

We deposited most of our TiO_2 thin films at the transition mode. As showed in Figure 3.4, the transition mode can be operated within a small range of oxygen partial pressure (0.07 pa to 0.12 pa). We observed little influence of oxygen partial pressure within that range on the phase composition of sputtered titania thin films. The stoichiometry of Ti:O determined by oxygen partial pressure will be discussed in a later chapter.

3.3.4. The influence of the deposition angles

Since the sample holder is placed on a rotating table, we were able to sputter the films at different angles by rotating the sample holder to a specific position. Figure 3.5 shows the two different sample positions we used: (a): one side of the sample holder is parallel to the target. Samples parallel to the target receive the normal angle deposition while the samples displayed to the sides received deposition at 30° or less depending on their relative positions on that side. (b): when the sample holder is rotated so that the vertex of the hexagon sample holder faces the target, samples can receive 60° or less angle deposition depending on the relative positions of the samples on that side. Sample 1 is farther than Sample 2 from the target.

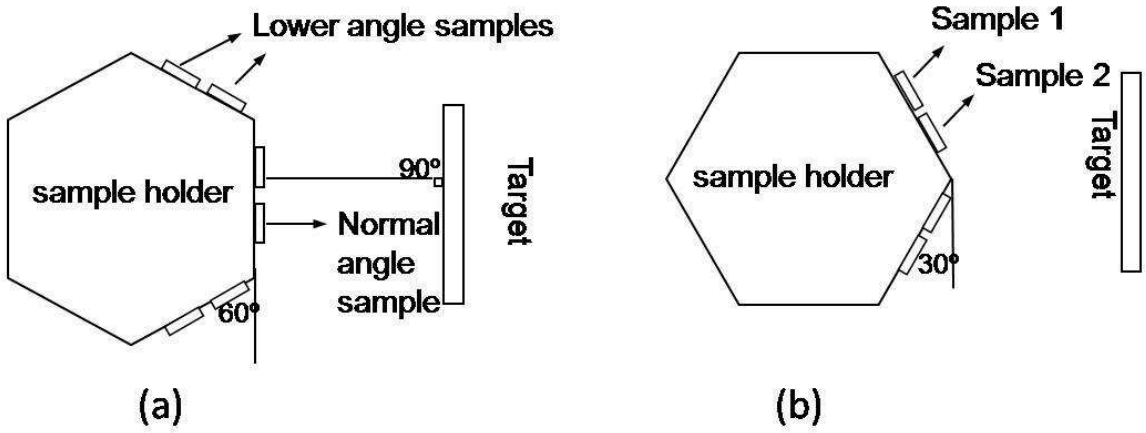

Figure 3.5. Two sample positions relative to the target used for sputtering TiO_2 thin films

In Figure 3.6 (a), the XRD intensity plot shows the influence of deposition angle (Figure 3.5 (a)) on the phase composition of films. When the samples were sputtered at the normal angle, they received a higher intensity and momentum of bombarding atoms. They were also closer to the target. Thus, the higher angle deposition tended to produce stable phases at a higher energy level, i.e., rutile, or a higher proportion of rutile. Lower angle deposition tended to produce anatase or a higher proportion of anatase than under the same conditions at the normal angle deposition. In addition to influencing phase composition, deposition angle also have an effect on film morphology and reactivity. These aspects will be discussed in the following chapters. Figure 3.6 (b) shows the XRD results of the samples prepared at deposition position in Figure 3.5 (b). Sample 1 (almost pure anatase) has a slightly lower deposition angle and longer distance from target compared to Sample 2. Thus, Sample 2 received more energy intensity compared to Sample 1 and displays a mixed phase of anatase and rutile while Sample 1 is merely pure anatase.

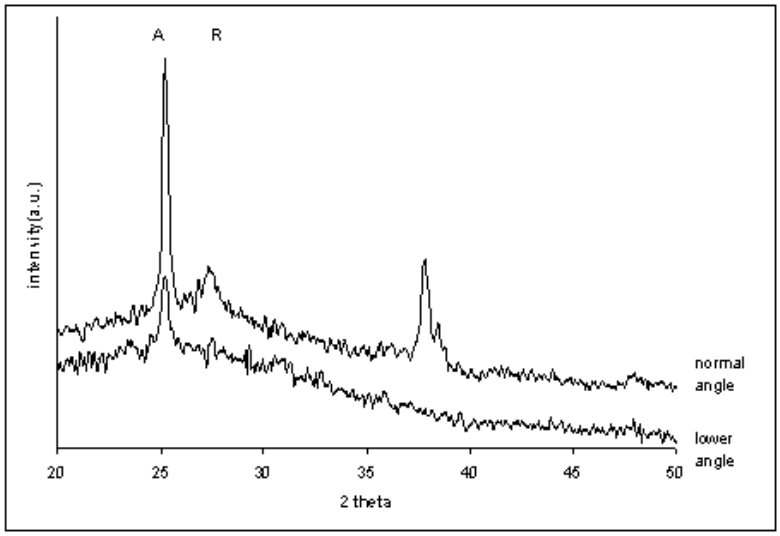

(a)

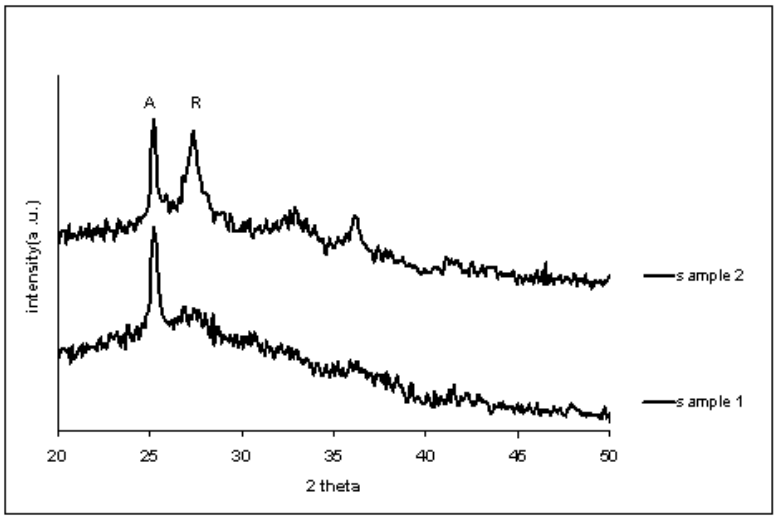

(b)

Figure 3.6. (a) XRD for samples prepared at different angles of deposition with the sample holder in the (a) position; (b) XRD for samples prepared at different angles of deposition and with the sample holder in the (b) position. All other deposition parameters were the same for (a) and (b)

.

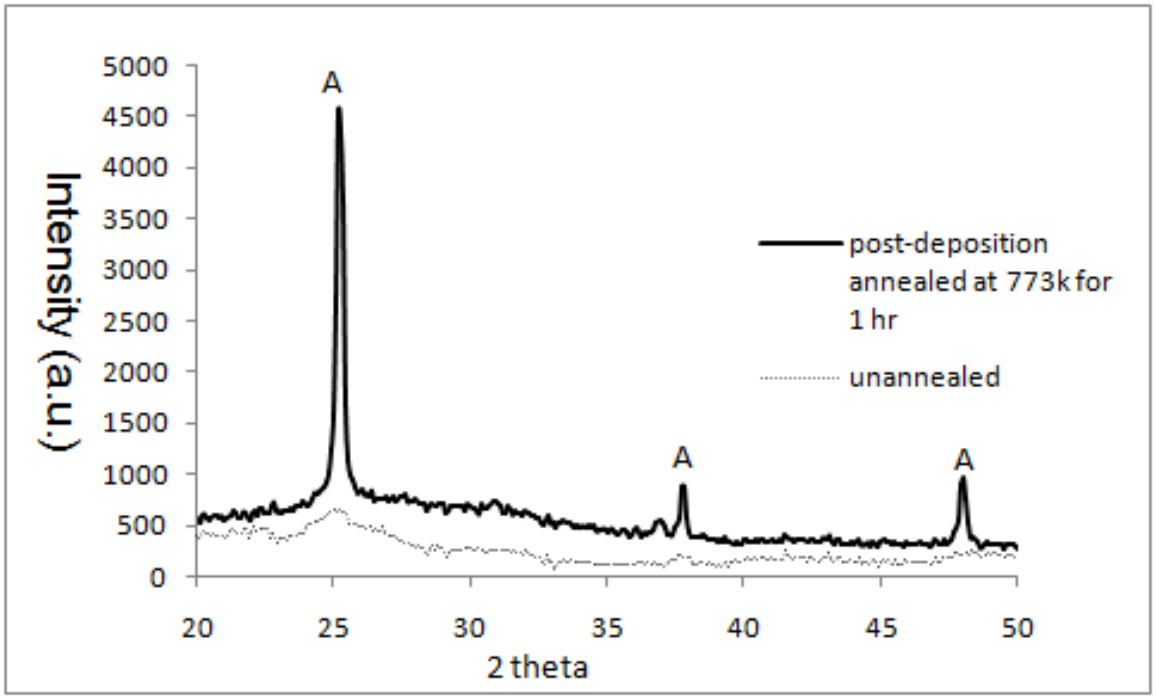

Figure 3.7. Comparison of XRD measurements for a titania thin film before and after annealing

.

3.3.5. The influence of the post-deposition annealing

Annealing of powders or thin film samples after synthesis is widely used to increase the crystallinity of the films [87, 148], transform the phase composition from anatase to rutile [117, 114] and create stoichiometry or non-stoichiometry depending on the annealing conditions[12, 20, 70].

In general, the TiO_2 phases are more thermally stable in films than in powders. In powder form, anatase begins to transform to rutile around annealing temperature from 773K [101]. In contrast, for TiO_2 films, anatase does not transform to rutile until 1073K to 1373K [117, 186].

Figure 3.7 compares the XRD intensities of a sputtered TiO_2 film before and after annealing. Before annealing, the films looked almost amorphous with only small trace of anatase. After annealing in ambient air at 737K for an hour, the film showed a much more enhanced anatase crystal peak.

Figure 3.8 shows the influence of post-deposition annealing on a sputtered mixed phase TiO_2 thin film. Similar to Figure 3.7, anatase was significantly enhanced after annealing. However, rutile peak did not change in either intensity or size after annealing. Thus, for the mixed phase film, annealing does not have the same effects on the growth of anatase and rutile. At the annealing temperature we used, no conversion of rutile was observed. According to the annealing experiments by Lőbl et al.[98], for the TiO_2 films deposited by reactive DC magnetron sputtering, below 873K anatase grows faster than rutile. This agrees with our observations very well.

3.3.6. The influence of substrates

Substrates are very critical for monocrystalline thin film deposition due to the epitaxy effect where the substrate acts as a seed crystal and the deposited film takes on a lattice structure and orientation identical to those of the substrate. Although we deposit polycrystalline TiO_2 thin films by sputtering, the substrate influence needs to be studied as well.

According to the literature, substrates do play a role in sputtered TiO_2 polycrystalline films. For example, films deposited on FTO (fluorine doped tin oxide) substrates showed better crystallinity than those on glass substrates [3]; when using soda-lime glass support,

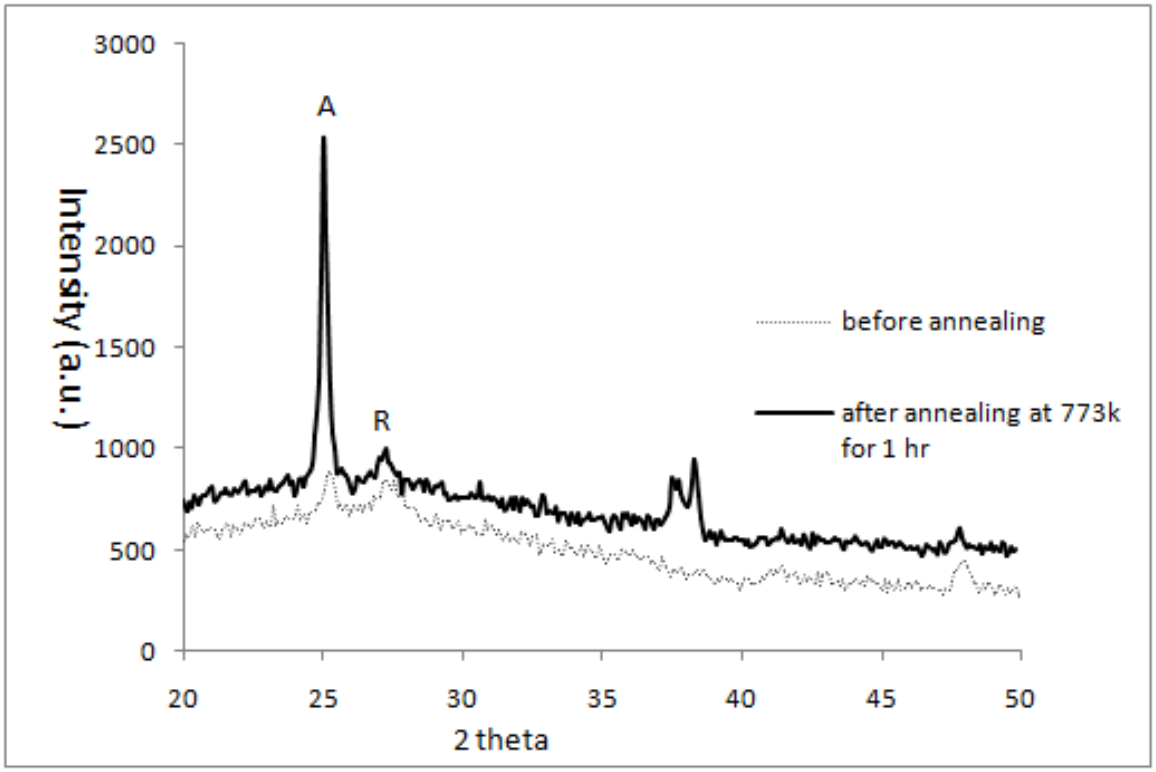

Figure 3.8. Comparison of XRD measurements for a mixed phase titania thin film before and after annealing

.

sodium diffuses into the TiO_2 film upon annealing, suppressing anatase crystallization and decreasing its photocatalytic activity [171].

In my study, I compared three different kinds of substrates to explore the substrate influence: amorphous microscope glass slides (borosilicate), crystalline quartz and single-crystalline Si wafer. The deposition conditions (same power, total pressure, oxygen partial pressure and deposition angle) were the exactly the same for the samples with three different substrates. All the substrates were well cleaned by soap water and followed by acetone. Figure 3.9 and Figure 3.10 show the XRD results of TiO_2 films deposited on three different substrates at normal angle and low angle (30°)(position 3.5(a)) respectively.

There are large differences in phase composition due to the substrate effect. Films deposited at normal angle on glass and quartz substrates showed mixed phase characteristics (about 55% anatase mixed phase film on quartz slide and less than 10% anatase mixed phase film on glass slide) in contrast to the film deposited on Si wafer (pure rutile), as illustrated in Figure 3.9. For the low angle deposited films (Figure 3.10), all the samples displayed mixed phase characteristics, but with different proportions of phase compositions (about 90% anatase on Si wafer, about 40% anatase on glass slide and about 50% anatase on quartz slide). For both of the normal angle and low angle samples on quartz slides, the phase compositions were similiar (about 50%-55% anatase mixed phase for both normal angle and low angle deposited films) and only the crystallinity decreased from the normal angle sample to the low angle one. Thus, quartz tends to improve the thermal stability of the deposited TiO_2. In contrast, for the films deposited on the glass slides, anatase is observed to transform to rutile from the low angle deposition to the normal angle deposition. A more complete phase transformation occurs with the films deposited on the Si wafers with rutile for the normal angle deposited sample and almost pure anatase for the low angle deposited sample. It is very interesting to notice that single crystalline Si wafer favors the single phase growth. The different influences of substrates on the films can also be explained by the fact that heat conducting ability varies from substrate to substrate and may result in the a substrate temperature differences during sputtering and eventually affect the phase composition of the films.

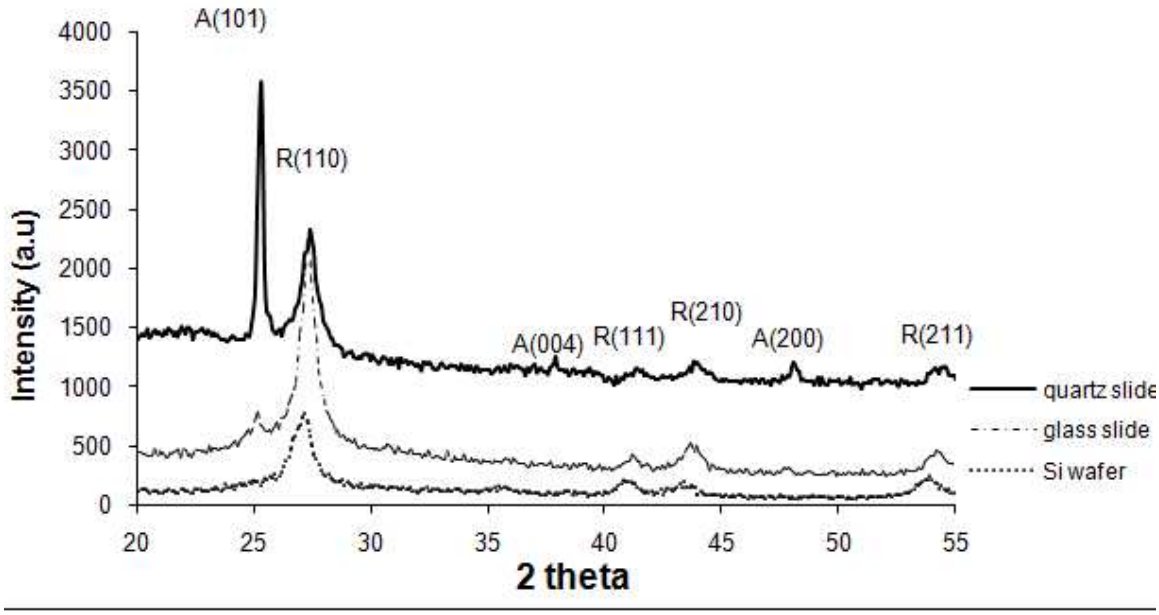

Figure 3.9. Comparison of XRD measurements for normal angle deposited titania thin films deposited on a quartz slide, a glass slide and a Si wafer.

3.4. The crystal particle size of sputtered TiO_2 films

The average crystal particle size was calculated by Scherrer's equation based on the information from XRD measurements. For the sputtered films, rutile crystals were about 10-15 nm in diameter and anatase crystals were larger with diameters of 20-40 nm. Similar results were also reported by Choi et al.[32], Asanuma et al.[17], etc.. In contrast, the mixed phase sol-gel and P25 crystallites, tended to have smaller anatase (around 10 nm) than rutile (around 20-30 nm)[101, 66].

As mentioned above [98], for sputtered films, anatase has higher thermal stability compared to regular TiO_2 powders and grows faster than rutile below 600°C which can explain larger crystal particle size of anatase in comparison to that of the rutile in our mixed phase samples. For the hydrothermal or flame hydrolysis synthesized samples like

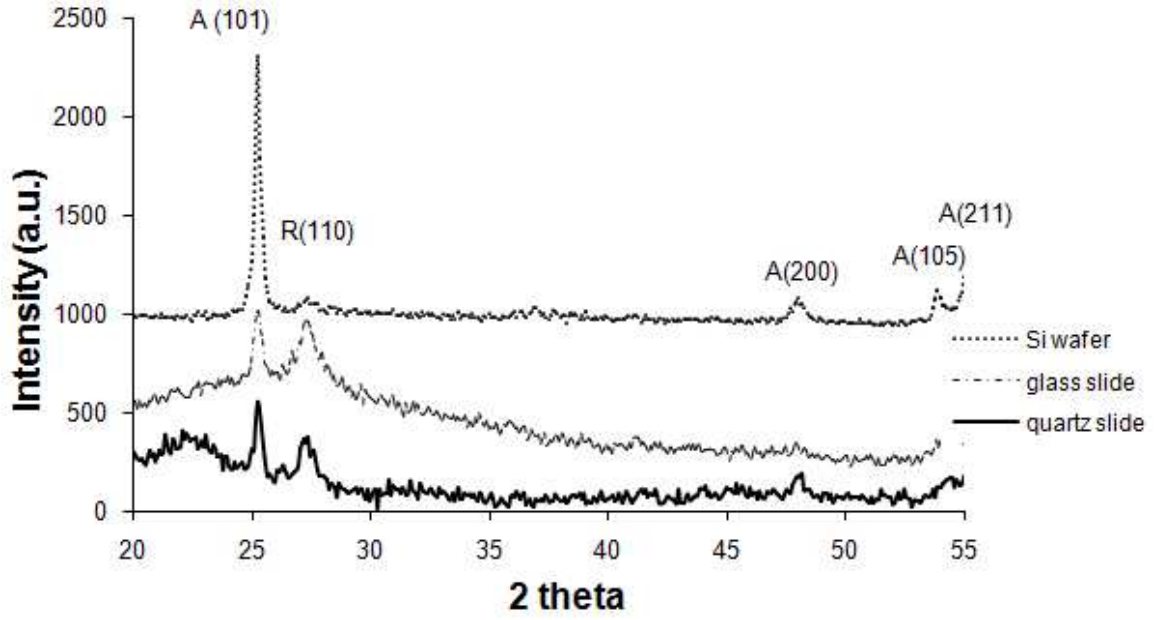

Figure 3.10. Comparison of XRD measurements for low angle deposited titania thin films deposited on a quartz slide, a glass slide and a Si wafer.

sol-gel or P25, the thermally stability of anatase is relative low and anatase transforms to rutile, a more thermal stable phase before the crystals grow bigger.

3.5. Conclusions

The sputtering process is described in this chapter. The influences of the different controlling parameters are also discussed. In conclusion, the target power, substrate bias, total pressure and deposition angles affect the phase composition of anatase and rutile during the sputtering. high power and bias input, low total pressure as well as high angle deposition, tended to promote the growth of high-energy-stable crystals like rutile. Post-deposition annealing and substrates provide additional tuning on the phase composition. Oxygen partial pressure during the sputtering process, however, is not critical to the phase

composition according to our characterization results but determines the stoichiometry of the films. For a sputtered mixed phase TiO_2, anatase has larger crystal particle than rutile, which is opposite to the hydro-thermally synthesized mixed phase TiO_2.

CHAPTER 4

Oxidizing Acetaldehyde by Sputtered Mixed Phase TiO_2

With an understanding of the basics of synthesizing TiO_2 films by sputtering, I will explore the relationship between the film structures and their photocatlytic reactivities. This chapter is focused on the study of the oxidation photoactivity of sputtered TiO_2. I discuss the influence of structural characters such as phase compositions, film thickness and surface morphology, etc. on the reactivity of acetaldehyde oxidation and compared the oxidation reactivity of sputtered films with P25 and sol-gel samples. We hypothesize that the by sputtering, we can synthesize TiO_2 based nanocomposites with high solid-solid interfacial densities which gives rise to a high oxidation reactivity.

4.1. Brief introduction of acetaldehyde

Acetaldehyde, an organic chemical compound with the formula CH_3CHO or MeCHO is a colorless flammable liquid with a fruity smell. It is one of the Urban Hazardous Air Pollutants, estimated by EPA's National Air Toxics Assessment (1999). EPA also lists acetaldehyde as a probable human carcinogen. Acetaldehyde is produced as an intermediate to synthesize other chemicals in industry. It is used in the production of perfumes, dyes and polyester resins, in fuel composition and as a solvent in the rubber, tanning and paper industries. It is also used as a food flavoring and preservative.

Acute exposure to acetaldehyde by inhalation may cause irritation of the eyes, nose, throat and lungs. At higher exposures, there may be coughing, pulmonary edema and

respiratory paralysis and death. chronic exposure produces changes in the lining of the nose and trachea, growth retardation and increased kidney weight and an increase in embryonic resorptions and skeletal malformations. .

The oxidation of acetaldehyde by TiO_2 based photocatalysts for environmental treatment purpose has been studied widely[47, 27, 145, 128]. Most of them use hydro-thermal synthesized TiO_2 based photocatalysts. In this chapter, I investigate the photo-oxidative ability of my sputtered mixed phase TiO_2 thin films by degrading acetaldehyde and relate it to the sputtered film structures. These activity results are compared with those of the hydro-thermal synthesized TiO_2 photocatalysts as well as P25.

4.2. Experimental details

4.2.1. Sample preparation

Table 4.1 shows the details of the typical controlling parameters I used to prepare the TiO_2 thin films with different phase compositions for this study based on the investigation of sputtering conditions described in the previous chapter. The substrates used are clean microscope glass slides (borosilicate) which were chosen due to their low cost compared to quartz and Si wafers I also studied in the previous chapter. The glass slide substrates were etched in the chamber for about 5 mins at substrate bias at 1000 KW before the deposition. Pure titanium (99.95%) was used as the sputtering target. High-purity argon and oxygen were used as sputtering and reactive gas respectively. The base pressure in the coating chamber was controlled below 5.3×10^{-4} Pa. The oxygen partial pressure was set and maintained at 0.1 Pa. Since all the films deposited at the conditions listed

Films	**Deposition angle**	**Target power and substrate bias**	**Total pressure**
Anatase	Low angle (Fig 3.5a)	4 kw power and -300 V bias	0.55 pa
Rutile	normal angle	5.9 kw power and -150 V bias	0.4 pa
Mixed phase (70%anatase)	Low angle	5.5 kw power and -120 V bias	0.55 pa
Mixed phase (70%rutile)	Low angle	5.8 kw power and -120 V bias	0.4 pa

Table 4.1. Sputtering Conditions

in the table display sufficient crystallinity according to the XRD measurements, no post-deposition annealing is necessary for those films. In addition to the samples listed in the Table 1.1, I was also able to sputter mixed phase TiO_2 films with other phase proportions by slightly adjusting the target power or substrate bias.

Both the sol-gel mixed phase samples and P25 samples were used to compare to my sputtered mixed phase films in oxidizing acetaldehyde.

The sol-gel mixed phase TiO_2 samples were prepared by Dr. Gonghu Li from our lab [101, 102]. He was able to monitor the phase composition of the sol-gel TiO_2 by simply controlling the acidity in the preparation and the calcination temperatures [101, 102]. The 70%anatase mixed phase sol-gel powders were mixed with water and sonicated to form a more uniform suspension and then dip-coated on the clean glass slides. Degussa P25 TiO_2(usually contains 70%-80% of anatase, 20%-30% of rutile) was used as a commercial standard. They were sonicated in ethanol solution first and then dip-coated on clean glass slides to form films the same as the sol-gel samples.

4.2.2. The gas phase acetaldehyde degradation reactor

The oxidative activities of the prepared samples were tested in a gas phase batch reactor system (Figure 4.1) consisting of a square Teflon™ container connected to a circulating pump and injection port. One square inch of glass slide covered with TiO_2 was placed at the bottom of the container and a UV light filter covered the top of the container underneath a Black Ray® UV lamp. The UV lamp provided light at a wavelength of 365nm and an energy power of 100W. Before the reaction, the surface of the catalysts was oxidized by passing hydrated air over at the room temperature. A 500 ppm aliquot of acetaldehyde gas was injected into the closed reactor through the injection port at the beginning of the reaction and samples were taken at different time intervals. The decay of acetaldehyde was monitored by a HP 5890 gas chromatography equipped with a flame ionization detector. For each sample, I tested at least twice to increase the accuracy.

4.2.3. characterization methods

In addition to X-ray Diffraction for characterizing the phase composition, I also used other characterization approaches.

4.2.3.1 Texture analysis system

Texture analysis systems generally use stylus profiling to measure, analyze and control the surface textures. The stylus profilers use a variety of diamond-tipped styli to detect minute surface variations in surface topography. In a profiler, the stylus is mechanically coupled to the core of an LVDT (Linear Variable Differential Transformer). A precision stage moves the sample surface across an optically flat reference surface beneath the stylus. As the stage moves the sample, the stylus rides over the surface, detecting roughness variations

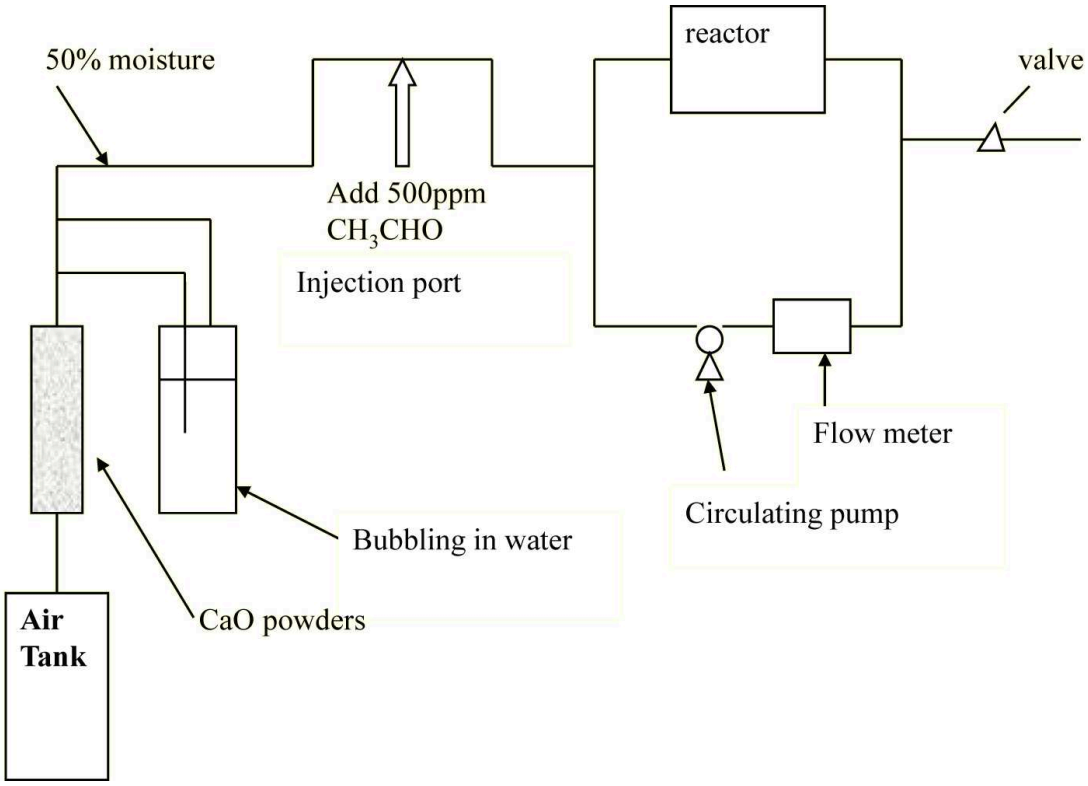

Figure 4.1. Schematic illustration of the batch reactor system for the acetaldehyde oxidation test.

as small as ten angstroms in height. The LVDT produces an analog signal corresponding to the vertical stylus movement. This signal is amplified, conditioned, digitized and stored for manipulation, analysis and display [135].

We used Dektak 3030 ST profilometer as the surface texture analysis system in the lab for measuring the film thickness. Dektak 3030 ST can measure surface texture less than 10 nm and film thickness up to 131 μm with a 10 to 20 Angstroms resolution.

In order to measure the thickness by the texture analysis system, I created some unsputtered areas on the sample as references. Thus, before sputtering, I deposited certain areas of the substrates with an ethanol suspension of commercial titania powders. The

ethanol evaporated in seconds and left in its place the titania covering the selected surface of the substrates. After sputtering, the commercial titania was removed by cleaning with acetone to reveal the unsputtered substrate surface. Film thickness then can be measured by performing line-profiling using Dektak 3030 ST profilometer over the unsputtered reference surface and the neighboring sputtered surface and calculating the 'height' of the sputtered surface relative to the 'referece surface'. For some films such as low angle sputtered ones, the film thickness varies horizontally over the substrates as a function of the distance to the target during the sputtering. Multiple measurements were required to determine the thickness distribution of the films.

4.2.3.2 Atomic Force Microscope

The atomic force microscope (AFM) is a high-resolution type of scanning probe microscope, with demonstrated resolution of fractions of a nanometer, more than 1000 times better than the optical diffraction limit. AFM can image samples in air and under liquids.

AFM (Figure 4.2) operates by measuring attractive or repulsive forces between a tip and the sample [24]. In its repulsive "contact" mode, the instrument lightly touches a tip at the end of a leaf spring or "cantilever" to the sample. As a raster-scan drags the tip over the sample, the detection apparatus measures the vertical deflection of the cantilever, which indicates the local sample height. Thus, in contact mode the AFM measures hard-sphere repulsion forces between the tip and sample.

In the tapping mode, the AFM measures topography by "tapping" the surface with an oscillating probing tip. Tapping mode overcomes problems associated with friction,

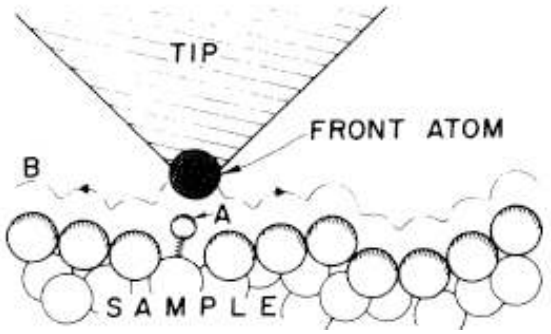

Figure 4.2. The principle of AFM operation [24].

adhesion, electrostatic forces, and other difficulties that can plague conventional AFM scanning methods.

In my study, I used AFM(JSPM-5200) by tapping mode to directly observe surface morphology and quantitatively analyze of the surface root-mean-square (r.m.s) roughness and surface area of the films.

4.2.3.3 Scanning Electron Microscope

The scanning electron microscope (SEM) is a type of electron microscope that images the sample surface by scanning it with a high-energy beam of electrons. The electrons interact with the atoms and some of them are scattered from the nucleus of the involved specimen to be collected to form an image of the surface. There are two kinds of scattering from electron-specimen interaction: elastic scattering and inelastic scattering. SEM characterizes the specimen based on the elastically scattered electrons such as forward scattered electrons, secondary electrons and backscattered electrons.

In SEM, imaging is typically obtained using elastically scattered secondary electrons for the best resolution of fine surface topographical features. Alternatively, imaging with

backscattered electrons from the specimen gives contrast based on atomic number to resolve microscopic composition variations, as well as topographical information. Qualitative and quantitative chemical analysis information can also be obtained using an energy dispersive x-ray spectrometer with the SEM (such as Energy Dispersive Spectroscopy (EDS) analysis) [38].

The SEM instruments I used for my study are Hitachi S-4500 and LEO Gemini 1525. Hitachi S-4500 is a standard SEM with both imaging and analysis functions. Leo Gemini 1525, on the other hand, is only focused on imaging and is equipped with a Schottky field emission gun for high resolution and excellent beam stability. Since I used SEM mainly for characterizing surface morphology (imaging) of the films, I used Leo more frequently for easy operation and better and stable imaging for the rest of my research.

The surface charge accumulation due to the diffusion of trapped space charge or from the multiplication of secondary electrons may happen to insulator or semiconductor samples such as TiO_2 during SEM imaging. The surface charge problem makes it impossible to operate the SEM imaging under high voltage and thus, only low resolution images can be obtained. In order to overcome the problem, I sputtered a very thin layer (5 nm to 7 nm) of gold or platinum over the surface of my thin film TiO_2 samples (with size about 2 cm by 2 cm) before SEM imaging.

4.2.3.4 Transmission Electron Microscope

Transmission electron microscopy (TEM)(Figure 4.3) is a microscopic technique whereby a beam of electrons is transmitted through an ultra thin specimen, interacting with the specimen as it passes through it. Compared to SEM, TEM has enhanced resolution (1

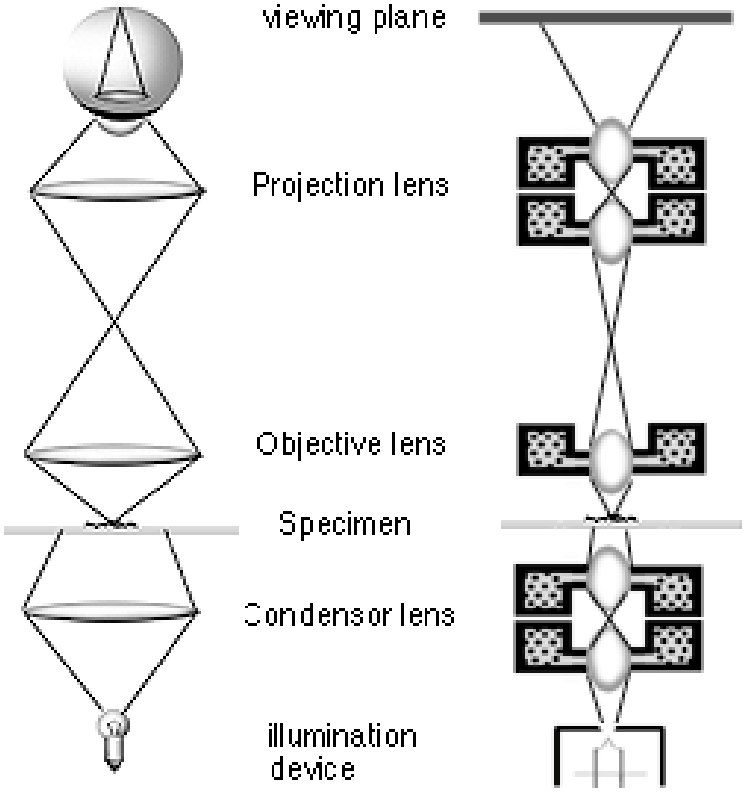

Figure 4.3. The structure of a transmission electron microscope

nm for SEM and 0.01 nm for TEM) allowing more focused analysis on fine structures (not just surface structure) by studying inelastically transmitted electrons.

TEM instrument resembles that of a regular optical microscope. The "light source" at the top of the microscope emits the electrons that travel through vacuum in the column of the microscope. Instead of glass lenses focusing the light in the light microscope, the TEM uses electromagnetic lenses to focus the electrons into a very thin beam. The electron beam then travels through the specimen under study. Depending on the density of the material present, some of the electrons are scattered and disappear from the beam. At the

bottom of the microscope the unscattered electrons hit a fluorescent screen, which gives rise to a "shadow image" of the specimen with its different structures displayed in varied darkness according to their density. The image can be studied directly by the operator or photographed with a camera. [38]

Since TEM can provide fine structure information of selected small areas, as well as high resolution images, it can help to characterize the interfaces of individual crystal of mixed phase TiO_2. The high resolution imaging can provide the shape, dimensions and position of the microcrystals of different phases and their interfaces observed on the sample. The analysis based on the inelastically scattered electron loss can characterize the defects in the atomic scale and chemical composition of the mixed phase TiO_2. TEM also has X-ray diffraction and Energy Dispersive Spectroscopy aimed at atomic scale analysis.

Unlike SEM samples, TEM samples do not need a coating of conducting materials before observation. However, they are required to be ultra thin (70μm) so that the electrons can transmit through the films. Figure 4.4 shows the procedures to make an ideally sized plain-view TEM sample from a bulk material. For a cross-section TEM sample, two small pieces need to be cut in the beginning and glued together(film to film). The rest of the procedures are the same as the plain-view sample preparation. TEM powder sample preparation is much simpler by merely spreading a diluted drop of powder suspension over a metal grid supporter.

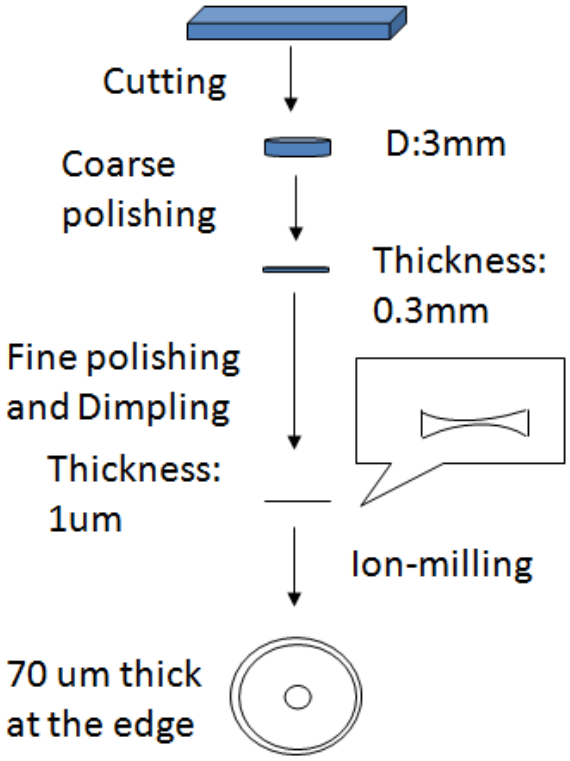

Figure 4.4. The procedures to make a plain-view TEM sample from a bulk material.

4.3. The oxidative photo-activity of sputtered TiO_2 films with different phase compositions

4.3.1. The optimization of the sputtered TiO_2 films

A screening by acetaldehyde oxidation test was carried out to search for the sputtered TiO_2 samples with optimal phase composition and fabricating conditions.

4.3.1.1 The optimal phase composition

The influence of phase composition was explored by testing acetaldehyde oxidation of a series of sputtered TiO_2 samples with different phase compositions (Figure 4.5): pure

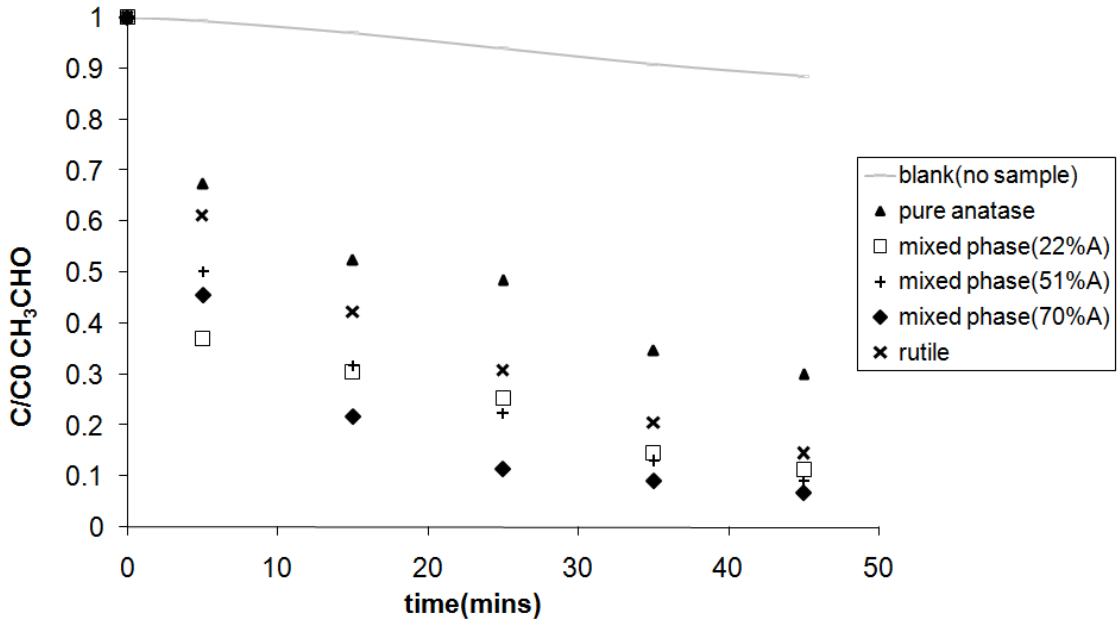

Figure 4.5. Degradation of acetaldehyde by various samples normalized by the surface areas of the films. The surface area is expressed as the ratio of the measured surface area to the nominal or projected area. Pure anatase, surface area $1.10\mu m^2/\mu m^2$; mixed phase (22% anatase), surface area $1.22\mu m^2/\mu m^2$; mixed phase (51% anatase), surface area $1.12\mu m^2/\mu m^2$; mixed phase(70% anatase), surface area $1.12\mu m^2/\mu m^2$; pure rutile, surface area $1.06\mu m^2/\mu m^2$.

anatase, 22%anatase, 52% anatase, 70% anatase and pure rutile. In order to correct for the surface area effect, the 70% anatase sputtered sample's surface area was set as a standard and all other films' surface areas were normalized to the standard. Exposed surface areas were measured by AFM showed in Figure 4.5. *The reactivity test results in this and following chapters are normalized by the surface areas.*

For both of the overall reaction and the initial 5 minutes' degradation, the mixed phase sputtered samples have better photocatalytical performance in oxidizing acetaldehyde than pure phase sputtered samples. There are slight differences among the mixed phase

TiO_2. The mixed phase (22% anatase) has the highest intial degradation rates (63% of the initial acetaldehyde concentration, C_0, was degraded after 5 mins) but lowest extended degradation rates (about 5% C_0/min for the last 40 mins) among all of the mixed phase samples. The mixed phase (70% anatase), on the other hand, demonstratesthe best overall photocatalytic performance (90% of C_0 was degraded after 45 mins) with high intial degradation rate (55% of C_0 was degraded after 5 mins) as well. The mixed phase (51% anatase), with the intermediate phase composition between 22% anatase and 70% anatase, also displays the intermediate photocatalytical reactivity. Thus, about 70% anatase of the mixed phase TiO_2 is the optmial phase composition based on the overal photocatalytic performance. What is more, it concides with the phase composition of the highly active commercial TiO_2 product, Degussa P25.

In contrast to the conventional knowledge that anatase is more active than rutle, the sputtered rutile film shows higher reactivity than sputtered anatase film in the experiment. In addition to the reactivity difference, the rutile film appeared to be much darker compared to the transparent colorless anatase film. These rutile characteristics (color and activity) suggest that there are unique structural features to the rutile films. Further investigation and exploitation of the unique structure features needs to be made for energy application, and is the focus of subsequent chapters.

4.3.1.2 The optimal synthesis conditions

As explained in the previous chapter, the effects of a number of sputtering parameters such as target power, substrate bias, total pressure etc. on film structure were determined. But

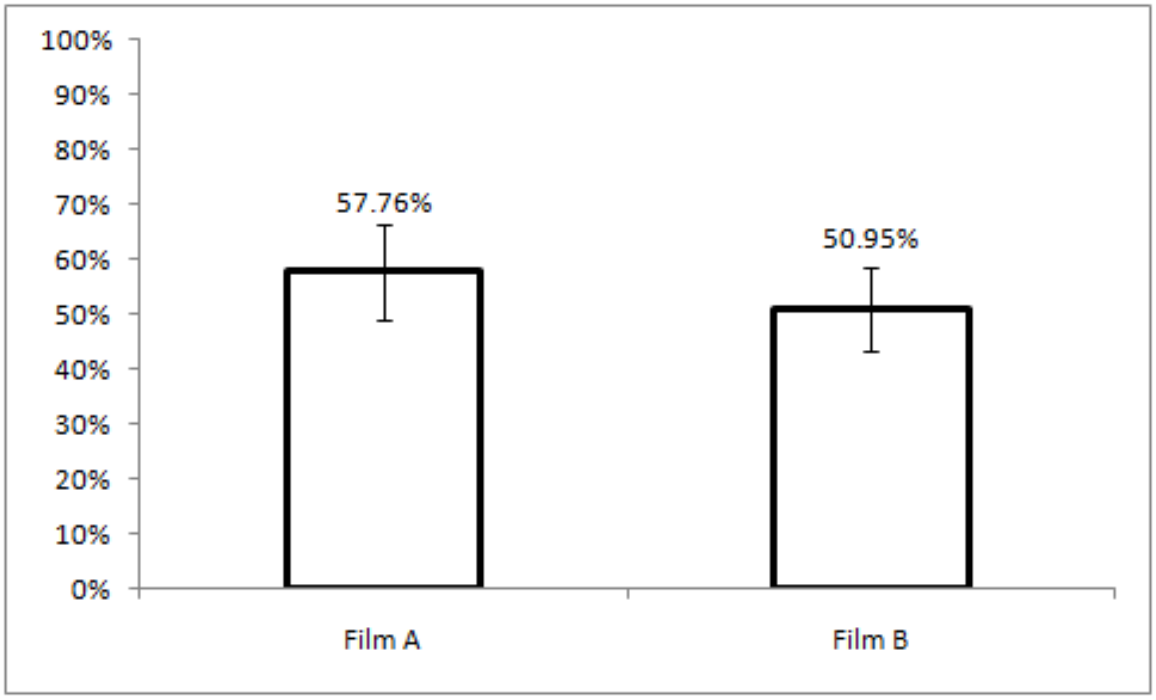

Figure 4.6. The CH_3CHO removal percentage after five minutes degradation for Film A and Film B

I investigated the effect of film thickness and deposition angles on the functional features of the films.

Figure 4.6 shows the influence of film thickness on reactivities. In general, the film thickness depends on 1) deposition rate determined by the sputtering conditions previously discussed and 2) deposition time. Film A and Film B in Figure 4.6 were prepared under the same sputtering conditions, so the deposition rates were the same for these two deposition processes as well. However, Film A and Film B were deposited for different time – 1 hr and 30 mins respectively. The average film thickness is about 600 nm for the Film A and 300 nm for the Film B. I also observed that film partially peels off from the substrates if it is excessively thick (> 800-1000 nm). Both Film A and Film B are mixed phase films with 70% anatase.

From the figure, there is no significant difference in reactivities for films with thicknesses that vary by a factor of 2. This also agrees with the findings of Zeman et al.[193] that film thickness has a minor influence on the photocatlytic activity of the films. In addition, this implies that film porority and unexposed surface area which should be larger for the thicker film, does not contribute to the reaction.

Recall that two sample positions were used for the film deposition (Figure 3.5) and I was able to make the optimal phase composition (70% anatase of mixed phase) at any deposition angle. Three mixed phase TiO_2 films (70% anatase) deposited at different angles were selected to compare the effect of deposition angle and film morphology on film photo-activity as measured by acetaldehyde degradation. Film (1) was deposited at a low angle (about 30 degrees) in Figure 3.6 (a), Film (2) was deposited at normal angle in Figure 3.5 (a) and Film (3) was deposited at 'Sample 2' position (about 60 degrees) in Figure 3.5 (b). The films deposited at different positions but all other conditions being the same have different film thickness. Film (1) had decreasing film thickness (from about 400 ± 23 nm to about 200 ± 15 nm) from the edge closer to the target to the edge farther from the target. Film (2) had smaller variation of film thickness (from around 500 ± 17 nm to 450 ± 11 nm). Film (3) was almost uniform with average film thickness around 600 ± 25 nm.

Figure 4.7 showed the acetaldehyde degradation reaction results for these three films. All of the films display high reactivities for acetaldehyde decay. The differences among them are small, yet a trend can still be noted that the lower the angle at which the film was deposited, the higher reactivity the film displays. These results reinforced the findings shown on Figure 4.6 that reactivity does not increase with film thickness, indicating that

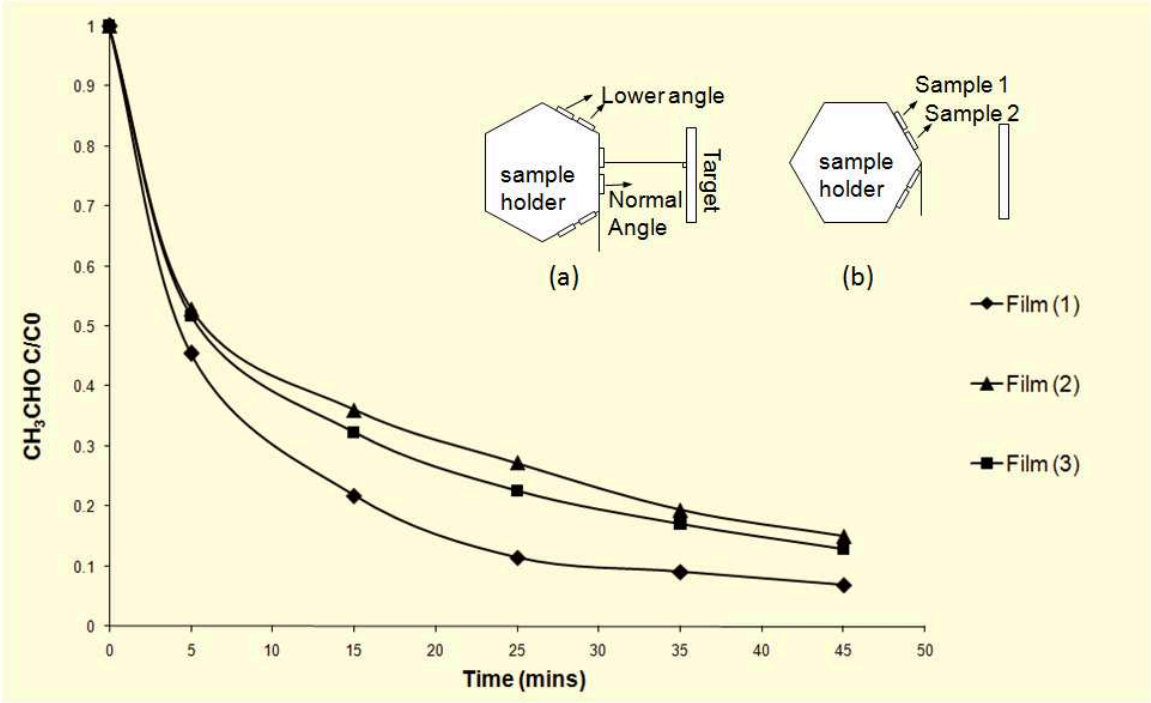

Figure 4.7. Oxidation of acetaldehyde by mixed phase TiO_2 films (70% anatase) deposited at different angles: Film (1) was deposited at low angle position as in Figure 3.5 (a), Film (2) was deposited at normal angle in Figure 3.5 (a) and Film (3) was deposited at 'Sample 2' position in Figure 3.5 (b).

the reactive surface area does not increase with film thickness. Thus, the difference in the reactivity can be attributed to the surface structural differences which will be discussed in the next section.

Based on these screening results, I found out the optimal sputtered film: 70% anatasse of mixed phase film deposited at the low angle (Figure 3.5 (a)). In the following section, I will compare the best sputtered sample with the sol-gel synthesized TiO_2 and Degussa P25 in terms of acetaldehyde oxidation.

4.3.2. The comparison of sputtered TiO_2 with sol-gel TiO_2 and Degussa P25

The decay of acetaldehyde was followed on the four films in the batch reactor: Two magnetron sputtered samples (low angle deposition from Figure 3.5 (a) position): a pure anatase sample and a mixed phase sample, one sol-gel mixed phase sample, and one Degussa P25 sample (all the mixed phase samples including Degussa P25 had around 70% anatase and 30% rutile).

Both of the sol-gel samples and Degussa P25 samples were dip-coated on the glass slides. Unlike the sputtered films, which generally have dense and uniform thin films with comparable surface areas, the dip-coated films are much thicker and have more porous and uneven, rough surfaces. It is a big challenge to use AFM to measure the surface areas for the dip-coated films since AFM can only provide the topographic information of the films within certain reach limits (a few microns). Thus, the abundant inner surface areas and the big aggregates over the surface which could influence the photo-activity greatly is not measurable by AFM. The average surface areas of the dip-coated films from AFM analysis by sampling multiple spots over the film surface are underestimated from the actual surface areas. We also tried to run adsorption-desorption experiments by chemical ionization mass spectrometry [149] by collaborating with colleagues from Department of Chemistry and failed to collect data due to insufficient film masses. We encountered the same problem with BET surface analysis. After trials and errors, we came back to AFM analysis and tried to improve our measurements by making dip-coated films as smooth as possible.

Figure 4.8 compared the reactivity results of the selected TiO_2 films after normalizing the surface areas. The photo-decay of acetaldehyde was followed over 45 minutes of

irradiation time. Both the mixed phase sol-gel sample and the sputtered samples showed better photocatalytic performance in decomposing acetaldehyde than the dip-coated Degussa P25 film, which had the worst film quality due to the largely varied particle sizes (could be tens of nanometers to over 100 nanometers) and the inevitable particle aggregates (e.g. around 1 micron). Given these films features and the high porosity, we might expect a higher reactive surface area, but unaccounted for higher surface area would only worsen the P25 relative performance. The mixed phase sol-gel film and the pure anatase, sputtered film had similar initial degradation rates (35% of C_0 was degraded in the first 5 mins) for the first 5 minutes, but the sol-gel mixed phase sample sustained a higher degradation rate for the rest of the time. The mixed phase sputtered film, which had a similar phase composition to the sol-gel's, demonstrated the highest initial degradation rate (55% of C_0 was degraded in the first 5 mins) and also the best overall photocatalytic performance.

4.4. The morphology and structure of the films

Both AFM and SEM were used to characterize the surface of the sputtered film. Figure 4.9 and Figure 4.10 show respectively, the AFM and SEM images for both pure anatase and mixed phase sputtered films used for the activity test. Both of the films were deposited at the low angle and displayed columnar microstructure with comparable surface roughness (r.m.s. for pure anatase film is 8.9 nm and for mixed phase film is 13.5 nm) and columnar aggregates around 200 nm in diameter containing rutile crystals about 10-15 nm in diameter and anatase crystals about 20-40 nm in diameter. Especially for the mixed phase film, the columns were grown at an angle less than 90 to the substrate surface,

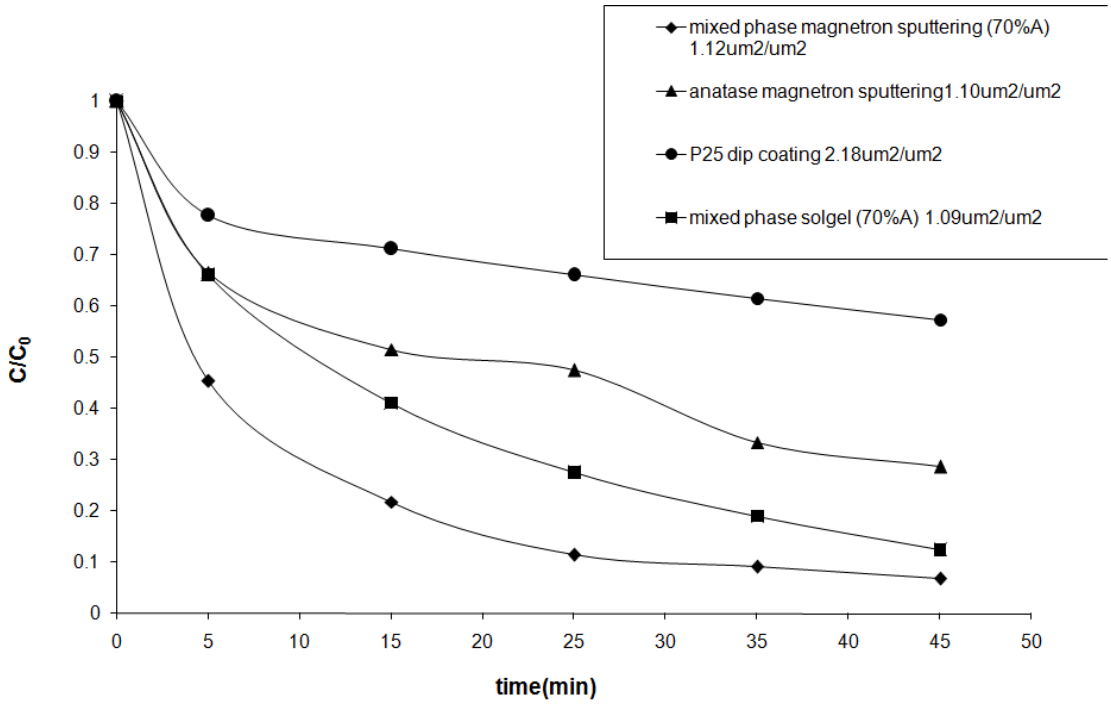

Figure 4.8. Degradation of acetaldehyde by various samples normalized by the surface areas of the films. The surface area here is expressed as the ratio of the measured surface area to the nominal or projected area. (1) Degussa P25, dip-coated film with surface area no smaller than $2.18\mu m^2/\mu m^2$; (2) anatase, magnetron sputtered film with surface area $1.10\mu m^2/\mu m^2$; (3) mixed phase, sol-gel film (70% Anatase) with surface area $1.09\mu m^2/\mu m^2$; (4) mixed phase magnetron sputtered film (70%Anatase) with surface area $1.12\mu m^2/\mu m^2$

and formed a scale-like surface. This special dual-scare columnar structure resulted from combined effects of limited atom or molecular mobility [169, 118] and shadowing effects during growth. Figure 4.11 shows a normal angle deposited mixed phase TiO_2 film and the film appeared to be very dense and smooth compared to the low angle deposited films. No columnar structures with distinctive boundaries could be found from the normal angle deposited film. The difference in film morphology between the normal angle deposited and low angle deposited films may explain the difference of photoactivity showed in the

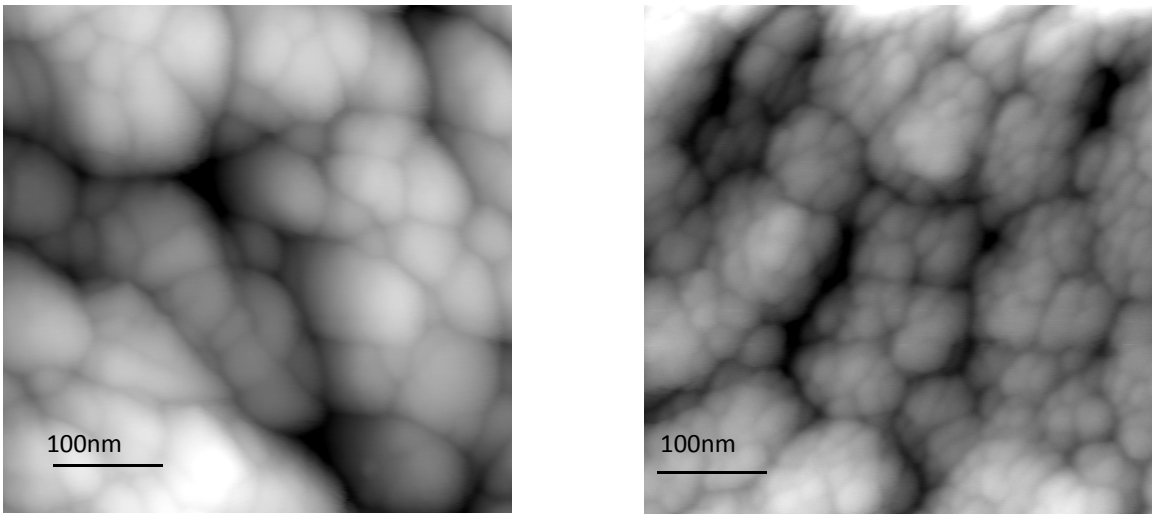

Figure 4.9. AFM images of the mixed phase and pure anatase films obtained by the sputtering method.

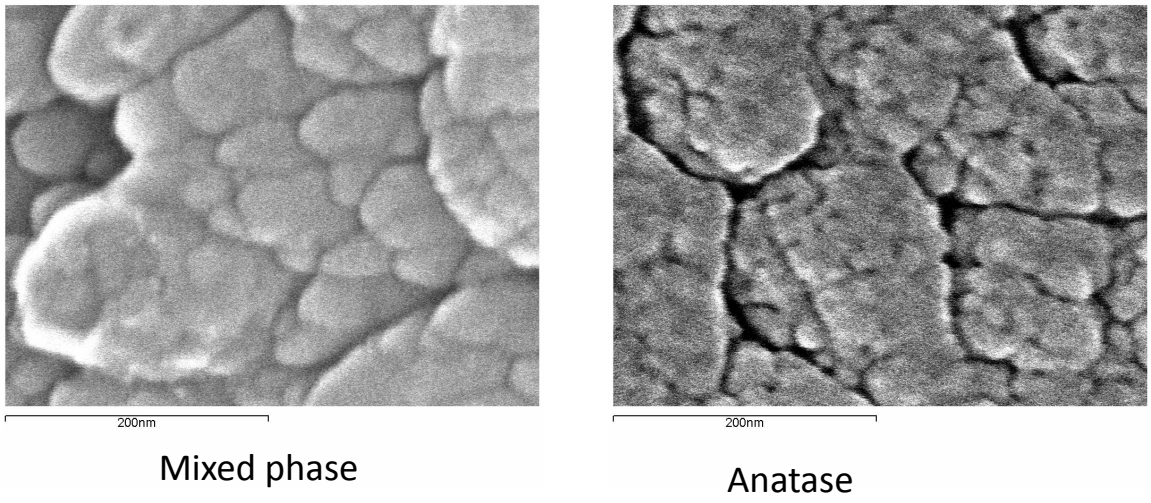

Figure 4.10. SEM images of the mixed phase and pure anatase films obtained by the sputtering method.

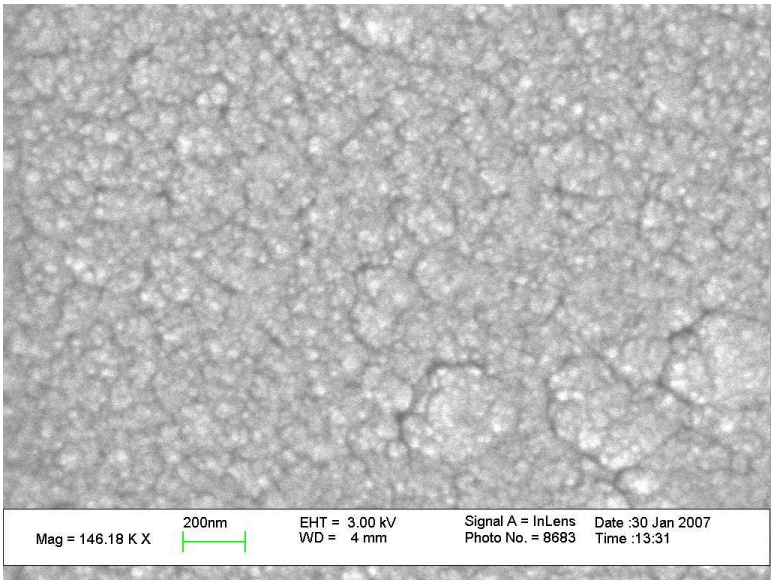

Figure 4.11. SEM images of the mixed phase titania film sputtered at normal angle.

previous section. There are abundant boundaries among the columns and crystals within the columns indicating a potential of high interfacial density. We hypothesize that the special morphology of the low angle deposited samples may favor the creation of certain crystal defects at the interface of phases and thus account for the enhanced photoactivity of the films.

A closer look at this highly reactive mixed phase sputtered film was made using TEM. The high resolution images of film nanostructures were obtained with Transmission Electron Microscopy (Hitachi H-8100) plan-view observation, and the selected area electron diffraction patterns of prepared films were observed using TEM (Hitachi HF-2000). Figure 4.12 shows the plan-view bright field image of the mixed-phase sputtered film. The film was composed of highly textured polycrystals with random orientations in the plane normal to the sputtering direction. Also from the diffraction pattern Figure 4.13, both

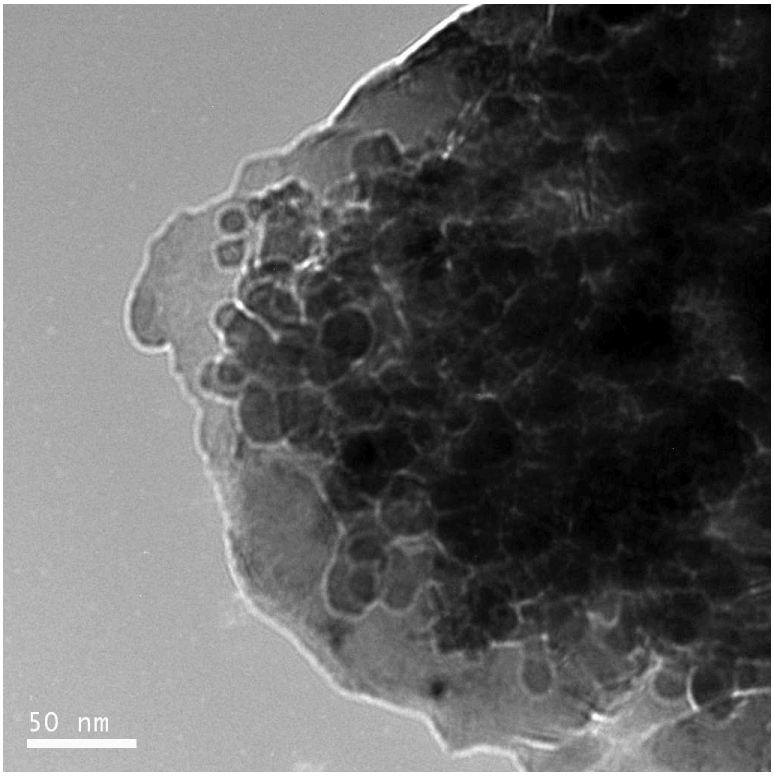

Figure 4.12. TEM plan-view image of the mixed phase film prepared by magnetron sputtering.

the anatase and the rutile diffraction patterns are identified. More diffraction patterns were obtained from random locations on the sample, and all of them had the reflections of both anatase and rutile crystals. These data provide evidence that all anatase and rutile crystals were completely mixed together, and indicate that a high density of rutile-anatase interfaces were created. These results are consistent with the hypothesis that the solid-solid interface plays a major role in promoting high photocatalytic activity of mixed phase TiO_2 materials.

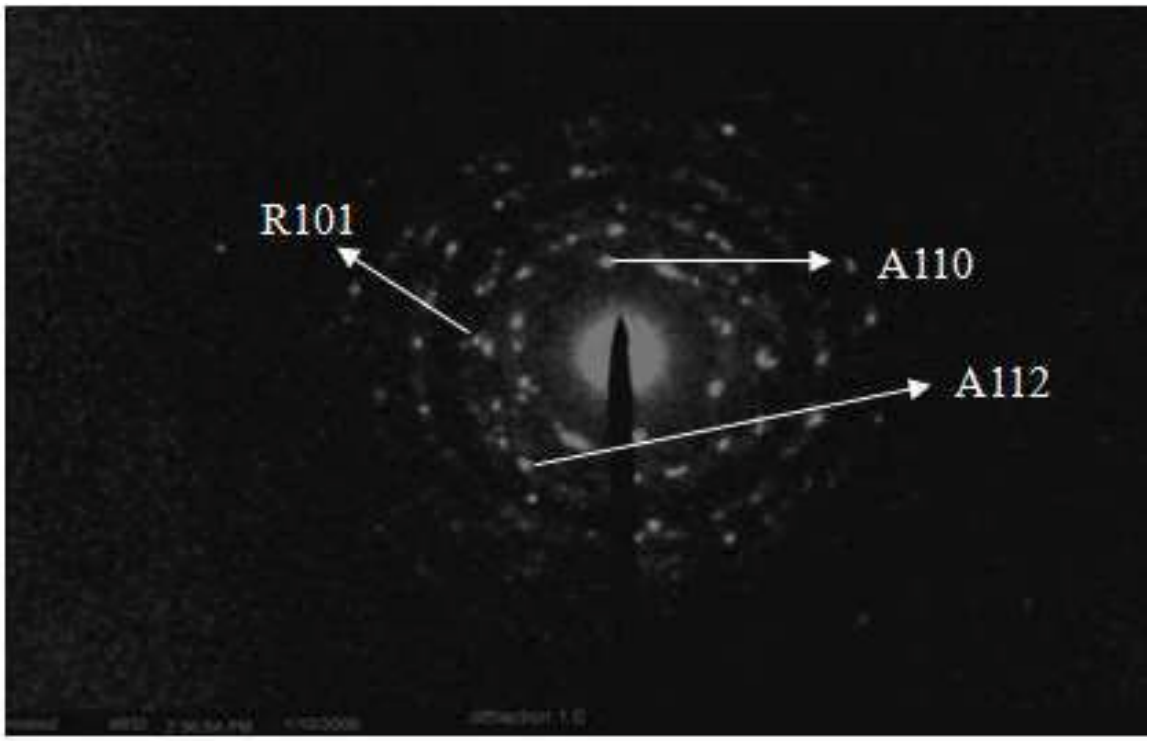

Figure 4.13. TEM plan-view selected area diffraction pattern of the sputtered mixed phase film.

4.5. Conclusions

DC magnetron sputtering was used to prepare a variety of TiO_2 films with different phase compositions on glass slides (borosilicate supports). A screening by oxidizing acetaldehyde under UV illumination was carried out to find out the most oxidatively reactive sputtered TiO_2 photo-catalysts. After comparing the different phase composition, the deposition angles and deposition time, we found out the mixed phase with 70% anatase TiO_2 deposited at the low angle showed the highest reactivity. Then, the mixed phase with 70% anatase sputtered film and a pure anatase sputtered film were compared to a 70% anatase sol-gel film, and a Degussa P25 film relative to their reactivities in degrading acetaldehyde. The sputtered mixed phase film proved to be far superior to the other films

as measured by the decay rate and extent of oxidation with acetaldehyde. For example, the 70% anatase sputtered film displayed up to 55% C_0 for the first 5 mins and a total 90% C_0 degradation after 45 mins while the 70% anatase Degussa P25 coated film was only able degrade 20% C_0 for the first 5 mins and a total 35% C_0 degradation after 45 mins. From AFM and SEM observations, columnar structures characterized the sputtered films. TEM gave proof of well mixed and crystallized anatase and rutile structures, uniformly distributed. This confirms the existence of abundant anatase-rutile interfaces which play an important role in photocatalytic performance of the films. The sputtered films' special characteristics may contain the structural defects that serve as active sites and that account for the superior performance, compared to sol-gel films and Degussa P25 films.

In the following chapters, I will not only demonstrate the reductive photoactivity of sputtered mixed phase TiO_2, but also further characterize the solid-solid interfaces and the interfacial defects served as reactive sites to explore the potential of the titania based nanocomposites for enhanced reactivity and red-shifted photoresponse.

CHAPTER 5

Reducing Carbon Dioxide by Sputtered Mixed Phase TiO_2 under UV and Visible Illuminations

Previous chapters demonstrated the feasibility of fabricating highly active sputtered mixed phase films and illustrated the relationships among fabrication, structure and function for acetaldehyde oxidation. In this chapter, I present results from the the study of the reductive photo-activity of sputtered mixed phase TiO_2 to further explore the relationship among fabrication, structure and function for reductive chemistry. In addition, I attempt to characterize the reactive interfacial sites so that I can tailor the fabrication and structure for enhanced photoactivity under the visible conditions which will be described in the next chapter.

The mechanism and significance of carbon dioxide reduction by TiO_2 to produce fuels was described in the second chapter. In short, this application provides a way to convert solar energy to storable and carbon-neutral chemical energy. Consequently, it is critical to extend the photo-response of the TiO_2 based photocatalysts into the visible range for more efficient solar energy harvesting. This chapter explores the feasibility of using visible light to initiate the catalytic reaction.

5.1. Experiment details

5.1.1. Sample preparation

We installed a new Ti target at the time we started this part of research. The oxidation status and the area of the sputtering region relative to the substrate are somewhat different between an old and a brand new target. Thus, the sputtering conditions needed to be modified slightly to fabricate titania thin films with phase compositions similar to previous work. The new target was 99.95% pure titanium. I continued to use glass slides as substrates.

To determine the influence of total pressure on TiO_2 phase composition, two levels were used in this study: 0.35 Pa for rutile or rutile-dominant mixed phase films and 0.5 Pa for anatase or anatase-dominant mixed phase films. The partial pressure of oxygen remained constant at 0.1 Pa in the transition mode. The sputtering power levels were varied from 4.7 kW to 5.5 kW to cover the transition from anatase to rutile-dominant films. Higher power levels promoted the formation of the rutile phase. An RF substrate bias (-100 volts) was also applied as an extra energy input to foster the growth of rutile. We used a stationary mode to control the deposition angles in order to study the influence of deposition angle on film structure and morphology. Based on earlier work, low angle (around 30 degrees and film thickness averaged about 400-500 nm) and normal-angle deposition (film thickness was about 800-1000 nm), as illustrated in Figure 3.5 were chosen for the sputtering process. Table 5.1 lists the sputtering parameters for different phase compositions. A mixed-phase TiO_2 thin film was also prepared from Degussa P25 by dip-coating [101] on glass slides and was used as a reference for photoactivity comparison.

Films	**Deposition angle**	**Target power and substrate bias**	**Total pressure**
Anatase	Low angle (Fig 3.5a)	4.7 kw power	0.5 pa
Rutile	Low angle	5.5 kw power and -100 V bias	0.35 pa
Mixed phase (70%anatase)	Low angle	5.3 kw power and -70 V bias	0.45 pa
Mixed phase (70%rutile)	Low angle	5.4 kw power and -90 V bias	0.4 pa

Table 5.1. Modified Sputtering Conditions

We repeated the sputtering deposition on cleaned Al foil substrates and dissolved the Al substrate in HCl solution without altering the film structures. Then, the collected films were ground into powders. This allowed us to prepare sputtered powders for Electron Paramagnetic Resonance (EPR) analysis.

5.1.2. Structural characterization

5.1.2.1 XRD

The crystalline phase composition of the prepared samples was determined by XRD (Rigaku) using Cu-Kα radiation operated at 40 kV-200 mA. The ratio of peak areas of the different phases was interpreted as the weight percentage of different phases of the films [163].

5.1.2.2 SEM and AFM

Observation of surface morphology and the quantitative analysis of surface area of the films were determined by SEM (LEO Gemini 1525) and AFM (JSPM-5200), respectively.

5.1.2.3 TEM

The high resolution images of cross-section of the film nanostructures were obtained with TEM (Hitachi HF-2000). The preparation of cross-section TEM samples was introduced in the Chapter 4.

5.1.2.4 UV-Visible Spectroscopy

UV-Vis spectroscopy is routinely used in the quantitative determination of solutions of transition metal ions and highly conjugated organic compounds [80, 50, 22] by measuring the solution's absorbance. In this study, the UV-Vis spectroscopy (Hitachi U-2000) was used to characterize the optical properties of TiO_2 photo-catalysts by simply scanning the films to obtain their UV-Vis spectra. Since the films were deposited on glass slides instead of in solution form, it would be difficult to measure the photo-response of the films accurately. However, it can still be used for qualitatively comparing different films on the same substrates.

5.1.2.5 Electron Paramagnetic Resonance

Electron Paramagnetic Resonance (EPR) is a spectroscopic technique that detects chemical species that have unpaired electrons. A great number of materials contain such paramagnetic entities, which may occur either as electrons in unfilled conduction bands, or as free radicals, various transition ions, bi-radicals, triplet states, impurities in semi-conductors. By application of a strong magnetic field (B) to material containing paramagnetic species, the individual magnetic moment arising via the electron spin of the unpaired electron can be oriented either parallel ($M_s = 1/2$) or anti-parallel ($M_s = -1/2$) to the applied field.

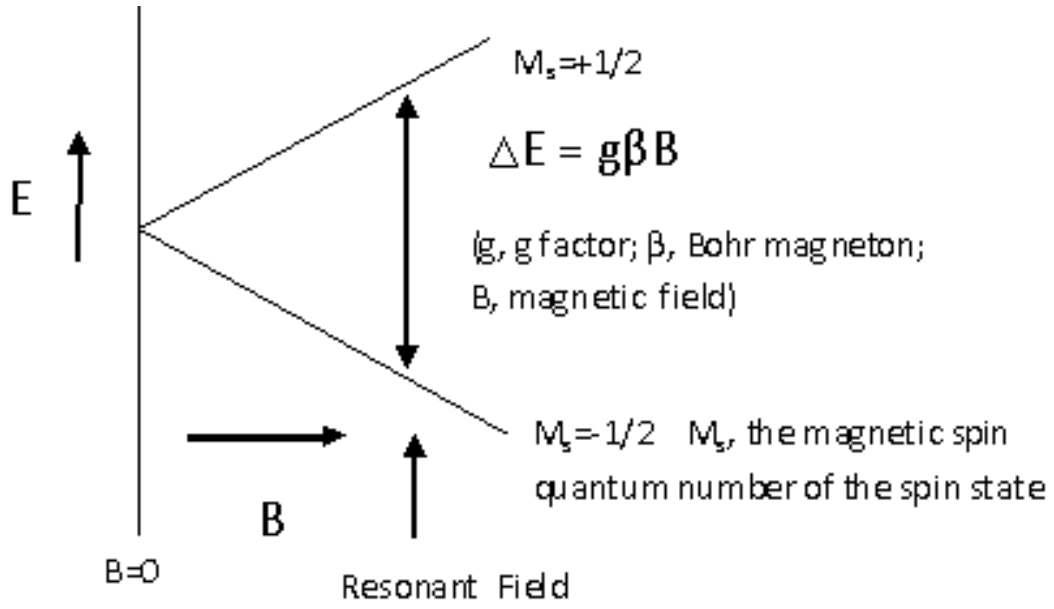

Figure 5.1. Energy-level diagram for two spin states as a function of applied Field, B.

This creates distinct energy levels for the unpaired electrons (ΔE, illustrated in Figure 5.1), making it possible for net absorption of electromagnetic radiation (in the form of microwaves) to occur. The situation, referred to as the resonance condition, takes place when the magnetic field and the microwave frequency are matched (i.e., the energy of the microwaves corresponds to the energy difference of the pair of involved spin states)[185].

EPR is a highly sensitive technique that is very suitable to study photo-initiated charge pair separation, trapping, recombination and reactions with organic substrates. Using EPR, the surface and lattice trapping sites can be identified for both electrons and holes. Additionally, by working at low temperatures the migration between these sites can be monitored.

The electronic structure of each paramagnetic center can be characterized by 'the g-factor' (Lande splitting energy), defines the field position of an EPR signal. The g-factor is determined by measuring the field and the frequency at which resonance occurs ($g=\Delta E/(\beta B)=h\nu/(\beta B)$, ν is the frequency of the electromagnetic radiation applied perpendicular to the field B). The g-factors resembles the 'finger prints' and are characteristic of atomic or molecular states of free radicals or other paramagnetic species.

In Hurum and Li's work [66, 68, 65, 101], EPR was used to folow the charge formation, separation, trapping, transfer and recombination at the solid-solid interface for Degussa P25. Since the fabrication methods are different for Degussa P25 and sputtered TiO_2, the solid-solid interfaces in sputtered TiO_2 are likely to vary structurally and quantitatively. The EPR method is proposed here to characterize the solid-solid interface and to explore electron and hole behavior in sputtered mixed phase TiO_2.

The EPR characterization was carried out by Dr. Gonghu Li and collaborators in Argonne National Lab.

5.1.3. CO_2 photoreduction test

The sputtered TiO_2 thin films were used to photoreduce CO_2 to methane or methanol in a gas phase batch reactor system (Figure 5.2). The system consisted of a square Teflon™ container connected to a circulating pump, injection port, and pretreatment equipment. The pretreatment procedure included evacuating O_2 by flowing CO_2 and nitrogen with water vapor over the film surface for 45 mins; water in the system served as a hole scavenger. Typically, much stronger hole scavengers, such as isopropanol, are employed in other studies [177, 13], and initially, we also used isopropanol. However, we conducted

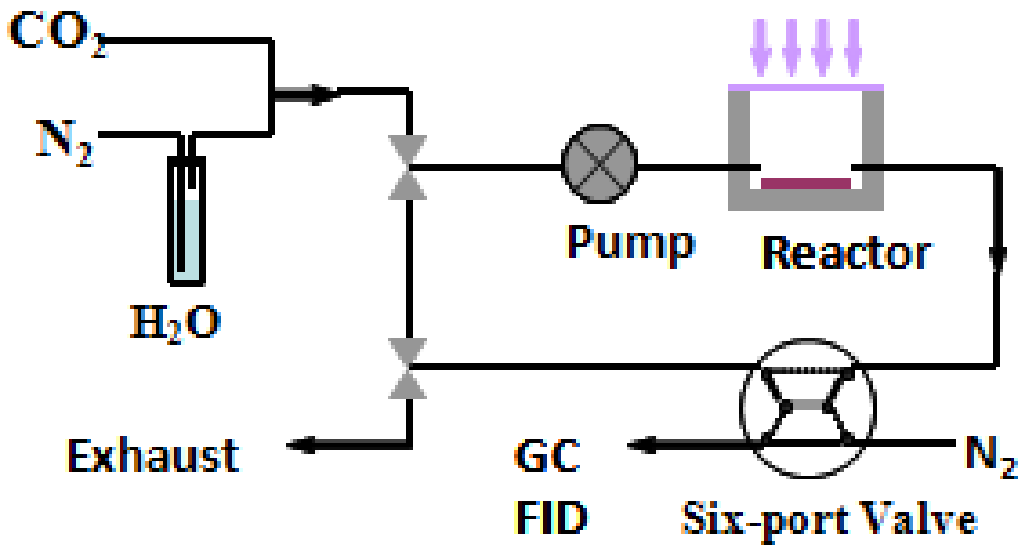

Figure 5.2. Schematic illustration of the batch reactor system for the CO_2 photoreduction test.

a series of experiments with only CO_2 and water. A 1-inch square glass slide covered with TiO_2 was placed at the bottom of the Teflon TM container, which was covered by a UV light filter (cut off at 400nm). The system was illuminated from above with either UV or visible light. The UV lamp was a mercury vapor UV lamp (100W), providing an energy density of $\sim$21.7mW/cm^2. The visible lamp was a solar light lamp (SVLVANIA, 20W) (full solar spectrum). An HP 5890 gas chromatograph equipped with a flame ionization detector (FID) monitored the products of CO_2 photoreduction.

Optimization of reaction conditions was carried out after we determined the feasibility of CO_2 photoreduction and identified the sample with the best photoactivity. First, we pretreated samples by thermal evacuation under helium flow and oxidation at 300°C (without causing phase transition) to vacate the surface and trapping sites [11]. Then, we investigated the effects of three factors in order to optimize the reaction conditions:

reaction temperature, CO_2 concentration, and reaction volume (amount of reactive gases). In addition to the room temperature, high level of temperature was achieved by by placing the reactor on a hot plate, heated to around 80°C. CO_2 partial pressure was tested at low (around 0.06-0.08 atm) and high (around 0.45-0.5 atm) levels, and was monitored using the GC with thermal conductivity detection (TCD). The volume was increased using a gas bottle (70 ml) attached to the reaction system (50 ml) as a way to increase the total mass in the system.

5.2. Results and Discussions

5.2.1. The reductive photo-activity of sputtered TiO_2 films with different phase compositions

The phase composition has been characterized by XRD and was discussed in the previous chapters. Similar to the mixed films deposited by the older target, the films deposited with the new target showed rutile crystallites about 10-15 nm in diameter and much larger anatase crystallites size with a diameter of 20-40 nm.

The photoreduction of CO_2 was compared for five films in the batch reactor (Figure 5.3): four magnetron sputtered samples (pure anatase, pure rutile, and two mixed phase deposited at different angles), and one P25 sample. All the mixed phase samples including Degussa P25, were composed of approximately 70% anatase and 30% rutile (Figure 5.3). In order to correct for the effect of varying surface area, the surface area of the most reactive sample, the low angle 70% anatase sputtered sample (curve (1) in Figure 5.3) was set as a standard and all other films' surface areas were normalized to the standard. Exposed surface areas were measured by AFM.

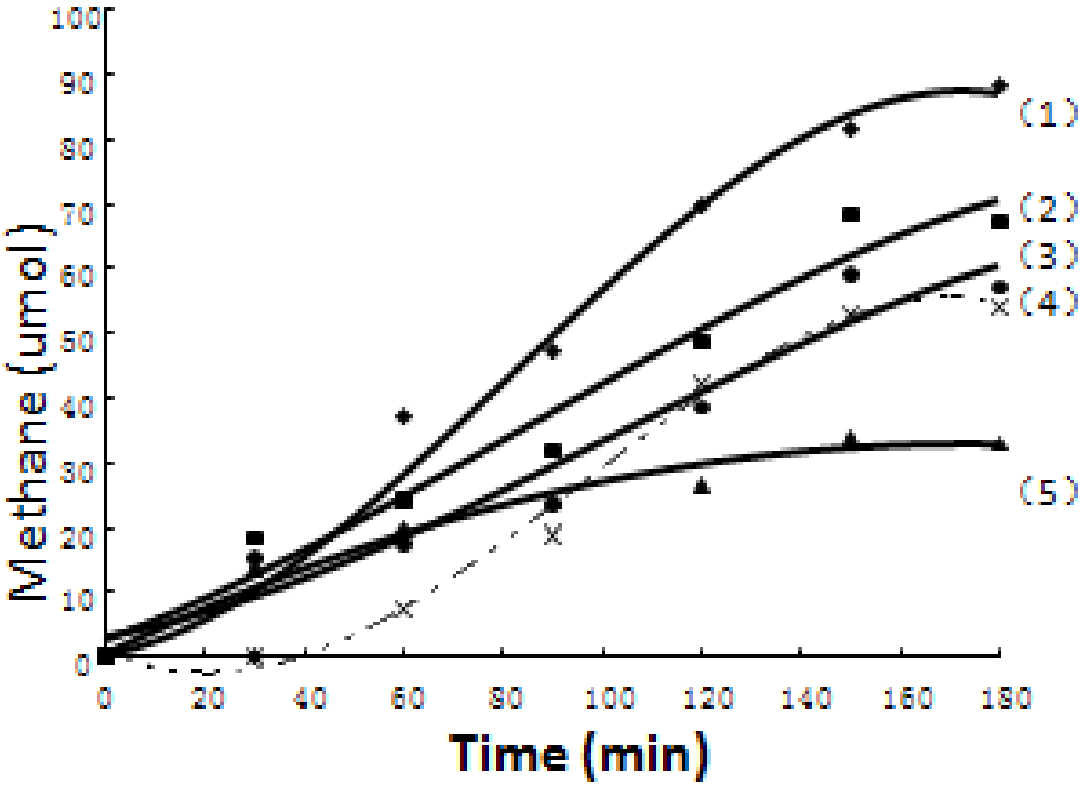

Figure 5.3. Production of methane from CO_2 reduction by various samples normalized by the surface areas of the films under UV light and with isopropanol added. The average error of the results is approximately 5-10%. The surface area here is expressed as the ratio of the measured surface area to the nominal or projected area. (1) mixed phase magnetron sputtered film (70% anatase, low angle) ($1.12\mu m^2/\mu m^2$); (2) mixed phase magnetron sputtered film (70% anatase, high angle) ($1.085\mu m^2/\mu m^2$); (3) anatase, magnetron sputtered film ($1.10\mu m^2/\mu m^2$, low angle); (4) P25, dip-coated film (at least $2.26\mu m^2/\mu m^2$); (5) rutile magnetron sputtered film ($1.09\mu m^2/\mu m^2$).

The main product detected and measured from the reaction of each film was methane. We also detected trace amounts of methanol but the concentrations were too low to quantify. Figure 5.3 compares the methane production from CO_2 reduction for the five samples under UV exposure and in the presence of isopropanol. We chose the initial

reaction conditions (room temperature, CO_2 to water ratio approximately 3:1) based on the existing experimental set-up and the literature. The results showed that sputtered films, especially the mixed phase composition created at low deposition angle (Film (1)), had the best overall photocatalytic performance with the highest methane yield, about 88 μmol which is approximately 1.7 times of P25's methane yield. The CO_2 conversion was around 5% according to TCD measurement. All the sputtered films (Film (1), (2), (3) and (5))had similar initial rates (0.3-0.4μmol methane/min) over the first 30 minutes. In comparison, the P25 sample shows a lag in methane production in the early stage and does not have detectable methane for the first 30 mins which might imply a different CO_2 adsorption and reaction mechanisms from sputtered films. All the mixed phase samples displayed greater extension rates of reaction (0.4 μmol methane/min for low angle mixed phase film and 0.37 μmol methane/min for high angle mixed phase film) compared to single phase samples (0.28 μmol methane/min for anatase and 0.14 μmol methane/min for rutile). In addition, at the same phase composition, the low angle deposited film (88 μmol total methane yield at 180 mins) displayed higher (about 30%) activity than the films deposited at a normal sputtering angle (65 μmol total methane yield at 180 mins). The pure phase rutile film displayed the lowest methane yield. Typically rutile is considered inactive except in the presence of scavengers. The difference in activity for low angle and normal angle films may be explained by the differences in the surface structures which were pointed out in the previous chapter, and will be further discussed later in the chapter. These trends in CO_2 reaction are consistent with previous observations concerning the degradation of acetaldehyde, indicating that mixed phase sputtered TiO_2 films have enhanced reactivity for both oxidation and reduction reactions. Although the

Experiment	CO_2 partial pressure	Temperature	Extra volume
Exp.1	low (Approx 0.08 atm)	room temperature	no, reactor volume:50 ml
Exp.2	high (Approx 0.45 atm)	80°C	no, reactor volume:50 ml
Exp.3	low (Approx 0.06 atm)	80°C	yes, reactor volume:120 ml
Exp.4	high (Approx 0.49 atm)	room temperature	yes, reactor volume:120 ml

Table 5.2. fractional factorial experiment of the reaction optimization

mixed phase P25 films had relatively slow initial rates, they displayed an extent of reaction comparable to the pure phase anatase film.

We also sought to optimize the reaction conditions for greater CO_2 conversion. The optimization was carried out with the most reactive, low angle deposited mixed-phase sputtered sample under UV illumination. A fractional factorial experimental design was used to compare the effects of temperature, reactor volume and CO_2 partial pressure on methane production (Table 5.2). As shown in Figure 5.3, very high methane yields were produced under the optimal combination of high CO_2 partial pressure (approximate 0.45 atm) and elevated temperature (approximately 80°C) without extra volume (Exp.2). In contrast, much less methane was produced for Exp. 3 (low CO_2 partial pressure and elevated temperature) as well as Exp.2 and Exp. 4 (both have high CO_2 partial pressure and room temperature). These results indicate that there is a synergistic effect between CO_2 concentration and temperature. At the end of the reactivity test, the CO_2 conversion was 12% calculated from Thermal Conductivity Detection (TCD) measurement based on directly measuring CO_2 concentration in comparison to 5% CO_2 conversion before optimization. This finding concurs with literature reports that elevated reaction temperature

increases the reaction efficiency. The addition of heat also caused the production of several other hydrocarbons, albeit at small yields. The products have been identified as C_2H_6 and C_3H_8, and possibly C_2H_4 and C_3H_6, in addition to methane. The ratio of water vapor to carbon dioxide is very critical to the reaction as well [11, 79]. In our current reaction system which is under atmospheric pressure and ambient temperature (only the reactor container could be heated), the water vapor concentration which is dependant on carrier gas (nitrogen) partial pressure (assuming X atm, X<1), was relatively low and could not be adjusted independent of CO_2 partial pressure ((1-X)atm). Thus, the ratio of water vapor to CO_2 (about 1:10 in this experiment) was reflected by CO_2 concentration in this study. Further modification of the reactor system will be necessary to be able to separately control the water vapor while keeping CO_2 concentration constant.

5.2.2. Structural characterization

I chose the most reactive low angle deposited mixed phase sputtered film for SEM imaging. The mixed phase films deposited under low angle conditions display a columnar structure and scale-like surface texture (Figure 5.5(a) from sputtered titiaia film on glass substrate and 5.5(b) from sputtered titania film pieces without substrate used for EPR characterization). In the previous chapter (Chapter 4), We showed that this unique structure is associated with high photocatalytic oxidative activity. The cross section images from both SEM (Figure 5.5(c)) and TEM (Figure 5.6) show the side profiles of the column bundles (about 100-300 nm in diameter) growing close together at an angle of about 45° to the substrate. These larger bundles are made up of anatase and rutile crystals (10-40 nm). Overall then, these films exhibited a dual-scale interfacial structure, between anatase and

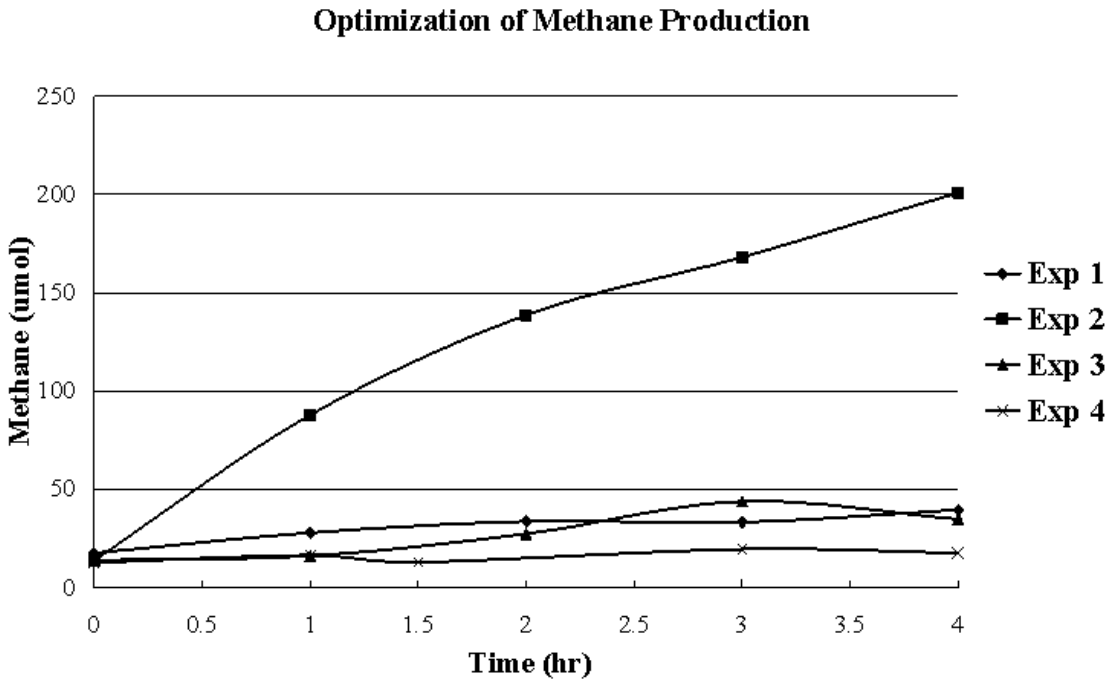

Figure 5.4. The results of optimizing reaction conditions (on mixed sputtered low angle film under UV condition) by fractional factorial designed experiment. Exp 1: Low CO_2 Concentration (Approx 8% vol), Room Temperature, No Extra Volume; Exp 2: High CO_2 Concentration (Approx 45% vol), Heated Reactor (Hot Plate Temperature was approx 80°C), No Extra Volume; Exp 3: Low CO_2 Concentration (Approx 6% vol), Heated Reactor (Hot Plate Temperature was approx 80°C), Extra Volume; Exp 4: High CO_2 Concentration (Approx 49% vol), Room Temperature, Extra Volume

rutle crystals and between bundles, that is perhaps of a different nature. The arrangement of the crystals within the bundles is not resolved in this image or in any other image we have seen. Based on the tendency of the films to exhibit columnar growth, we propose that the crystals are also arranged nano columns that then form large bundles.

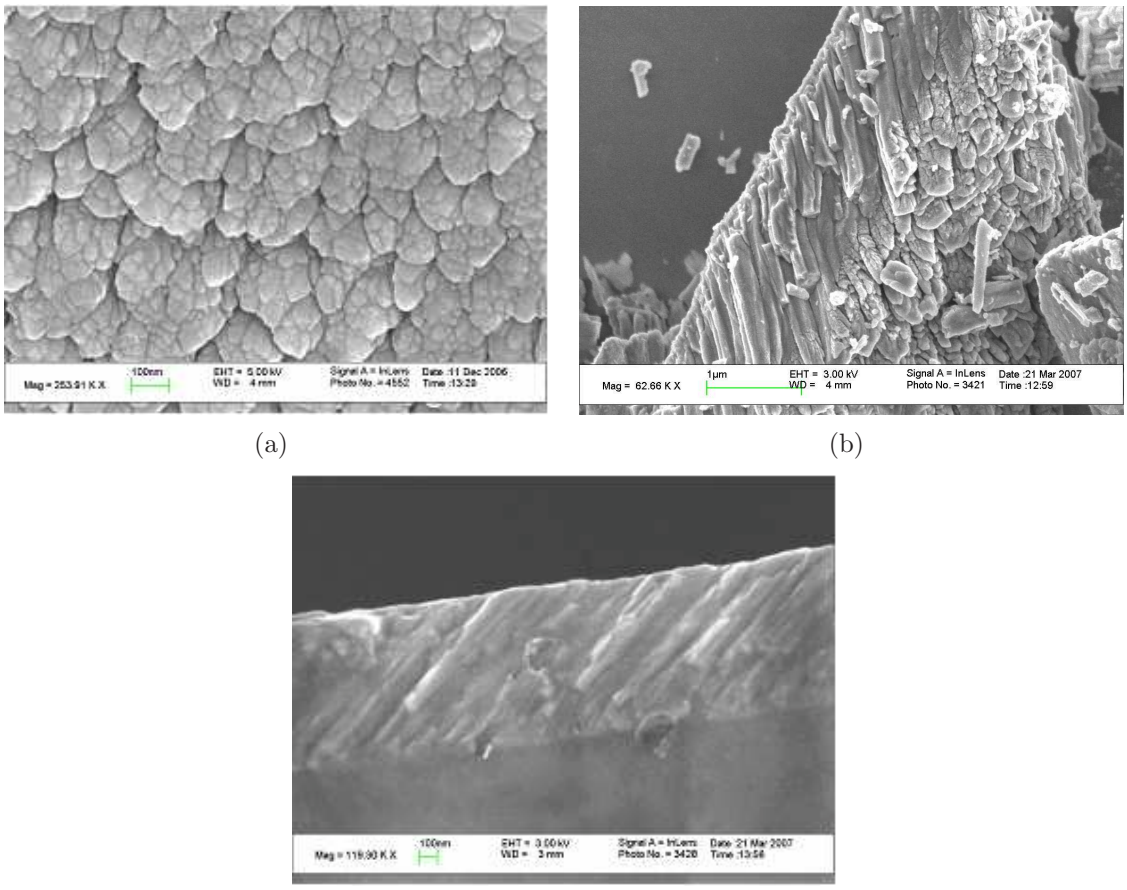

(a) (b)

(c)

Figure 5.5. SEM (LEO Gemini 1525) images for low angle mixed phase TiO_2 films. a) Plain-view of small crystals within columns; b) Small sputtered film piece (no substrate) c) Cross section of the film composed of column bundles grown at certain angle.

5.2.3. Visible light photo-response

We hypothesized that mixed-phase TiO_2 photocatalysts with a high density of reactive interfacial sites will display enhanced photoactivity. In addition , the presence of rutile has the added benefit of slightly shifting the photoresponse to longer wavelengths. We

Figure 5.6. TEM cross section image for low angle mixed phase TiO_2 films.

compare the spectral characteristics of our low angle sputtered mixed phase films with mixed phase P25.

Figure 5.7 shows the UV-Visible absorption edges for the sputtered mixed phase film in comparison with P25. A strong red shift is observed in the low angle sputtered mixed phase film.

Figure 5.8 shows that the low-angle-deposited mixed-phase TiO_2 film was able to reduce CO_2 under visible light with only water serving as the oxidant. Under these conditions of lower light intensity and energy as well as no additional hole scavenger, however, the methane yield was merely 1/10 of that produced under UV illumination in the presence of a hole scavenger. In contrast, P25 showed no detectable photoactivity under these conditions without an additional hole scavenger other than water. Since the light absorption range (up to 550 nm wavelength) of the mixed phase sputtered sample

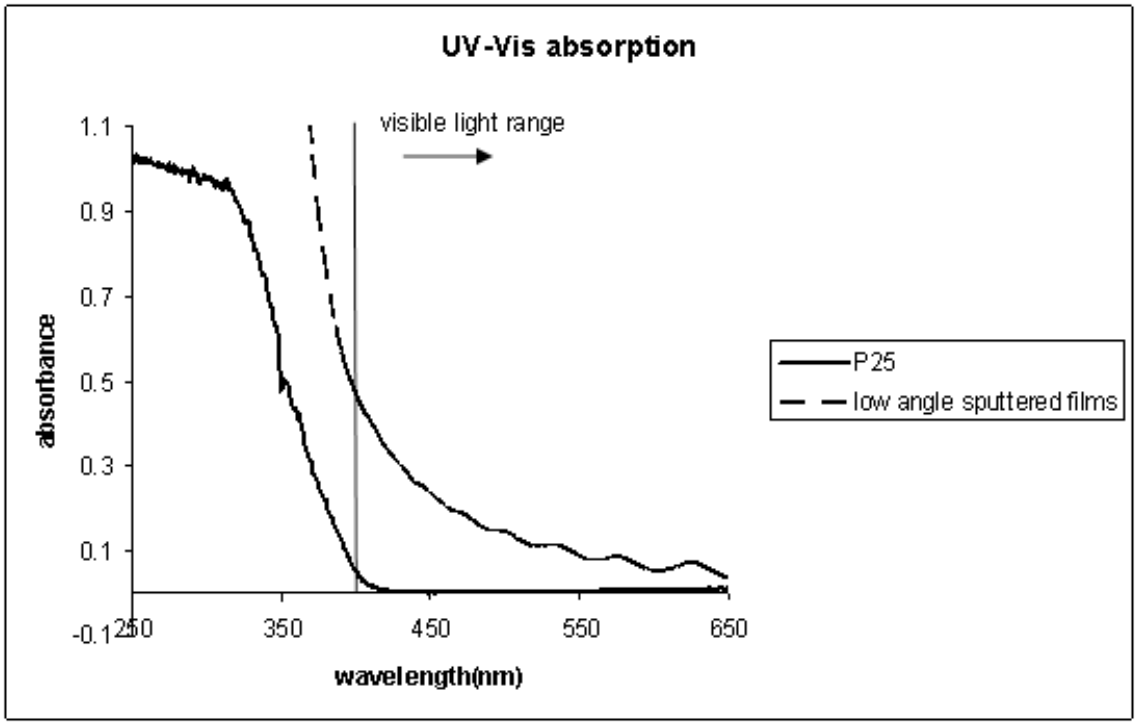

Figure 5.7. UV-Visible absorption spectra of mixed phase low angle sputtered TiO_2 and P25 films.

far exceeded that of rutile (around 410 nm in wavelength), the sputtering process creates other color centers or surface states that cause the strong red shift.

Figure 5.9 [101] compares the EPR spectra of sputtered titaina films, sol-gel titania and P25 (all of them are mixed phase samples with about 70% anatase) under UV/Vis conditions. In the absence of oxygen, electrons trapped by anatase (g of the trapping sites is 1.995) and rutile (g of the trapping sites is 1.977) can be clearly identified for Degussa P25 and the solgel sample. The EPR spectrum of the sputtered titania film, however, shows a small and broad signal of trapped electrons, suggesting that the domain of crystallinity is small. In addition to the hole signals which are characterized around g = 2.016, there is a strong resonance with a g factor at 2.0065, possibly an axially symmetric

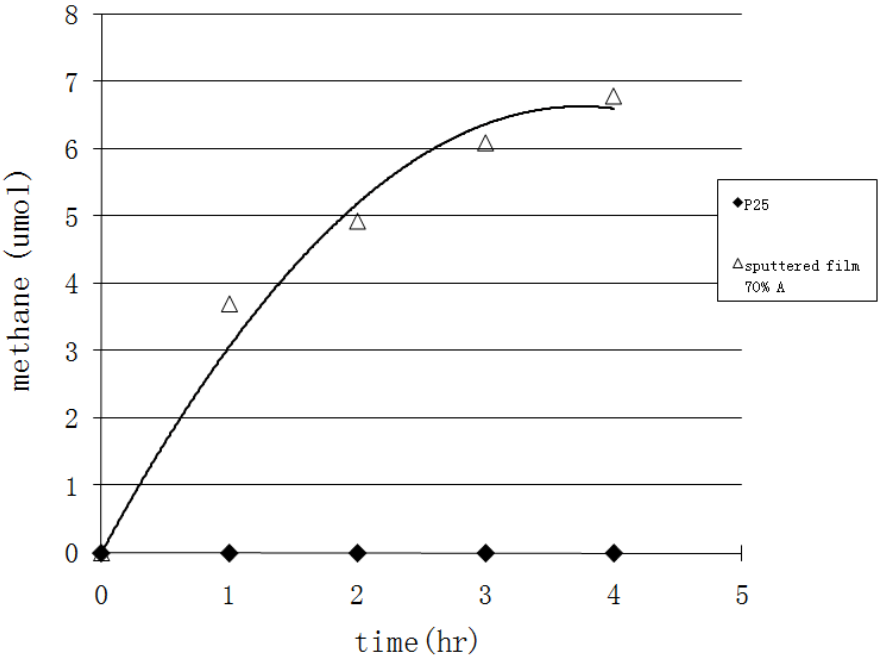

Figure 5.8. Production of methane from CO_2 reduction by mixed phase magnetron sputtered film (70% anatase, low angle) and dip-coated P25 film under solar lamp without isopropanol.

signal within the anatase interior, is prominent for the sputtered titania sample. The reduced crystallinity may be the consequence of a high proportion of interfacial area relative to the anatase and rutile nanocrystalline areas which was shown by TEM selected area X-ray pattens from the previous chapter. These data are a preliminary indication that the sputtered materials contain a different population of trapping sites in comparison to Degussa P25 and the solgel sample [101].

Due to the small mass and crystallinity, the sputtered thin films were largely limited from the further characterization by EPR. Thus, we gathered sputtered film pieces (the preparation methods were described in the 'Experiment' section) and ground them into powders. Figure 5.10 shows the EPR signature of sputtered powder samples under dark

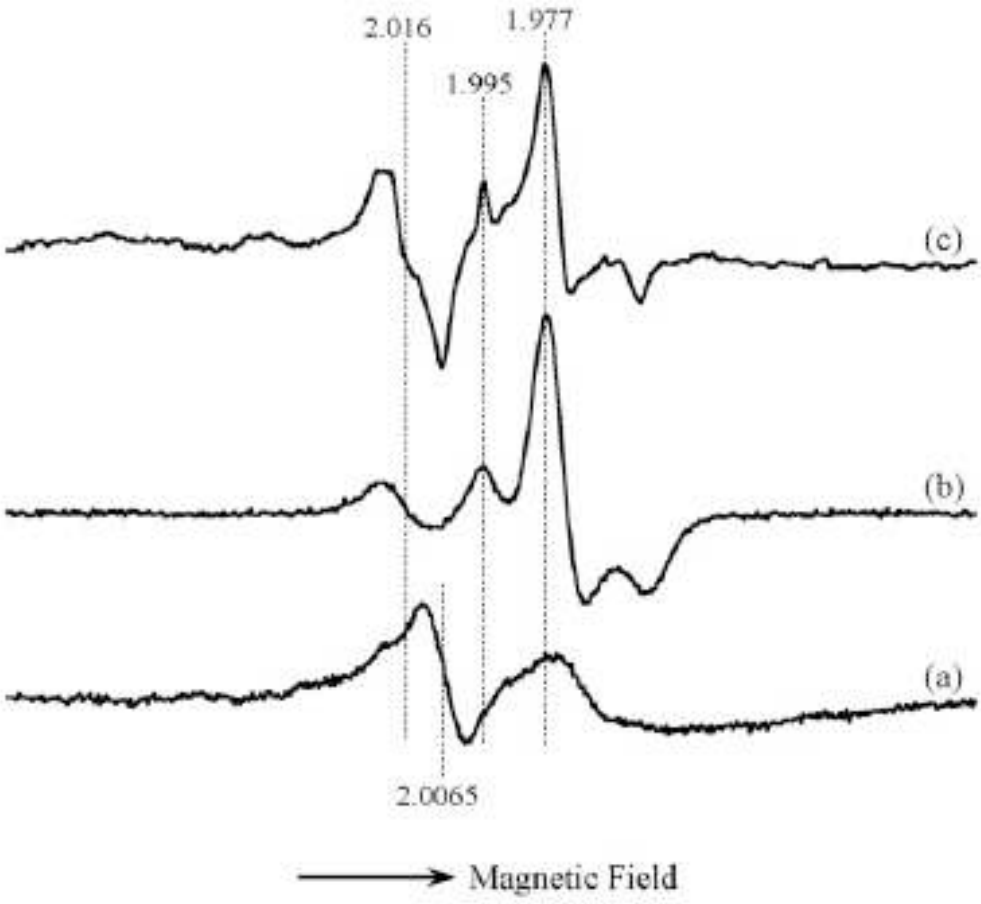

Figure 5.9. EPR spectra of different titania samples under UV/visible light illumination: (a) a mixed phase titania thin film prepared by magnetron sputtering, (b) a mixed phase titania in powder form prepared by a modified sol-gel method, and (c) Degussa P25. Background signal in dark was subtracted from the corresponding spectrum. The mixed phase titania samples have phase compositions similar to that of Degussa P25 [101].

conditions. The EPR spectrum of Ti_2O_3 shows a strong resonance at g = 1.97 characteristic of paramagnetic Ti^{3+} sites. Although the sputtered powder sample is greyish in comparison to the black Ti_2O_3, the EPR signatures of the two powder samples are very similar to one another. This indicates the existence of a significant amount of partially

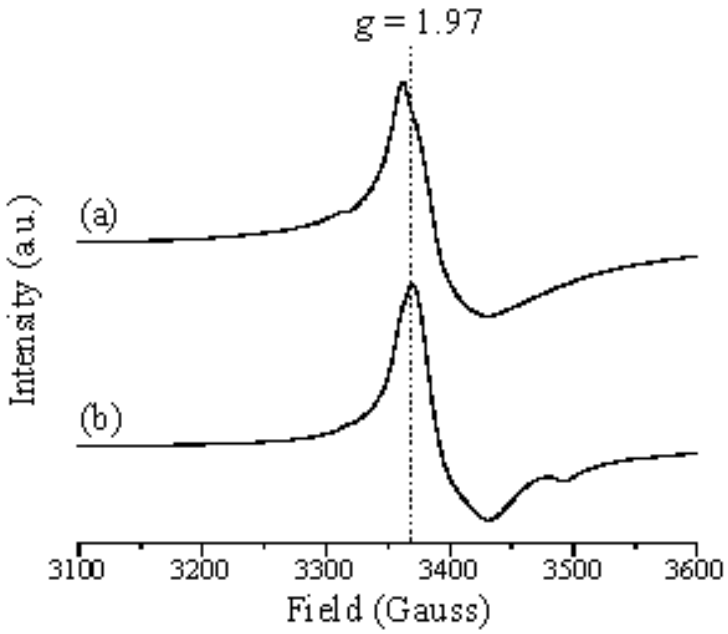

Figure 5.10. X-band EPR spectra of (a) sputtered powder sample and (b) Ti_2O_3. The spectra were recorded in dark at 4.5 K. The resonance characteristic of Ti^{3+} at g = 1.97 is labeled.

oxidized Ti in the sputtered powder sample bulk, whereas XRD patterns of the films' surface and top layers are consistent with mixed phase TiO_2. Oxygen vacancies are commonly observed in the sputter deposition of metal oxides. Some studies have pointed out that non-stoichiometry may account for the visible-light response of the deposited materials [75, 92], which is consistent with our activity test and optical measurement.

Figure 5.11 shows the CO_2 reduction results for the powders made from sputtered films with different annealing temperatures, commercial Ti_2O_3 powders as well as P25 powders. Although my sputtered powder samples (Sample (4)) show a spectrum similiar to that of Ti_2O_3, they display a much enhanced photo-activity in comparison to Ti_2O_3 (Sample (2))

(Figure 5.11). All of the powder samples were weighed for 0.05g and then dip-coated over glass slides respectively. The CO_2 reduction test was carried out under visible light condition (SVLVANIA, 20W) with water as hole-scavenger. Both of the sputtered powders and Ti_2O_3 powders underwent some annealing treatments in the air ambient. P25 (Sample (1)), again, did not show detectable activity in the reaction. In addition to the activity difference between the sputtered powders and the Ti_2O_3 powders, annealing also showed marked influence on the photo-reduction performances of powder samples. Both sputtered powders (Sample (6)) and Ti_2O_3 powders (Sample (3)) showed almost doubled methane yield after annealing at 723K (under 773K to avoid phase transformation) and 773K respectively. However, the sputtered powders annealed at 873K (Sample (5)), a higher temperature, showed a significant phase transformation from mixed phase to predominantly rutile, and did not show significantly improved activity compared to the unannealed mixed phase sample. Sample 5 was only half as reactive as the mixed phase sample annealed at 723K (Sample (6)). Annealing samples which have the reduced or non-stoichiometric composition (such as sputtered powders and Ti_2O_3) in the ambient air results in the re-oxidation of the samples(the color changes from dark before annealing to light after annealing) and change of the stoichiometry, as well as the phase transformation. Phase transformation was already shown to have the influence of photo-activity from this and previous chapter (in general, reactivity: mixed phase > anatase > rutile) and should be at least partially responsible for the reactivity difference between Sample (5)(mixed phase) and Sample (6)(predominantly rutile). The role of the stoichiometry change, on the other hand, needs to be further explored.

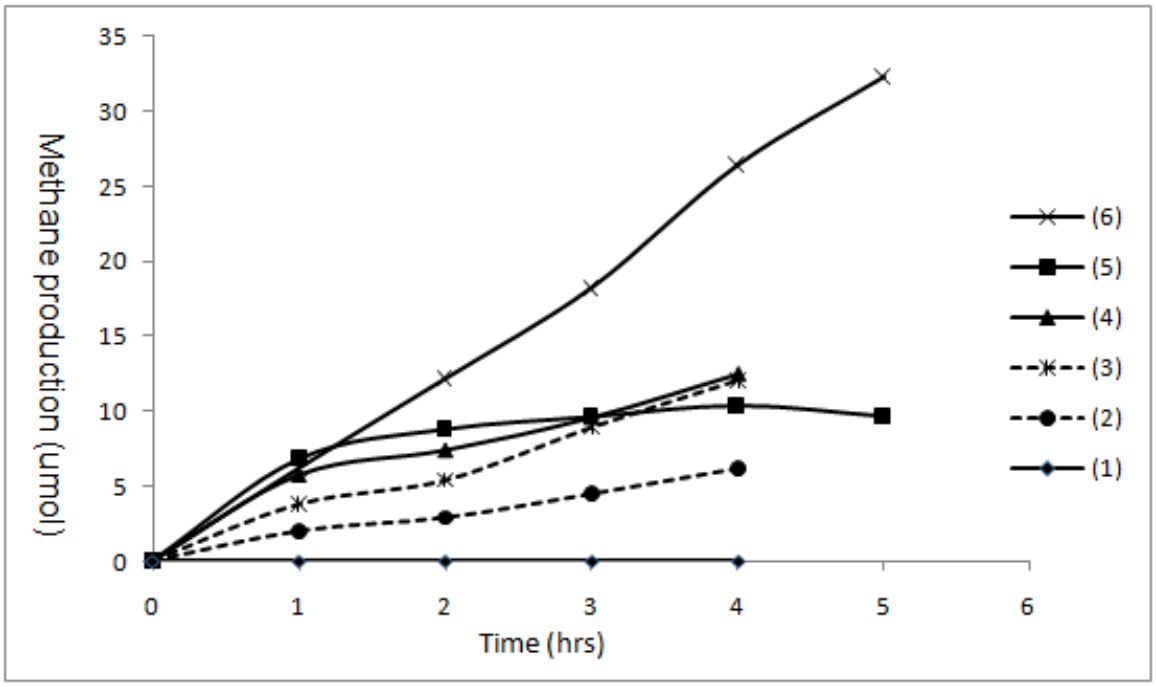

Figure 5.11. Comparison of CO_2 reduction results under visible illumination by various powder samples (0.05g/load): (1) P25 powders, white; (2) Ti_2O_3 powders, black; (3) Ti_2O_3 powders, annealed at 773K for 1 hr, brown; (4) unannealed sputtered powders, grey, 70% anatase; (5) sputtered powders, annealed at 873K for 1 hr, white, predominantly rutile; (6) sputtered powders, annealed at 723K for 1 hr, light grey, 60% anatase

5.3. Conclusions

DC magnetron sputtering was used to prepare a variety of mixed phase TiO2 films on borosilicate glass slides. A series of sputtered films prepared at different deposition angles and having different phase compositions, were compared to a P25 film in a test that measured CO2 reduction under UV or visible illumination. A sputtered mixed-phase film (70% anatase, 30% rutile), deposited at low angle proved to be far superior to the other films as measured by the initial rate and extent of reduction with CO_2. Optimization of reaction conditions was also carried out, and the coupling of elevated temperature and high

CO_2 concentration produced an approximate 12% CO_2 conversion to methane compared to an approximate 5% CO_2 conversion before optimization. The catalytic performance of sputtered films are directly associated with the film structures controlled by different fabrication conditions. From both SEM and TEM observations, we see columnar bundles of anatase/rutile nanocolumns grown in the sputtered films. This confirms the existence of a high density of anatase-rutile interfaces, which we believe are associated with the enhanced photocatalytic performance of the films. Our sputtered films also displayed an enhanced visible light response and reactivity that is consistent with non-stoichiometric, oxygen deficient features. The results of this study demonstrate the important improvements in visible light harvesting and CO_2 reduction achieved with sputtered mixed phase TiO_2 composites. By coupling these enhanced material characteristics to optimized reaction conditions, we have also improved methane yields pointing to the feasibility of solar fuel generation by sputtered films.

CHAPTER 6

Study of Non-Stoichiometric Mixed Phase Titania

Inthe previous chapters(Chapter 4 and 5), we have successfully synthesized mixed phase titania nanocomposites with high density of solid-solid interfaces by reactive direct current (DC) magnetron sputtering. They showed enhanced photo-activity in both oxidative and reductive reactions as well as red-shifted photo-response compared to pure phase titania and mixed phase titania synthesized by solvo-thermal and flame hydrolysis methods. Further characterizations revealed that there are oxygen vacancies existing in the sputtered titania films. We hypothesize that the oxygen vacancies in the mixed phase titania films give rise to a red shift of photo-response and also may create reactive sites at the solid-solid interfaces to enhance photo-activity. Since most research related to on oxygen vacancy effects has been focused on single phase TiO_2 (or even single crystal), it is interesting to explore the combined effects of oxygen vacancy and mixed phase TiO_2.

In this chapter, I am going to 1)synthesize varying degrees of non-stoichiometric titania by controlling oxygen partial pressure during the sputtering process; 2)determine how film composition and morphology changes with varying stoichiometry (or oxygen partial pressure during sputtering); and 3) characterize the structure, photoresponse and reactivity of non-stoichiometric titania regarding photocatalytic oxidation and reduction.

Modification of the synthesis process for controlling oxygen levels is also discussed in this chapter.

6.1. Experiment details

6.1.1. Sputtering non-stoichiometric mixed phase titania by monitoring oxygen partial pressure

As mentioned in Chapter 3, there are three deposition modes based on the oxidation states of the target: the oxidation mode, the transition mode and the metal mode. In the metal mode, the process is operated at low oxygen partial pressure and the target surface therefore remains metallic. However, insufficient oxygen is introduced to form the oxide (TiO_2) in this mode. In the oxidation mode, the oxygen partial pressure is much higher and stoichiometric titania film can be deposited, but the deposition of Ti is hindered and deposition rates are slowed due to the formation of an oxide layer on the target (poisoned target). In the transition mode, the process is operated between the metal mode and oxidation mode and thus, relatively high deposition rates and near stoichiometric titania can be achieved. This is also the mode in which I can synthesize varying degrees of non-stoichiometric titania.

I used oxygen partial pressure to control the fabrication of non-stoichiometric titania films. In my previous experiments, my low angle mixed phase films were prepared at an oxygen partial pressure of 0.1 pa. In this experiment, the partial pressure of oxygen was set between 0.12 pa (near the oxidation mode) to make near stoichiometric titania and 0.07 pa and less to make non-stoichiometric titania. There is an 'hysteresis' effect [162] , which can seriously affect the control of oxygen. Oxygen is known to be difficult to control in the transition mode and starts to be more and more unstable when oxygen partial pressure approaches the turning point of the transition mode and metallic mode,

which is 0.07 pa in our situation. Oxygen is stabilized again at very low partial pressure (0.035pa) in the metal mode which is too low to form titania.

From our previous experience, we discovered that adding a small amount of nitrogen during the sputtering process helped to stabilize the oxygen flow control without being incorporated into the films. Others have shown [154, 21] that gases with lower reactivity (such as nitrogen) can be mixed in to reduce the hysteresis during sputtering from the target, but they are not incorporated into the films; rather, they are replaced by the more reactive compound-forming gas (like oxygen) on the substrates when depositing films. Thus, we explored the effect of adding a minimum amount of nitrogen gas to stabilize oxygen during deposition. The sputtering power levels were varied from 4.7 kW to 5.5 kW to cover the transition from anatase to rutile-dominated films. Higher power levels promoted the formation of the rutile phase. An RF substrate bias ($-60 \sim -80$V) was also applied as an extra energy input to foster the growth of rutile. Within transition range, the oxygen partial pressure does not detectably influence the phase compositions. I used a stationary mode to control the deposition angles. Low angle (around 30 degrees, Figure 3.5a) deposition was chosen for better reactivity based on previous studies.

6.1.2. Reactivity test

6.1.2.1. Acetaldehyde oxidation

Most details about reactor and the reaction procedures are described in Chapter 4. However the reactor was not optimized and thus, the reaction proceeded too fast to explore the initial decay kinetics(Figure 4.8). I decreased the initial acetaldehyde concentration from 500 ppm to 300 ppm and increased the total reactor volume by adding an extra 30

ml glass container.

6.1.2.2. CO_2 reduction

The reactor and procedures for gas phase CO_2 reduction are described in Chapter 5. Based on prior optimization of the reaction testing procedure, we applied the following reaction conditions: 0.5 atm CO_2 partial pressure, thus CO_2: H_2O = 10:1, and reaction chamber temperature equal to 80°C. Only water was added as a hole scavenger. Since the water content cannot be controlled independently of CO_2 concentration in the reactor, the water vapor partial pressure was kept constant as approximately 0.05 atm. The system was illuminated from above with either UV or visible light. The UV lamp was a mercury vapor UV lamp (100W), providing an energy density of around 21.7 mW/cm^2. The "visible" lamp was a commercial solar light lamp (SVLVANIA, 20W) (full solar spectra). A UV cutoff (filter) of 400nm wavelength was applied to the reaction with visible illumination. An HP 5890 gas chromatograph equipped with thermal conductivity detection (TCD) and a flame ionization detector was used to monitor CO_2 and the products of CO_2.

6.1.3. Characterization

The crystalline phase composition of the prepared samples was determined by X-ray Diffraction (XRD, Rigaku) using Cu-Kα radiation operated at 40 kV-200 mA. The ratio of peak areas of the different phases was interpreted as the weight percentage of different phases of the films [193]. UV-Visible Spectroscopy (Hitachi U-2000) was used to measure the spectral characteristic of the films. Observation of surface morphology and the quantitative analysis of surface area of the films were determined by SEM (LEO Gemini

1525) and AFM (JSPM-5200). XPS (X-ray Photoelectron Spectroscopy, Omicron ESCA probe) was used to analyze the chemical nature of the surface structures. TOF-SIMS (Time-of-Flight Secondary Ion Mass Spectrometry, Physical Electronics, PHI TRIFT III) was used for the depth-profile elemental analysis of the non-stoichiometric titania films. The high resolution images of cross-section film nanostructures and the analysis of the chemical composition and the defect levels that existed in the bulk of the films was probed by EELS (Electron Energy Loss Spectroscopy) using JEOL JEM-2100F FAST TEM. Below, I briefly explain XPS, SIMS and EELS as characterization techniques.

6.1.3.1 X-ray Photoelectron Spectroscopy

X-ray photoelectron spectroscopy (XPS) is a surface (of thickness in the nanometer range) analytical technique, which is based upon the photoelectric effect. Each atom in the surface has a core electron with the characteristic binding energy that is conceptually, although not strictly, equal to the ionization energy of that electron. When an X-ray beam encounters the sample surface, the energy of the X-ray photon is adsorbed completely by the core electron of an atom. If the photon energy, $h\nu$, is large enough, the core electron will then escape from the atom and emit out of the surface. The emitted electron with the kinetic energy of E_k is referred to as the photoelectron. The binding energy of the core electron is give by the Einstein relationship:

$$E_b = h\nu - E_k - \phi.$$

Where $h\nu$ is the X-ray photon energy; E_k is the kinetic energy of photoelectron, which can be measured by the energy analyzer; and ϕ is the work function induced by the analyzer, about 4-5 eV.

The core electron of an element has a unique binding energy, which is then used as a "fingerprint". Thus, almost all elements except for hydrogen and helium can be identified by measuring the binding energy of its core electron. By measuring and comparing the binding energy of the element, the elemental composition, empirical formula, chemical state and electronic state of the elements that exist within a material are measured. Furthermore, the binding energy of core electron is very sensitive to the chemical environment of element. The same atom bonded to the different chemical species, exhibits a change in the binding energy of its core electron. The variation of binding energy results in the shift of the corresponding XPS peak, ranging from 0.1 eV to 10 eV. This effect is termed as "chemical shift", which can be applied to studying the chemical status of an element at the surface [1].

The XPS (Omicron ESCA Probe), I used for the study, provides:

- Identification of the elements and chemical status with the electronic database.
- Quantification of chemical composition.
- Destructive depth profiling using an ion gun.
- Non-destructive depth profiling by the angle-resolved analysis.
- Neutralization of surface charging with the electron flood gun.
- Automatic peak fitting and target factor analysis, depth profile calculation, as well as curve smoothing, background removing with the loaded Multipak software.

I used XPS mainly to identify the stoichiometry of sputtered titania film surfaces and detect the existence of nitrogen at the surface for the films sputtered with nitrogen addition.

6.1.3.2 Time-of-Flight Secondary Ion Mass Spectrometry

The Secondary Ion Mass Spectrometry (SIMS) is the mass spectrometry of ionized particles which are emitted from the surface when energetic primary particles bombard the surface. The pulsed primary ions with the energy of 1-25keV, typically liquid metal ions such as Ga^+, Cs^+ and O^-, are used to bombard the sample surface, causing the secondary elemental or cluster ions to be emitted from the surface. The secondary ions are then electrostatically accelerated into a field-free drift region with a nominal kinetic energy of:

$$E_K = eV_0 = \frac{m\nu^2}{2}$$

Where V_0 is the accelerating voltage, m the mass of the ion, ν the flight velocity of the ion, and e its charge. The ions with lower mass have a higher flight velocity than the ones with higher mass. Thus they will reach the secondary-ion detector earlier. As a result, the mass separation is obtained in the flight time t from the sample to the detector. A variety of mass ions are recorded by the detector with the time sequence to give the SIMS spectrum [179].

The ToF-SIMS (PHI TRIFT III, Physical Electronics) I used for my study, provides,

- Identifying the elemental composition and the chemical status near the surface (around 5 angstrom) with high sensitivity (about 1ppm) and high mass resolution (about 9000).
- Distinguishing the different isotopes of the same element.

- Imaging the topography of surface using the secondary electrons.
- Line-scanning of chemical species.
- Mapping chemical species on the submicron scale.
- Ultra-thin depth profiling.
- Database of the compound spectra.
- Identifying automatically peaks with the database of fragments

I used Tof-SIMS for the depth profiling of the non-stoichiometric titania film sputtered with nitrogen addition.

6.1.3.3 Electron Energy Loss Spectroscopy

In electron energy loss spectroscopy (EELS) a material is exposed to a beam of electrons with a known, narrow range of kinetic energies. Some of the electrons will undergo inelastic scattering, which means that they lose energy and have their paths slightly and randomly deflected. The amount of energy loss can be measured via an electron spectrometer and interpreted in terms of what caused the energy loss. Inelastic interactions include phonon excitations, inter and intra band transitions, plasmon excitations, inner shell ionizations, and Cerenkov radiation. The inner-shell ionizations are particularly useful for detecting the elemental components of a material.

EELS is frequently used in association with Transmission Electron Microscopy (TEM) or Scanning TEM (STEM). In TEM or STEM, the losses predominantly occur in the bulk of the sample, as the electron beam travels through the thin specimen to the EELS detector the other side. In surface science techniques, the electron beam is usually reflected off the surface resulting in a sharp peak corresponding to elastically scattered electrons

Films	O_2 partial pressure	N_2 partial pressure	Phase composition
Film 1-0	0.07 pa	0	70% A
Film 1-1	0.07 pa	minimum 0.0035 pa	72% A
Film 1-2	0.07 pa	0.007 pa	75% A
Film 2-0	0.08 pa	0	70% A
Film 3-1	0.05 pa	minimum 0.005 pa	75% A
Film 3-2	0.05 pa	0.01 pa	80% A
Film 4-0	0.035 pa	0	70% A
Film 5-0	0.12 pa	0	70% A

Table 6.1. Sputtered films with different stochiometry

with a number of peaks at lower energy which correspond to plasmon or other excitations [39]. I used EELS to characterize and locate the oxygen vacancies.

6.2. Results and discussions

6.2.1. Sputtered titania samples

A series of mixed phase sputtered films with different stoichiometry were prepared under low angle deposition and the influence of nitrogen addition was considered as well. The sample conditions can be seen in Table 6.1.

As illustrated in Table 6.1, films were sputtered at different levels of oxygen partial pressure ranging from near-oxidation mode to the metallic mode.

Approaching the turning point of transition mode and metallic mode where the oxygen control is unstable, the minimum nitrogen needed to stabilize the system increases as oxygen partial pressure decreases (e.g. Film 1-1 and Film 3-1). However, no nitrogen is needed after the oxygen partial pressure further decreases into metallic mode. The phase composition measured by XRD is also influenced by the trace addition of nitrogen. The percentage of anatase slightly increases with the increase of nitrogen in the reactive gasses

at low levels. The initial slight enhancement of anatase in the beginning stage of nitrogen addition could be considered the result of the improvement of the crystallinity of the mixed phase titania under growth conditions at which anatase grows faster in size. It is likely that the general adatom mobility is enhanced with low level nitrogen additions [134]. The initial slight enhancement of anatase in the beginning stage of nitrogen addition could be considered the result of the improvement of the crystallinity of the mixed phase titania under growth conditions that favor anatase stability. At much higher nitrogen partial pressure, sufficient to make nitrogen doped titania, the phase composition influence is quite different(from mixed phase to rutile) and will be discussed in the next chapter.

6.2.2. Optical measurement

The film deposited at 0.12 pa (Film 5-0) oxygen partial pressure was transparent. In general, films looked less and less transparent as the oxygen partial pressure decreased and the film deposited at 0.07 pa oxygen partial pressure (Film 1-0) looked cloudy with a grey color due to lack of overall stabilization of oxygen during the deposition process. In contrast, the film deposited at 0.07 pa oxygen partial pressure with minimum nitrogen addition (1/20 of oxygen partial pressure) for stabilization (Film 1-1) was more clear and colorless than the Film 1-0 but not as clear as Film 5-0. In addition, the films deposited in the metallic mode (e.g. 0.035 oxygen partial pressure, Film 4-0) were deep grey to black and opaque. Thus, from dark to light/transparent, the films can be listed in the following order: Film 4-0, Film 1-0, Film 1-1, Film 5-0.

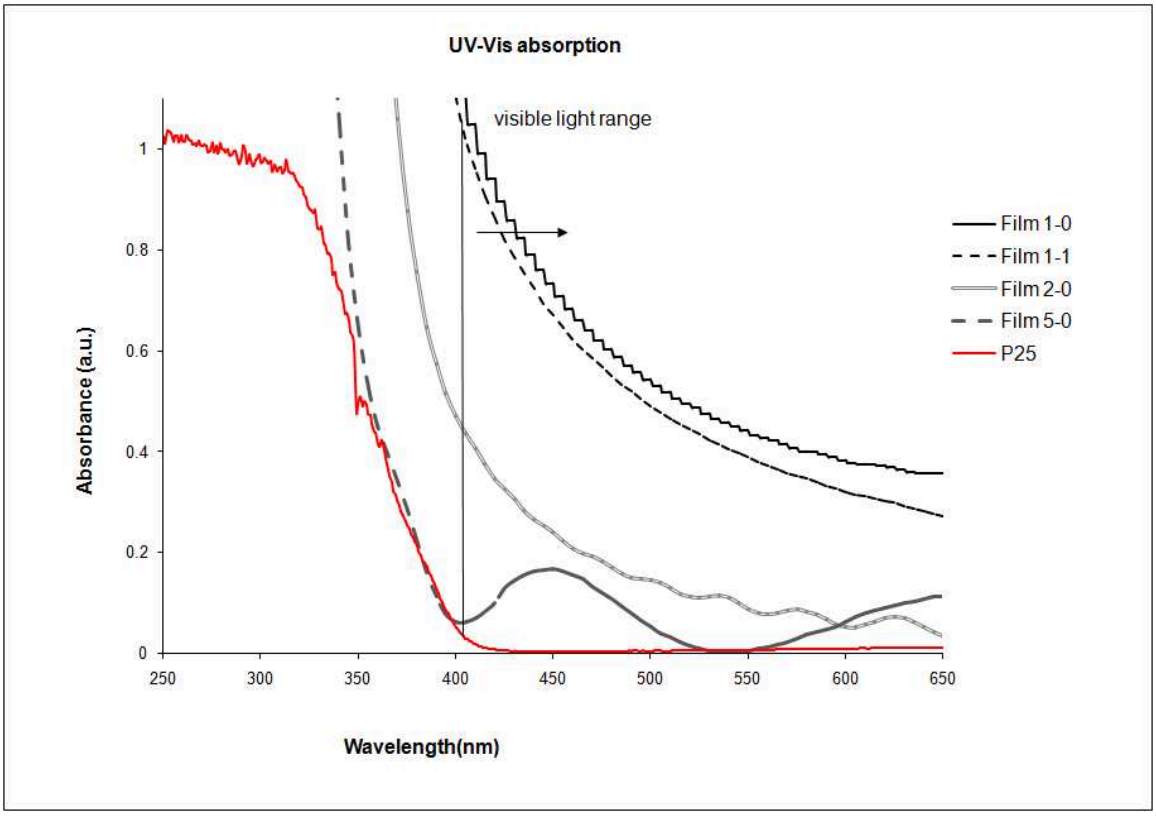

Figure 6.1. UV-Vis absorption spectra for Film 1-0: pO_2: 0.07 pa (not stable), no N_2; Film 1-1: pO_2: 0.07 pa, with minimum pN_2: 0.0035 pa; Film 2-0: pO_2: 0.08 pa (stable), no N_2; Film 5-0: pO_2: 0.12 pa and a commercial standard P25 coated film.

Figure 6.1 shows the UV-Vis absorption spectra for sputtered non-stoichiometric films deposited at different oxygen partial pressures (from 0.07 pa to 0.12 pa) and a P25 dip-coated film. The wavy absorption curves of the sputtered films in the visible range result from refraction of the films. Film 5-0 produces an absorption spectrum similar to P25 samples with onset of absorption around 400 nm. The lower the oxygen partial pressures used to make the films, the more red-shifted the films' photo-response become. On one hand, the oxygen vacancies may cause a change in the band gap and chemical structures

to produce a red-shift in the photo-response. On the other hand, due to charge compensation, they may change the valence of titanium in the lattice from Ti^{4+} to Ti^{3+} which is correlated with visible light absorption especially in the blue light range (wavelength: 450-495 nm) [40, 172] and serve as color centers [157, 152]. We suspect the oxygen vacancies have the combined influence (both creating 'color centers' and introducing intermediate band gap states to narrow band gap) on the red-shift of the sputtered non-stoichiometric titania photoresponse. In the following paragraphs, I identify Ti^{3+} by structural characterization and indirectly verify the band gap narrowing of the sputtered titania due to oxygen vacancies by carrying out reactivity test under visible light conditions.

The small input of nitrogen during sputtering did not significantly change the UV-Vis absorption spectrum of the film. Film 1-1 still showed a strong red-shift compared to the nearly stoichiometric (Film 5-0) and the P25 films, but slightly less red-shifted compared to Film 1-0 deposited under same oxygen partial pressure but without nitrogen addition. As Film 1-1 was clearer and more transparent than Film 1-0, we can attribute the slight difference of photoresponse to a decrease of color centers.

6.2.3. Photoreactivity tests

6.2.3.1 Acetaldehyde oxidation

Figure 6.2 shows the comparison of sputtered titania films with different phase compositions (pure rutile and anatase as well as 70% A mixed phase) and stoichiometry in terms of acetaldehyde oxidation under UV condition. The results are normallized by the surface areas. All the films display linear intial decay kinetics. The mixed phase sputtered titania films in general were more photo-active than pure phase films. The

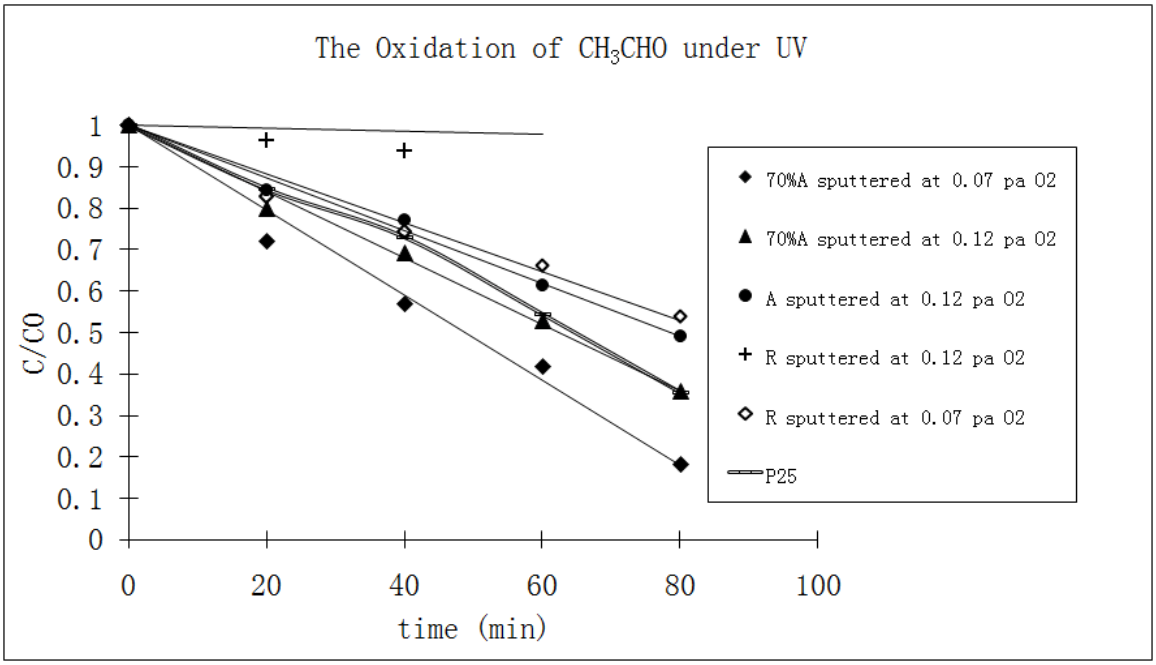

Figure 6.2. Oxidation of acetaldehyde by sputtered titania with different stoichiometry and phase compositions

non-stoichiometric titania films deposited under oxygen partial pressure of 0.07 pa are more reactive than the nearly stoichiometric films prepared under higher oxygen partial pressure (0.12 pa). For example, the rutile deposited under high oxygen partial pressure barely showed any reactivity as many other studies have reported[33, 165], presumably due to high recombination rate. However, the non-stoichiometric rutile deposited under low oxygen partial pressure showed an enhanced reactivity ($0.55\%C_0$/min) comparable to the near-stohiometric rutile ($0.04\%C_0$/min). Similar enhanced reactivity is observed for mixed phase titania prepared under 0.07 pa oxygen partial pressure as well($1.1\%C_0$/min compared to $0.85\%C_0$/min of near-stoichiometric mixed phase film). This indicates oxygen vacancies in the non-stoichiometric titania films might serve as trapping sites to hinder the charge recombination and thus, enhance the photo-acitivyt. All the films deposited

at 0.07 pa oxygen partial pressure display grey color indicating more oxygen vacancies whereas the films deposited at 0.12 pa are almost colorless. Recall that in chapter 4, the sputtered rutile film also showed relative high reactivity and displayed dark color. The influence of the non-stoichiometry on the photo-reacitivity will be further explored for the CO_2 reduction.

6.2.3.2 CO_2 reduction

Figure 6.3 compares the methane production from CO_2 reduction with water as hole scavenger under UV illumination by the low angle mixed phase titania deposited at different oxygen partial pressure. We were not able to detect any methane produced by P25 coated samples with merely water as hole scavenger.

There is a strong trend of increasing methane production with decreasing oxygen partial pressure within the transition deposition mode. The films (Film 1-0 and 1-1) deposited at the turning point(0.07 pa) of the transition mode and metal mode had the highest methane yields. Here, nitrogen not only stabilized the oxygen during the deposition process, but also contributed to the increase of the photo-activity (by about 40%) of the titania catalyst (Film 1-1) which was also deposited at the oxygen partial pressure of 0.07pa. The role of the nitrogen will be further discussed below. In comparison to the almost stoichiometric film deposited at the oxygen partial pressure of 0.12 pa (Film 5-0), the nitrogen stabilized non-stoichiometric film (Film 1-1) displayed more than a tenfold increase in methane yield. The CO_2 conversion for this catalyst was around 22% according to TCD measurement. However, when the oxygen partial pressure was further decreased (0.035)(Film 4-0) and deposited in the metal mode, there was a huge

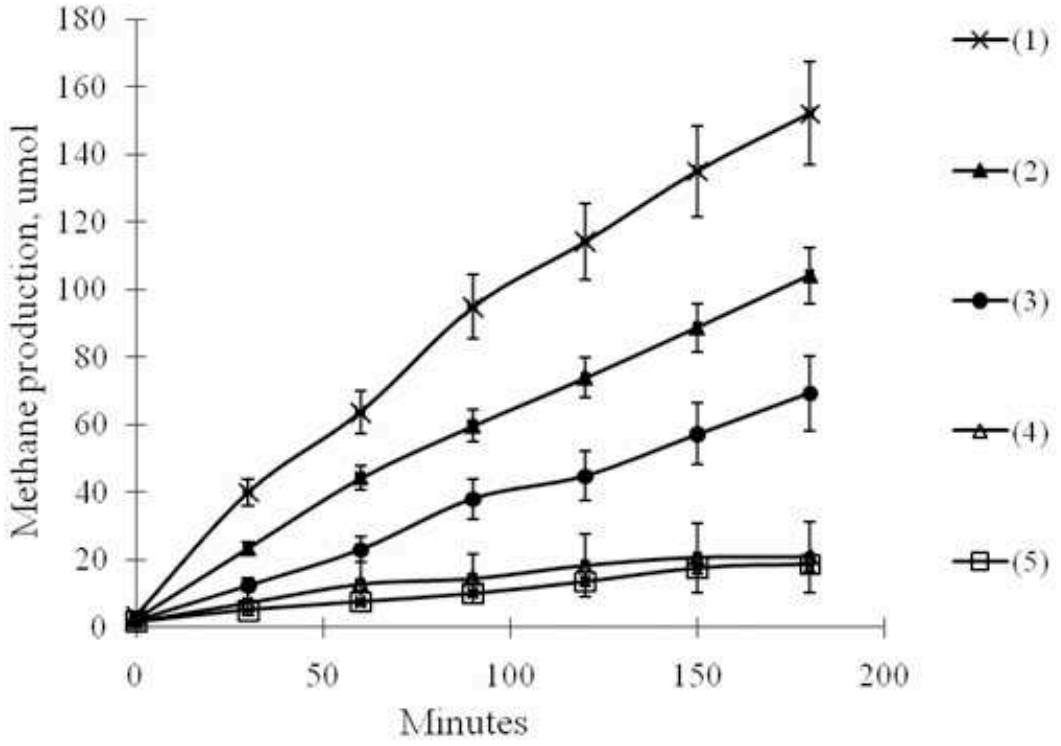

Figure 6.3. Comparison of CO_2 reduction to methane results under UV condition for films fabricated under varying oxygen partial pressures. Water is the hole scavenger.(1): Film 1-1, O_2: 0.07 pa, with minimum nitrogen; (2): Film 1-0, O_2: 0.07 pa, with no nitrogen;(3):Film 2-0, O_2: 0.08 pa; (4): Film 4-0, O_2: 0.035 pa; (5): Film 5-0, O_2: 0.12 pa

decrease in films' reactivities in comparison to Film 1-0 and 1-1 and is similiar to that of Film 5-0. We believe there is more than one role the oxygen vacancies play to affect the reactivity. Oxygen vacancies are strong adsorption sites to various gas molecules [170, 19, 116], which may contribute to the increasing reactivity with increasing non-stoichiometry. Beyond a certain poinnt, as more oxygen vacancies are futher introduced into the films, photocatalytic activity is decreased because of a decrease in the thickness of the space-charge layer [172] and the creation of recombination centers [168].

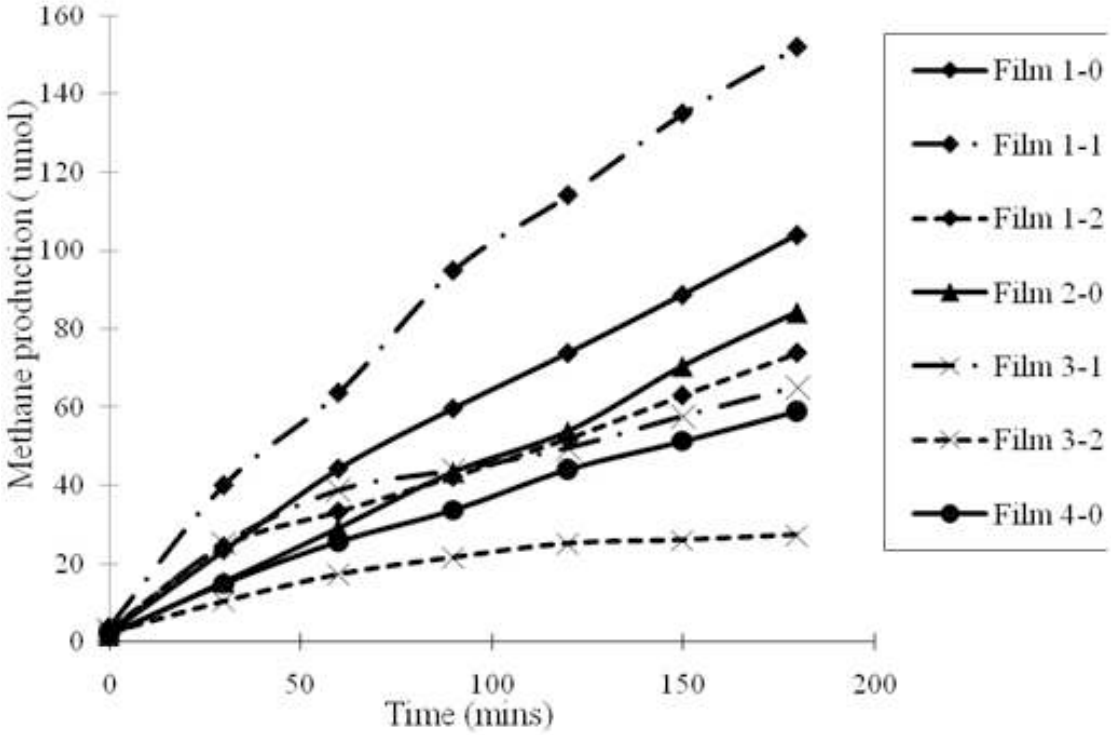

Figure 6.4. Methane production results from CO_2 photoreduction under UV illumination: the nitrogen influence. Film 1-1 (O_2: 0.07 pa, minimum N_2: 0.0035 pa, Film 1-0 (O_2: 0.07 pa, no nitrogen), Film 1-2 (O_2: 0.07 pa, N_2: 0.007 pa); Film 2-0 (O_2: 0.08 pa), Film 3-1 (O_2: 0.05 pa; minimum N_2: 0.005 pa), Film 3-2 (O_2: 0.05 pa; N_2: 0.01 pa), and Film 4-0 (O_2: 0.035 pa).

Figure 6.4 shows the influence of the nitrogen addition during the synthesis on photo-activity of sputtered titania films. Minimal addition of nitrogen during the process to stabilize the system promoted the photo-activity of the catalysts. However, the excessive nitrogen addition reduced the photo-activity dramatically. One of the reasons could be that the excessive nitrogen can decrease the average distances between trapping sites,

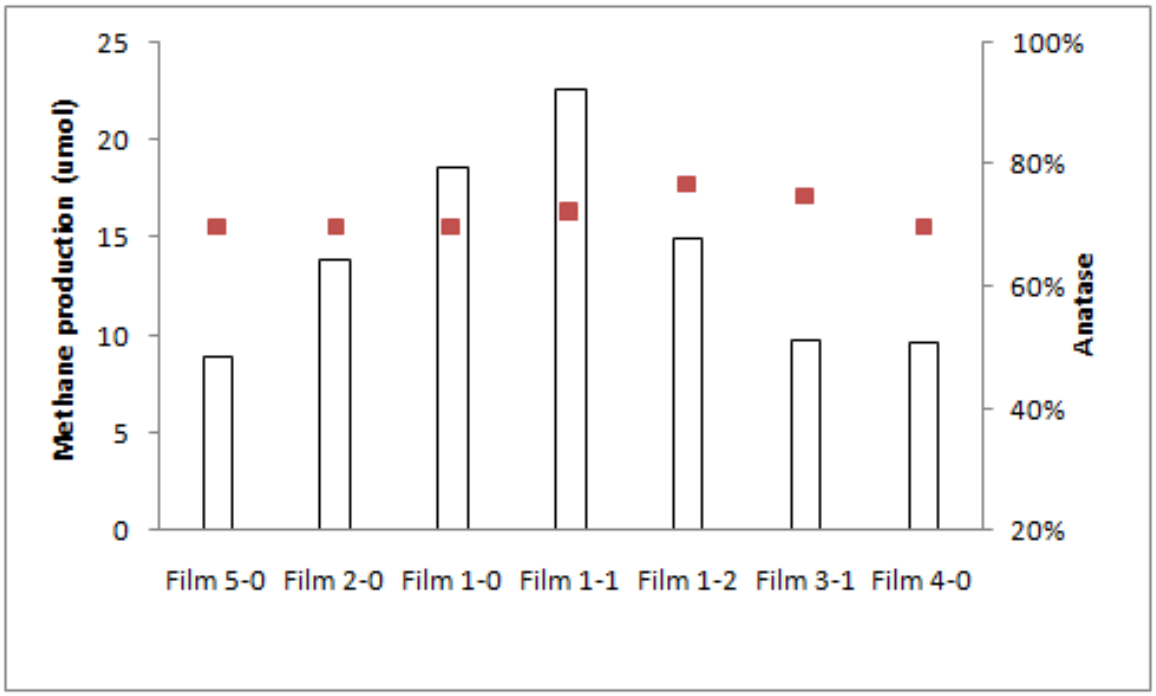

Figure 6.5. Comparison of CO_2 reduction results as well as phase compositions under visible condition for films fabricated under varying oxygen and nitrogen partial pressures. Water is the hole scavenger. Film 1-1 (O_2: 0.07 pa, with minimum N_2: 0.007 pa; Film 1-0 (O_2: 0.07 pa, no nitrogen); Film 2-0 (O_2: 0.08 pa); Film 3-1 (O_2: 0.05 pa; N_2: 0.005 pa); Film 4-0 (O_2: 0.035 pa); and Film 5-0 (O_2: 0.12 pa).

and thus, carriers are more easily captured by these sites causing the increase in the recombination rate [30] and a reduction of the reactivity.

Figure 6.5 illustrates the methane production from CO_2 after 4 hours' reaction under visible illumination conditions. The trends are similar to those observed in Figure 6.3 and 6.4 with an optimal non-stoichiometry and nitrogen addition observed to the films. Again, no methane was detected for P25 coated films. Film 1-1, deposited at 0.07 pa oxygen partial pressure with minimum nitrogen addition displayed the best reactivity under visible light conditions followed by the film deposited at the same oxygen partial pressure

but without nitrogen input. In general, the methane yields under visible condition for all the films are diminished from the results under UV conditions. The reduced reactivity under visible condition may be primarily attributed to the intensity difference of the light sources we applied during the reactions (100 W UV lamp and 20 W solar lamp). There is about six fold decrease in methane yield between the UV and visible light conditions and a five fold difference between the lamp intensity. This diminished yield may also be attributed to a small decay to the existence of 'color centers' which do not contribute to band gap narrowing and thus, do not promote the CO_2 reduction under visible conditions [40]. Although low in quantity compared to the methane yield under UV conditions, the methane was generated with the application of a UV cut-off (400 nm wavelength) above the reactor under visible illumination. Thus, there must be charge separation excited by photons in the visible light range. In addition, the ratio of methane yield under visible conditions versus UV conditions increases with the decrease of the oxygen partial pressure indicating the degree of band gap narrow induced by oxygen vacancies varies with the concentration of oxygen vacancies.

6.2.4. Structural characterizations

Figure 6.6 shows the SEM images for Film 5-0, Film 1-0, Film 1-1 and Film 1-2 deposited at oxygen partial pressures of 0.12pa, 0.07 pa (no nitrogen), 0.07 pa (minimum nitrogen input 0.0035 pa for stabilization) and 0.07 pa (nitrogen 0.007 pa), respectively. As is evident in Figure 6.6, oxygen partial pressure as well as minimum nitrogen addition influence film morphology and texture. All of the films show the characteristic columnar structures of mixed phase anatase and rutile that have been described in our previous

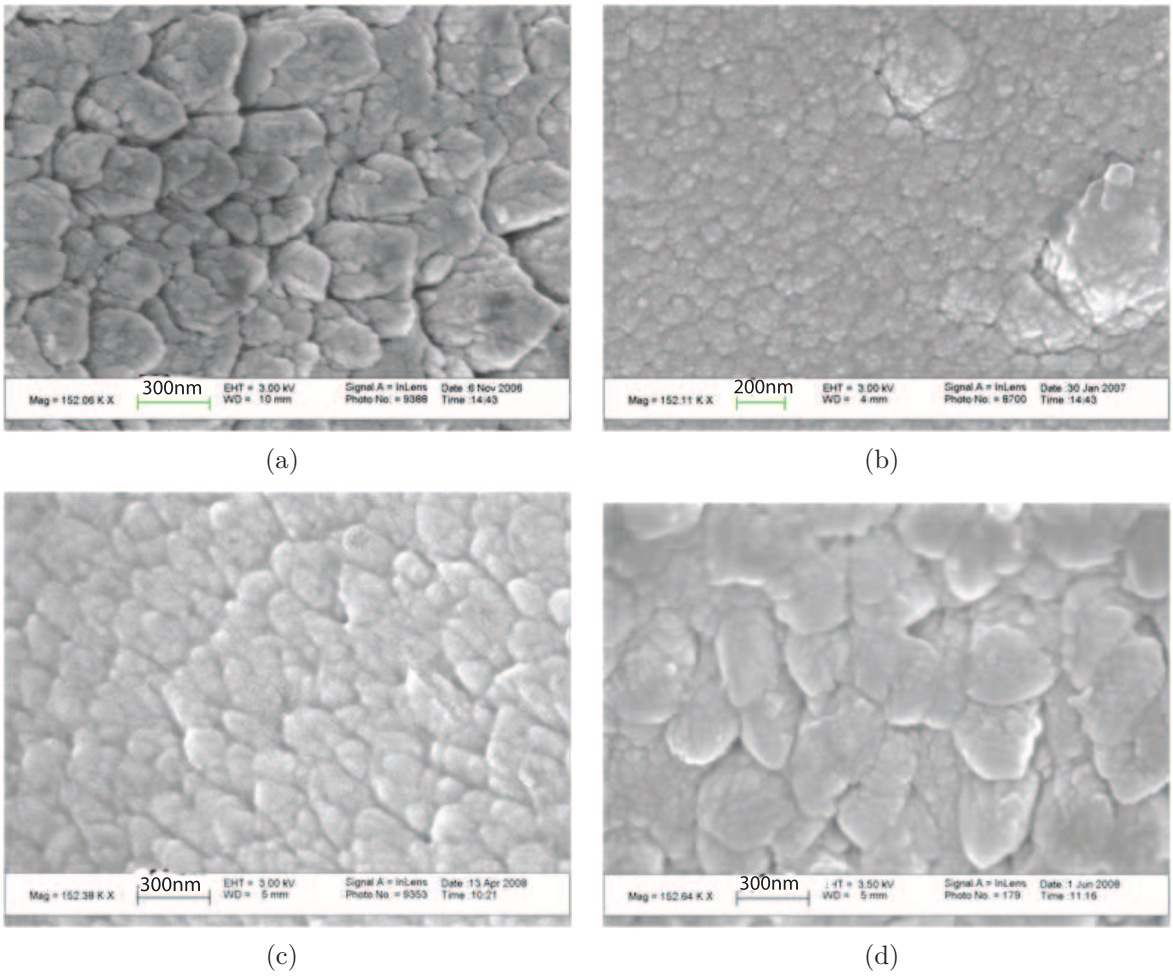

(a) (b)

(c) (d)

Figure 6.6. SEM images for (a)Film 5-0: prepared at oxygen partial pressure of 0.12 pa; (b) Film 1-0: O_2 0.07 pa, no nitrogen added; (c)Film 1-1: O_2 0.07 pa, minimum N_2 0.0035 pa; (d)Film 1-2: O_2 0.07 pa and N_2 0.007 pa. Magnification for all the figures are similar around 152K.

chapters. However, Film 5-0 deposited at the highest oxygen partial pressure showed the most distinguished and largest columns, around 300 nm in diameter (The columns in Figure 4.10 deposited under 0.01 pa oxygen partial pressure are around 200 nm in diameter). This structure creates two very distinctive types of boundaries: those within the columns between the individual anatase and rutile phases and those between the

columns. Film 1-0, however, had much smaller columns (about 50 nm in diameter) and the boundaries are less obvious. In addition, Film 1-0 displayed a rougher surface with clusters composed the size of 3-4 columns (about 200-400 nm in diameter). In general, as the oxygen partial pressure increases, Ti atoms sputtered from the target can effectively react with more abundant oxygen atoms on the substrate due to the atoms' bombardment, promoting atomic mobility and crystal growth. Thus, the columns grow larger (Film 5-0). In contrast, as the oxygen partial pressure decreases, the column size and crystallinity will be reduced accordingly (Film 1-0). In addition, the formation of the rough surface of Film 1-0 with clusters is also due to strong resistivity restricted within the small columns during growth resulting from the low atomic mobility[62]. However, the formation of small columns may promote greater solid-solid interfacial areas which contribute to the high reactivity of mixed-phase titania.

Film 1-1 and Film 1-2 exhibited the influence of nitrogen input during sputtering process. In Film 1-1 with minimum nitrogen input, the column size is 2-3 times as big as in Film 1-0 (about 100-150 nm in diameter), but still not as distinct and big as Film 5-0. The surface is much smoother compared to Film 1-0 as well. Film 1-2, on the other hand, have big columns comparable to the columns in Film 5-0. Thus, the interfacial area in different films might be in the order of Film 1-0 >Film 1-1 > Film 5-0 or 1-2. These results are also consistent with the findings from Prabakar et al.[134] that at the very early stage of nitrogen introduction into oxide sputtering, nitrogen with high kinetic energy serves as additional energetic particles to bombard the substrate causing an increased atomic mobility and larger column size. In addition, although nitrogen replaced argon when the total pressure and the oxygen partial pressure were kept constant, nitrogen has

slightly lower ionized energy (14.53 eV) than argon (15.76 eV) which contributed to higher concentration of the ionized or excited species. Thus, Film 1-1 with minimum nitrogen addition is more crystalline than Film 1-0. I confirmed this by XRD measurement that I found taller and sharper anatase and rutile peaks in Film 1-1 than in Film 1-0. The slight enhancement of anatase (shown in Figure 6.5) in Film 1-2 with more nitrogen addition could also be considered the result of the improvement of the crystallinity of the mixed phase titania under growth conditions and anatase (30-40 nm) tends to grow bigger than rutile (10-15 nm). However, the amount of nitrogen initially added to the system (1/20 of oxygen partial pressure) was so small and was replaced by more reactive oxygen at the surface of the substrate right away that the chemical composition of sputtered titania remained unchanged (no nitrogen was incorporated). Since both interfaces and crystalline mass are very critical for the reactivity of the mixed phase titania, from the point view of the surface structure, the minimum nitrogen influence on the film (Film 1-1) was to achieve a balance between crystalline mass and interfacial areas, and correspondingly, achieve the peak methane production from CO_2 reduction among all the tested samples.

Figure 6.7 showed the XPS spectra of Ti 2p2/3 and Ti 2p1/2 for titania surfaces prepared at different oxygen partial pressures ranging from 0.035 pa to 0.12 pa. The spectrum in Figure 6.7 for an oxygen partial pressure of 0.12 Pa exhibits a sharp peak corresponding to Ti^{4+} at about 458 eV indicating a nearly stoichiometric surface. On the other hand, the samples sputtered under oxygen partial pressure of 0.07 pa with or without nitrogen exhibit similar Ti 2p combined signatures of both Ti^{4+} and Ti^{3+} confirming the existence of TiO_x ($x < 2$) in addition to TiO_2 at the surfaces of both of the samples. The film deposited with trace nitrogen does not display a detectable nitrogen signal (binding

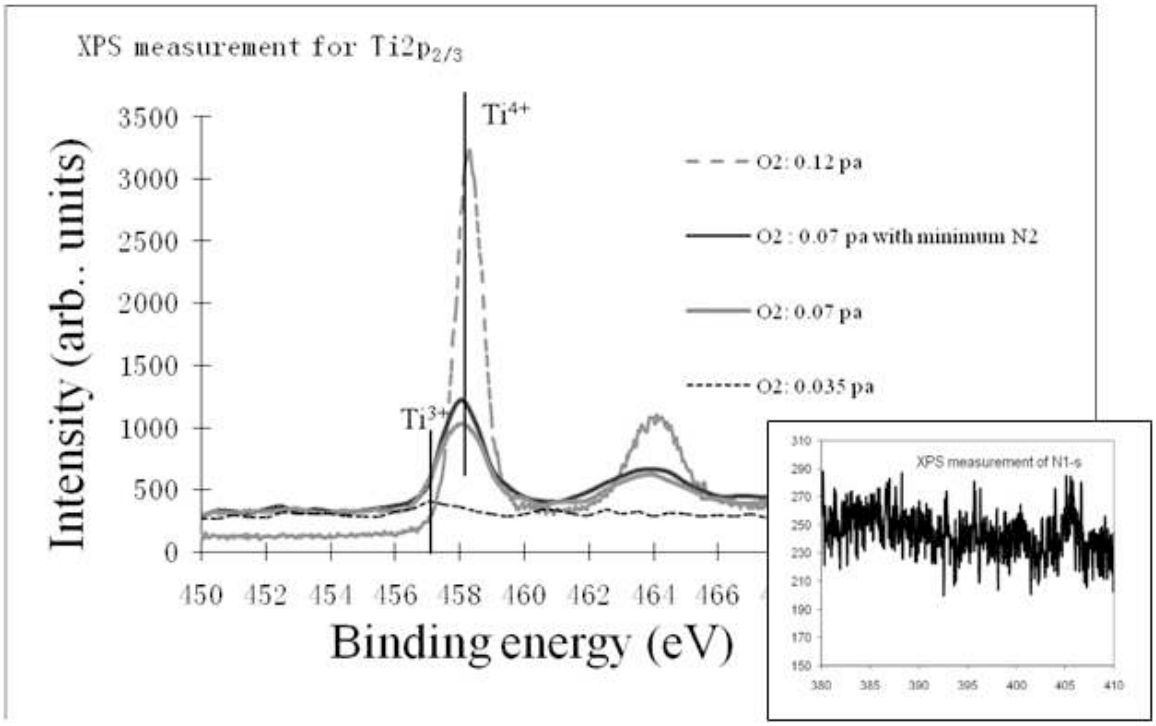

Figure 6.7. XPS analysis of Ti 2p for the films prepared under different oxygen partial pressures and detail scanning of N 1s for the film prepared by 0.07 oxygen partial pressure with minimum input of nitrogen.

energy around 395) at the surface (N1-s spectrum in Figure 6.7) and it displays a sharper signal in Ti spectrum, indicating better crystallinity compared with a film deposited at the same oxygen partial pressure without nitrogen input. The film deposited at 0.035 pa oxygen partial pressure contains mainly Ti^{3+} indicating the lack of sufficient oxygen during titanium oxide deposition in the metal mode. In addition, we did not detect any nitrogen in the Film 1-1 (0.0035 pa nitrogen partial pressure) and 1-2 (0.007 pa nitrogen partial pressure) by the depth profile of the ToF-SIMS.

In order to prepare better TEM samples for EELS analysis, we deposited our non-stoichiometric titania films onto Al-sheet substrates at 0.07 pa oxygen partial pressure, without nitrogen. Then, we dissolved the Al substrate in acid solution and collected the

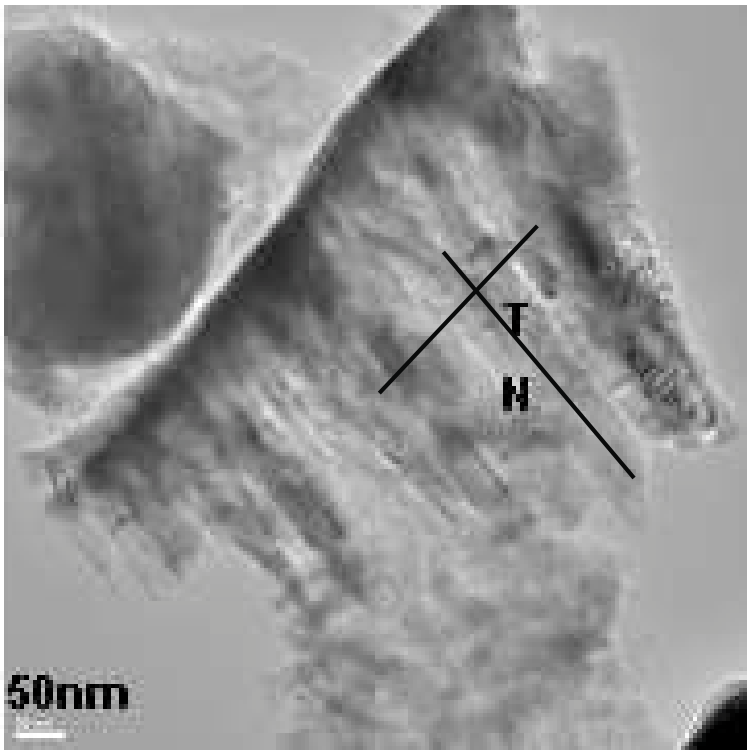

Figure 6.8. TEM image of the non-stoichiometric film piece sputtered under 0.07 pa oxygen partial pressure. T is a point in the column, and N is the point at the interface of the columns.

films and ground them into smaller pieces. Figure 6.8 showed the TEM image of one fine piece of the film and we carried out line profiles horizontally and vertically over it. Overall, the surface is more stoichiometric than the bulk, because after deposition, the surface has more access than the bulk to the air environment and oxidation. Both at the surface and in the bulk of the film, there is an interesting separation of areas where the oxygen is more stoichiometric and where it is deficient. In the individual column it is much more stoichiometric than in the solid-solid interface between neighboring columns. For example, N is a point at the interface of columns and T is a point in the bulk of the column (Figure 6.8).

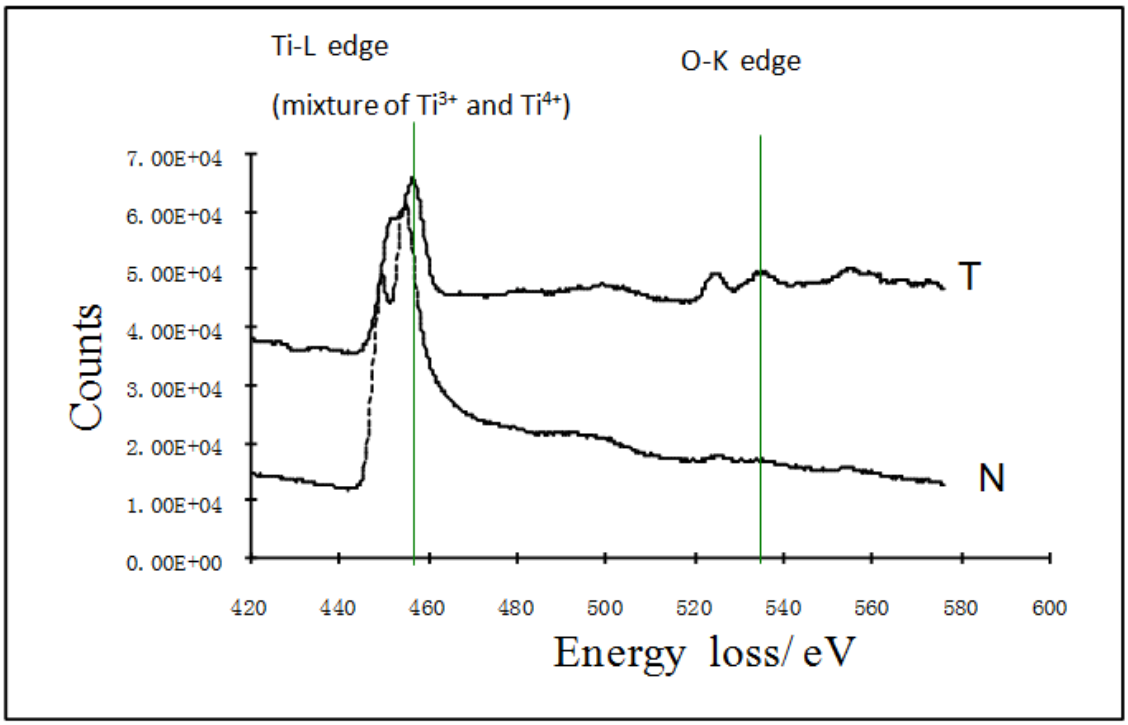

Figure 6.9. EELS spectra of point T and point N.

From the EELs analysis illustrated in Figure 6.9, we see that both of the points display a mixture of Ti^{3+} and Ti^{4+}. For point N, the Ti-L edge is shifted to a lower energy state compared to point T, indicating a lower average oxidation state of Ti (more Ti^{3+}). The O-K edge is much less distinctive for point N than point T, which also implies a lack of oxygen in the lattice. After quantitative calculation, the Ti: O mass ratio is 44:56 for point T and 70:30 for point N, which is almost stoichiometric.

Similar distribution of oxygen vacancies within and between the columns was also observed by Nogochi et al.[126] for their sputtered anatase thin films. However, they claimed the oxygen vacancies merely serve as recombination centers that hindered the quantum efficiency based on the MB degradation tests (UV condition). This differs from

our observation on the reactivity as a function of non-stoichiometry in the titania films and may be due to the fact that they only explored the metal mode and the oxidation mode instead of the transition mode. The film they made in the oxidation mode (stoichiometric) happened to be more reactive than their sample made in the metal mode (very non-stoichiometric). The fact that we were able to explore the non-stoichiometric titania synthesized in the transition mode led us to observe a peak of reactivity correlated with an optimal amount of oxygen vacancies.

At the solid-solid interfaces, the majority of the oxygen vacancies are created and thus, alter the lattice structure [49] to assist in the creation of reactive interfacial sites that promote charge separation and photo-response. This reinforces our conclusions from previous studies pointing to the importance of creating solid-solid interfaces with reactive interfacial sites.

6.3. Conclusions

Non-stoichiometric mixed phase titania catalysts were deposited at low angle by reactive DC magnetron sputtering in the transition mode to create highly reactive and visible light responsive photocatalysts. Oxygen partial pressure was controlled to synthesize different levels of non-stoichiometriy in the films. However, the system was difficult to stabilize at very low oxygen partial pressure approaching the turning point of the transition mode and metal mode. Thus, trace amount of nitrogen (1/20 of oxygen partial pressure) was introduced in the process to stabilize the system at that turning point without being incorporated in the films.

Oxygen vacancies have influences on both the photo-response and photo-activity of the titania films. As the oxygen partial pressure decreases, the sputtered non-stoichiometric films grow darker and cloudier. All the non-stoichiometric titania displayed a red-shifted photo-response.

These non-stoichiometric catalyst films successfully oxidized acetaldehyde under UV conditions and reduced CO_2 to fuel (methane) with the addition of water as a hole scavenger under both UV and visible illumination. In contrast, the P25 coated films showed no reactivity under these conditions. The photocatalytic reactivity increased with the decrease of oxygen partial pressure during the transition mode sputtering. The highest activity was observed in the two catalyst synthesized at the turning point of transition mode and metal mode (pO_2 0.07pa). The photo-activity then decreased for the films deposited in the metal mode. The oxygen vacancies likely serve at least two roles: adsorption or trapping sites and recombination centers. The trade-off effect between these two roles determines an optimal degree of non-stoichiometry of the titania in terms of photocatalytic reactivity. However, as the nitrogen partial pressure further increases, the deposited titania's photo-activity decreases accordingly.

The non-stoichiometric titania films displayed different structures. SEM showed the decreased column size and crystallinity ascribed to restricted atomic mobility and a lack of sufficient oxygen to form crystalline phase for non-stoichiometric films. Both EELS and XPS spectra showed the creation of oxygen vacancy induced Ti^{3+} for non-stoichiometric titania films. EELS results also revealed that more oxygen vacancies are located at the interfaces of columns than inside the columns. By combining characterization and activity results, we conclude that oxygen vacancies enhance visible light harvesting and there is

an optimal oxygen vacancy concentration in terms of photo-activity. Oxygen vacancies may serve as or trigger the creation of reactive interfacial sites at certain concentrations and then, beyond that level may function as recombination centers to hinder the photo-activity.

The trace nitrogen addition increased the mobility and the columns size. The non-stoichiometric titania film synthesized with minimum nitrogen addition for stabilizing the sputtering showed the optimal balance between the crystallinity and total interfacial surface areas reflected by the column size resulting in the highest methane production from photoreducing CO_2.

CHAPTER 7

Sputtering with Two Reactive Gases and Glancing Angle Deposition

This chapter is mainly focused on other attempts made, in addition to what has been described in the previous chapters, to fabricate titania based nanocomposites by DC magnetron sputtering. Sputtering nitrogen doped film is an extension of the previous work that uses nitrogen to synthesize non-stoichiometric titania films. I tried to use ion doping to further create and stabilize oxygen vacancies. Adding hydrogen during sputtering was also inspired by trace nitrogen addition described previously and was intended to explore hydrogen's influence on films' structures and activities. Glance angle deposition is a novel way to fully use the "shadow effect" which is also shown in low angle deposited highly reactive films, to create unique column structures. They were not the most successful attempts in terms of functional tests but they provided very interesting results and insights for future development of fabrication-structure-function relationships.

7.1. Sputtering with two reactive gases

7.1.1. Introduction

7.1.1.1 Sputtering nitrogen doped titania with nitrogen and oxygen reactive gases

In the previous chapter, the small amount of nitrogen addition during sputtering was

demonstrated to stabilize the deposition process and improve the films' atomic mobility. In that case, the nitrogen was in such small amount that it served as stabilizer or buffer to the system rather than a reactive gas. As we further increases the dose of nitrogen gas during the deposition, however, the nitrogen would eventually dope the films .

Nitrogen doped titania catalysts have been reported to produce a red-shifted photo-response due to the creation of intermediate oxygen vacancy electronic states between the conduction band and the valence band by nitrogen induced charge compensation[16]. This is an indirect way to introduce oxygen vacancies in the films. Nitrogen doped titania can be synthesized by solvo-thermal methods [74, 103, 112] as well as sputtering [30, 60, 88, 108]. However, most of the nitrogen doped titania by sputtering was prepared by reactive gas "flow control". As I stated in the earlier chapters, "Pressure control" is used for better control, and we were interested in exploring the feasibility of using "pressure control" to synthesize nitrogen doped titania and comparing it to our non-stoichiometric titania catalysts, which contain oxygen vacancies without any dopants.

7.1.1.2 Sputtering with hydrogen and oxygen reactive gases

Inspired by the trace nitrogen addition during the sputtering, I decided to explore the influence of other reactive gas on the deposited films.

Introducing hydrogen as an additional reactive gas is reported to improve the film's structure order [35] and mechanical resistance [23] as well as reducing or eliminating the arcing of the target during the process [180]. Inevitably, using hydrogen and oxygen as reactive gases will give rise to the increasing water vapor concentration during the deposition. Water vapor also influences the deposition process [127] as well as film properties

(e.g. phase composition and structure [141, 181]). In contrast to hydrogen's influence, water vapor during the sputtering tends to deteriorate the film's resistance and mobility [139]. In addition, excessive water vapor takes longer time for the pump to recover the high vacuum. Thus, the balance of the amount of the hydrogen introduced and the production of water needs to be controlled.

7.1.2. Experiment

The two reactive gases were controlled by the pressure ratio. The oxygen partial pressure was initially set by the 'master control valve'. The partial pressure ratio of the two reactive gases could be adjusted by the 'slave control valve'. By controlling the partial pressure ratio, as the partial pressure of the second reactive gas increases, the partial pressure of the oxygen will decrease gradually. Then, the 'master control valve' was adjusted restoring the oxygen partial pressure and keeping it constant.

For nitrogen doping, the oxygen partial pressure was set as 0.07-0.08 pa and the partial pressure ratio of oxygen to nitrogen varied from 5:1 to 1:3.5. In the case of hydrogen addition, the oxygen partial pressure was kept at 0.07 pa and the ratio of the oxygen to hydrogen was set at 20:1, 10:1 and 5:1. When the partial pressure ratio went below 5:1, the water vapor content was too high for the efficient pumping.

The other sputtering conditions were similar to those described in the previous chapters: low angle; total pressure 3.5 pa to 5.0 pa; power: 5.1-5.3 kw; substrate bias: -70 to -80 V.

Film characterization included: UV-Visible Spectroscopy (Hitachi U-2000), XRD (Rigaku, using Cu-Kα radiation operated at 40 kV-200 mA), XPS (X-ray Photoelectron Spectroscopy, Omicron, ESCA probe) and SEM (LEO Gemini 1525). The activity test was carried out for acetaldehyde degradation and CO_2 reduction. All the details about the methods and the processes can be found in previous chapters.

7.1.3. Results and Discussions

7.1.3.1 Structural characterization

In cases of films deposited with nitrogen and oxygen as the mixed reactive gases, they showed light yellow color when nitrogen partial pressure was at low level and the turned to bright yellow when the nitrogen partial pressure exceeded the oxygen partial pressure. Hydrogen influenced titania films, on the other hand, displayed a light blue color. All the films were transparent.

We did not find a significant influence of hydrogen addition on the films' phase compositions in contrast to reports in the literature [141, 181], probably due to the low and small range of hydrogen concentrations (to avoid excessive water vapor formation) we used for the sputtering. In the previous chapter, we already demonstrated the growth of the anatase X-ray diffraction peak as we added trace amounts of nitrogen during the deposition process. However as we further increased the nitrogen partial pressure (other sputtering parameters were kept constant), the anatase peak started to shrink (starting with 70% anatase and 30% rutile) and the rutile peak started to grow and the structure remained pure rutile regardless of the increasing nitrogen partial pressure until the nitrogen became dominant in the mixed reactive gas. After the nitrogen addition exceeded the

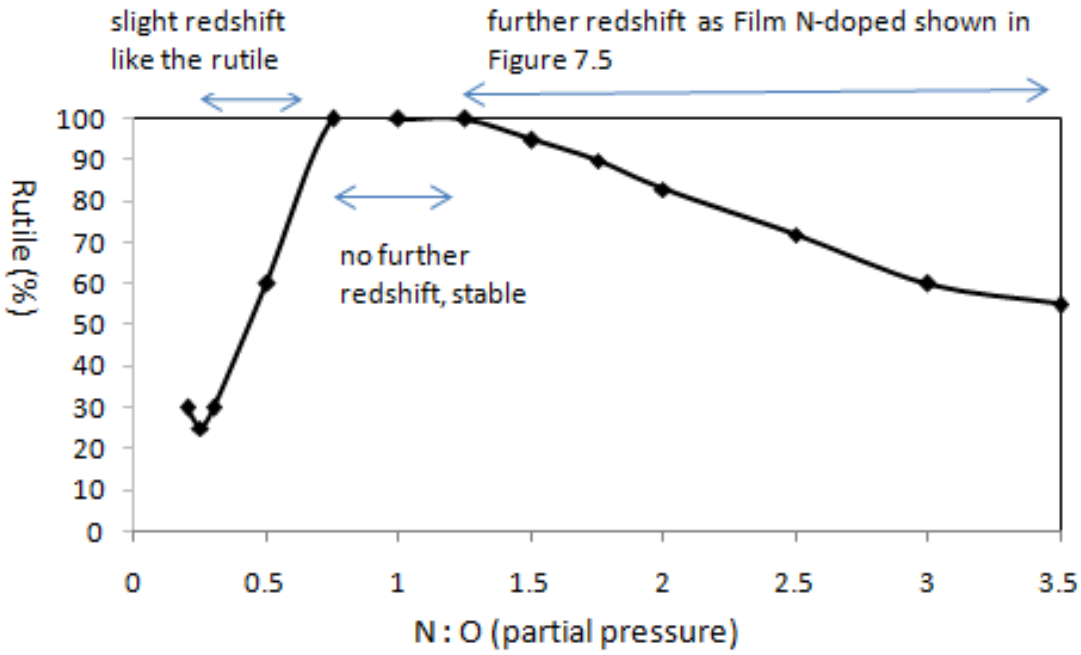

Figure 7.1. The influence of nitrogen addition on the rutile content and photoresponse of the sputtered titania films

oxygen (recall that the film color changed into bright yellow), the anatase peak started to grow again. The whole transition of the titania's phase composition under nitrogen influence is illustrated in Figure 7.1.

The initial slight enhancement of anatase in the beginning stage of nitrogen addition could be considered the result of the improvement of the crystallinity of the mixed phase titania under growth conditions that favor anatase stability. As nitrogen increases, it serve as additional energetic particles to bombard the substrate and cause the phase transition from mixed phase to pure rutile [134]. Furthermore, the deposition rate is increased due to the higher sputtering yield of the nitride compared to the corresponding oxide.The observation of phase transition from rutile to mixed phase again at high nitrogen partial pressure as consistent with the study by Lindgren et al [108]. When the nitrogen partial

pressure further increases, the target is eventually 'poisoned' by titanium nitride and the deposition rate will decrease again. Thus, not as many energetic particles bombard the substrate surface and result in the phase composition at lower energy level (mixed phase) again.

Figure 7.2 and Figure 7.3 shows the SEM images for the nitrogen doped titania film (prepared under N:O(p.p)=2:1) and hydrogen influenced film (prepared under H:O (p.p)=1:10). The target power and substrate bias were adjusted (not the same conditions used in Figure 7.1) during synthesizing these two films so that the phase composition of the films agreed with each other which was mixed phase with 70% of anatase. Compared to the undoped titania (Figure 4.10 and 5.4), the crystals are much bigger (expand to the whole column, 200-250 nm in diameter) in the nitrogen doped films for both low angle and normal angle deposited films confirming that during the sputtering nitrogen serves as additional energetic particles to bombard the substrate surface and assist in crystalline development. For the hydrogen influenced low angle deposited titania film, the columns are more uniform in size and shape but with much less distinctive column boundaries compared to the low angle deposited titania without adding hydrogen.

Figure 7.4 shows the XPS N1s spectra of nitrogen doped film compared to the non-stoichiometric films sputtered with trace nitrogen added. No nitrogen can be detected from those non-stoichiometric films and only very small peak can be assigned as nitrogen peak for the nitrogen doped films. After calculation, the N:O is 1:9 ($TiN_{0.2}O_{1.8}$). Thus, although the nitrogen partial pressure was twice as much as the oxygen partial pressure for sputtering the nitrogen doped films, only very small amount of nitrogen was able to be incorporated in the film since oxygen is much more reactive than nitrogen.

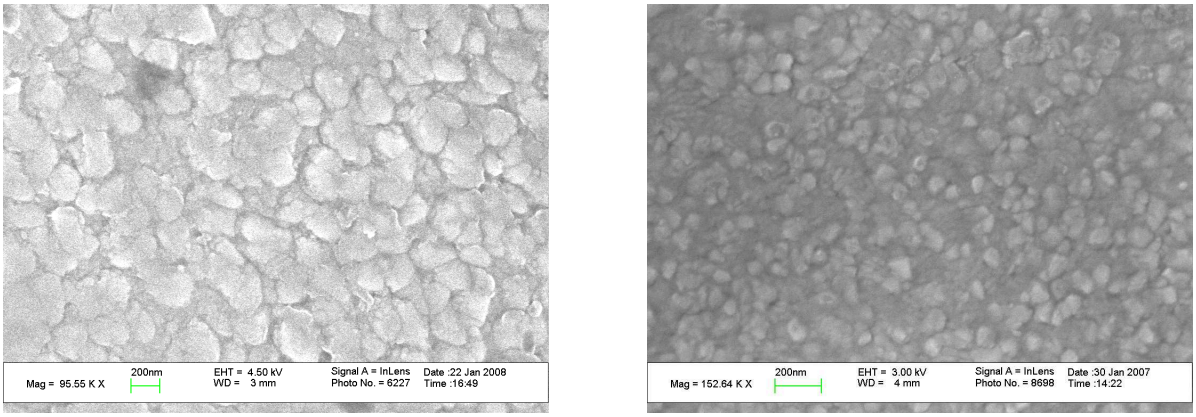

(a) (b)

Figure 7.2. The SEM image for the nitrogen doped titania (prepared under N:O=2:1). (a). Low angle deposition; (b). Normal angle deposition

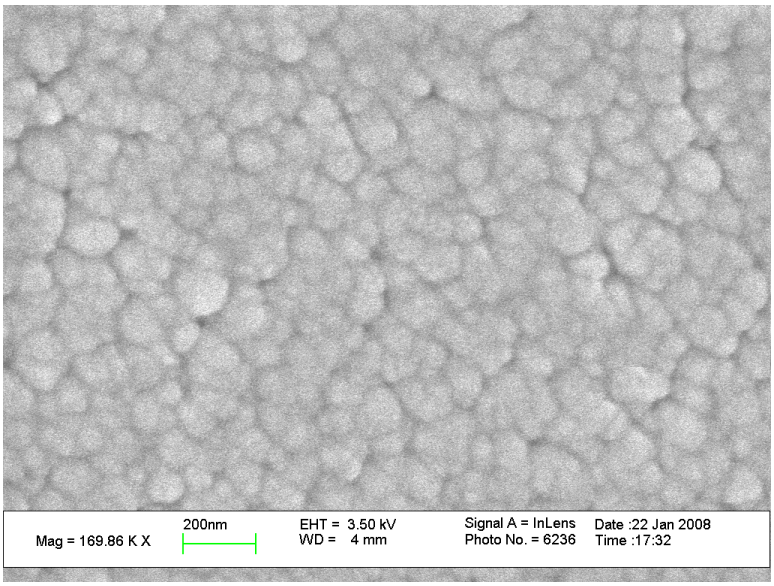

Figure 7.3. The SEM image for the hydrogen influenced titania (prepared under H:O (p.p)=1:10, low angle

7.1.3.2 Optical measurement

Figure 7.5 displays the UV-Vis absorption spectra of nitrogen doped titania (prepared

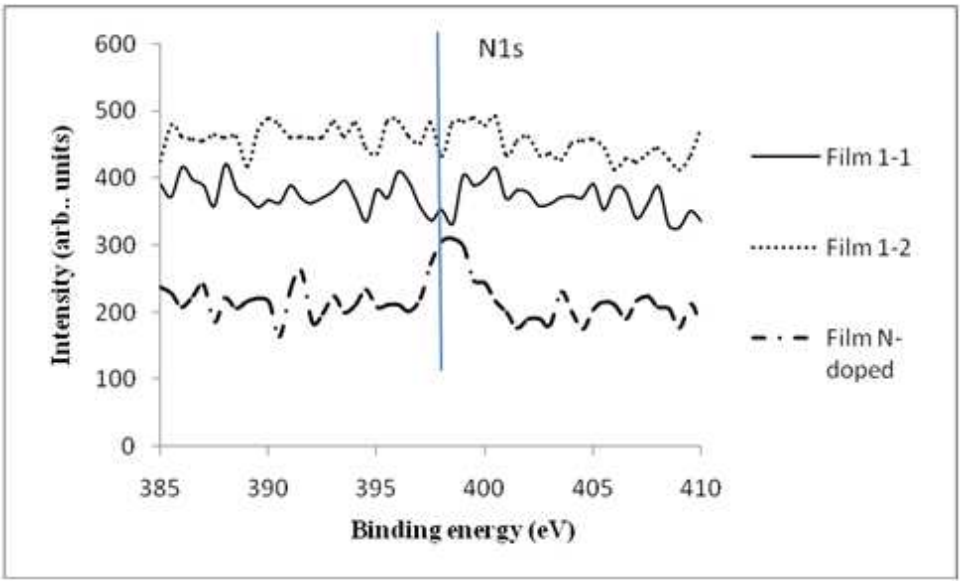

Figure 7.4. XPS spectra of N1s for the Film 1-1: O_2 p.p: 0.07 pa, with minimum N_2 p.p: 0.0035 pa; Film 1-2: O_2 p.p: 0.07 pa, N_2 p.p: 0.007pa; and a nitrogen doped film with N_2: O_2 (p.p)=2:1 (O_2 p.p. was about 0.08 pa)

under N:O=2:1) and hydrogen influenced titania (prepared under H:O (p.p)=1:10) compared to the non-stoichiometric titania as well as commercial standard, Degussa P25.

The nitrogen doped titania shows a redshift in photoresponse with an onset wavelength around 440 nm compared to standard P25. However, the nitrogen doped titania's photoresponse is not as extensive in the visible range as the non-stoichiometric titania sputtered under the oxygen partial pressure at the turning of the transition mode and the metallic mode. Hydrogen addition causes only slight redshift of the film's photoresponse which might be ascribed to the 'blue' color of the film.

I also ran the UV-Vis absorption measurements (summarized in Figure 7.1) over films deposited with other partial pressure ratios of nitrogen and oxygen. In the beginning, the redshift of the photoresponse was subtle and synchronized with the phase composition

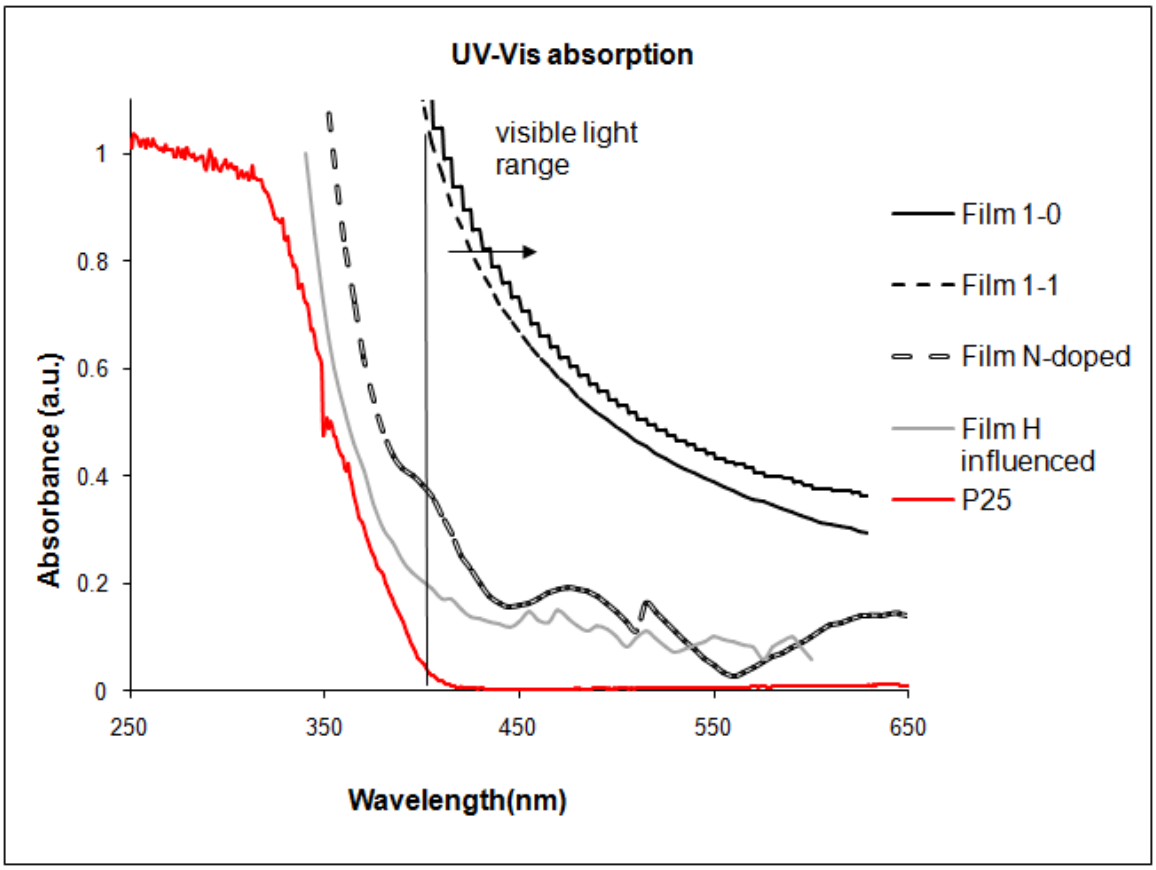

Figure 7.5. UV-Vis absorption spectra for Film 1-1: O_2 p.p: 0.07 pa, with minimum N_2 p.p: 0.0035 pa; Film 1-0: O_2 p.p: 0.07 pa, no nitrogen; a nitrogen doped film with N_2: O_2 (p.p)=2:1 (O_2 p.p. was about 0.08 pa); a hydrogen influenced titania (prepared under H:O (p.p)=1:10) and a P25 dip coated film as a standard.

change from mixed phase to pure rutile. After the phase composition was stabilized at pure rutile with increasing nitrogen partial pressure, the photoresponse also stayed unchanged for a while and then started to further redshift in the visible range again. The redshift in the second case can be attributed to the nitrogen doping. Although the phase composition changed from pure rutile to the mixed phase of anatase (anatase does not cause redshift) and rutile again, the photoresponse of the film continued to gradually

redshift.

7.1.3.3 Photo-activity tests

Figure 7.6 shows the acetaldehyde oxidation results of the nitrogen doped film and hydrogen influenced film compared to the stoichiometric (sputtered at 0.12 pa oxygen partial pressure) and non-stoichiometric (sputtered at 0.07 pa oxygen partial pressure) titania films under UV conditions (Mercury vapor lamp, 100W as been used in the previously experiments). The details of the reactions were introduced in Chapter 6. The surface areas of the films were normalized. The mixed phase nitrogen doped film was sputtered using a partial pressure ratio of N:O=2:1 and the hydrogen influenced film was sputtered using a partial pressure ratio of H:O=1:10. All the mixed phase films contained 70% anatase and 30% rutile. The surface areas were measured by AFM and the results were normalized by the surface areas.

Once again, the mixed phase titania films are more photocatalyicly active than the pure anatase titania. Hydrogen addition during titania deposition, shows the different influence on the photo-activities of different phases. Hydrogen influenced anatase had lower photo-activity compared to the ordinary undoped sputtered anatase. Hydrogen influenced mixed phase, on the other hand, showed enhanced photo-activity comparable to the most reactive non-stoichiometric mixed phase titania. However, more analysis and testing are needed to fully understand the role of the hydrogen added during the sputtering process. Nitrogen doped mixed phase titania, showed the lowest degradation rate and percentage among all the mixed phase samples. It has been suggested that the doped nitrogen ions may also serve as recombination centers and cause the quenching

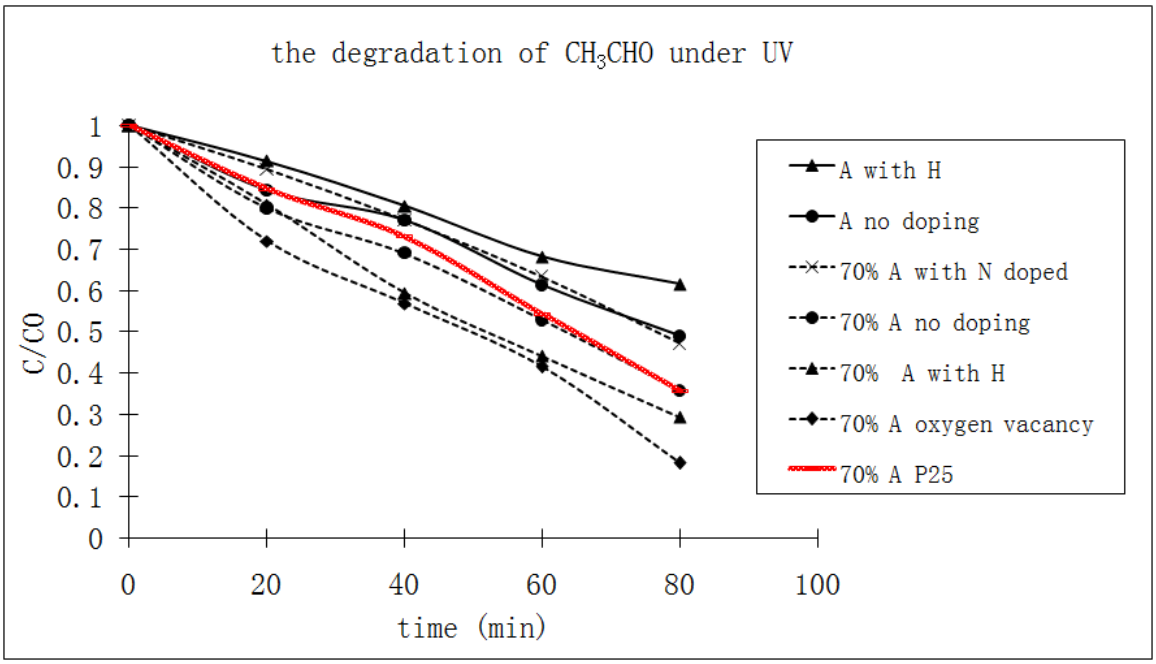

Figure 7.6. Acetaldehyde oxidation results under UV conditions.

of photo-activity for the nitrogen doped titania under UV illumination [110, 133]. In addition, nitrogen doped titania tends to have large crystals/columns (300-400 nm for low angle deposited film and 60-70 nm for high angle deposited film) shown in the SEM images which means it has less interfacial surface area compared to the undoped titania. We have already demonstrated the photocatalytic importance of the solid-solid interfaces in the previous chapters. Thus, the reduced interfacial surface area could may also contribute to the low photoactivity of nitrogen doped titania under UV illumination.

Although the nitrogen doped titania did not have as high a photo-activity as other mixed phase titania, including P25 film, under UV conditions, it showed better photocatalytic performance than P25 under visible illumination (Figure 7.7). After 4hrs reaction under visible conditions, the nitrogen doped film achieved about 35% acetaldehyde removal. It retained 70% of the photoactivity under UV condition (about 50% acetaldehyde

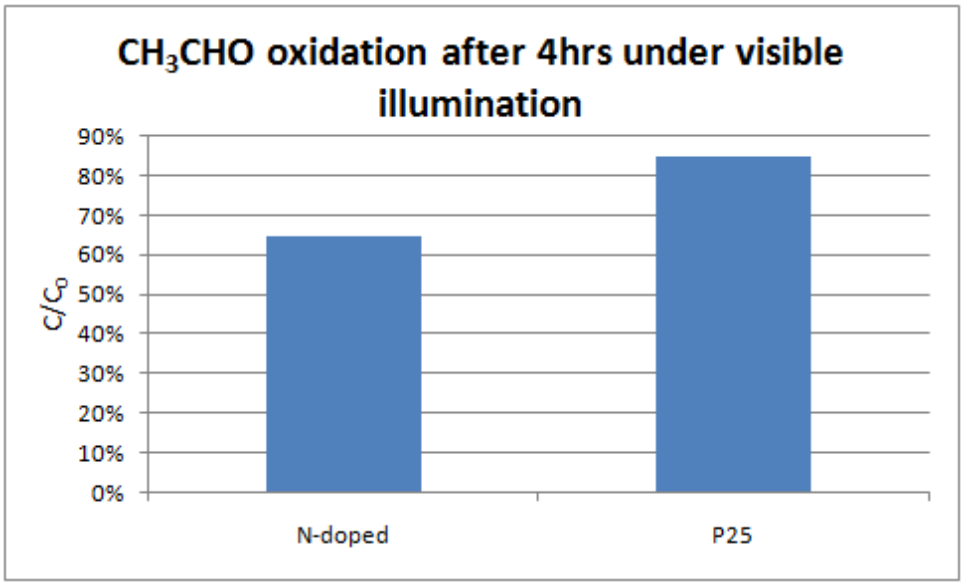

Figure 7.7. Acetaldehyde oxidation results under visible conditions.

removal). In contrast, P25 only achieved 15% acetaldehyde removal under visible light illumination which is a dramatic decrease compare to the reactivity under UV condition (about 60% acetaldehyde removal). Figure 7.8 compared the CO_2 reduction performance of nitrogen doped film with P25 again and only water was added as a hole scavenger. From the figure, P25 was not able to reduce CO_2, whereas the nitrogen doped titania showed its ability to reduce CO_2 (still not comparable to the non-stoichiometric titania shown in the previous chapter) under visible conditions.

7.2. Glancing Angle Deposition(GLAD)

7.2.1. Introduction

The GLAD (glancing angle deposition) technique has been around for several decades, and can be used as an approach to control three-dimensional film structure on the nanometer scale. In this process, a porous film of highly oriented columns is deposited by physical

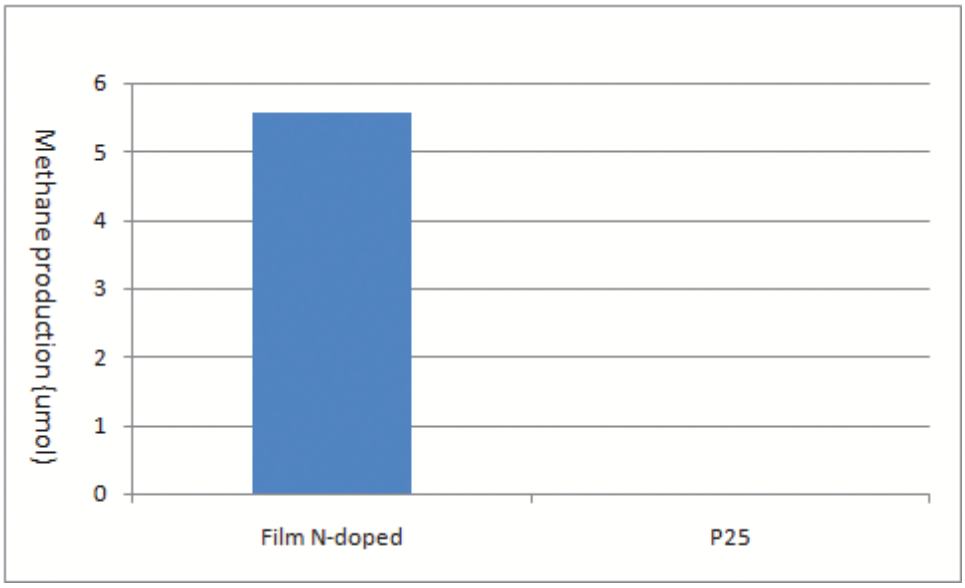

Figure 7.8. CO_2 reduction results under visible light illumination for 4 hours

evaporation or sputtering with the incident beam at glancing angle (usually $> 80°$ from the substrate normal). Often the film exhibits a microstructure that resembles columns with a high aspect ratio (length/width). The resulting columns are normal to the substrate or inclined depending on whether or not the substrate was rotated during deposition [9].

There are several film microstructures created by GLAD involving the rotation of substrate or target or both: oblique angle deposited columns, chevrons and helices [138, 34]. Oblique angle deposited columns are fabricated under highly oblique flux incidence angle (Figure 7.9a), while helices are fabricated by rotating the substrate more slowly (dependent on the film properties desired)(Figure 7.9c). Chevron structures are formed by rotating the substrate 180 to create each arm of the zigzag (Figure 7.9b). The highly oblique deposition angle enforces the shadowing effect on the surface between nuclei of previously deposited material, creating a porous film.

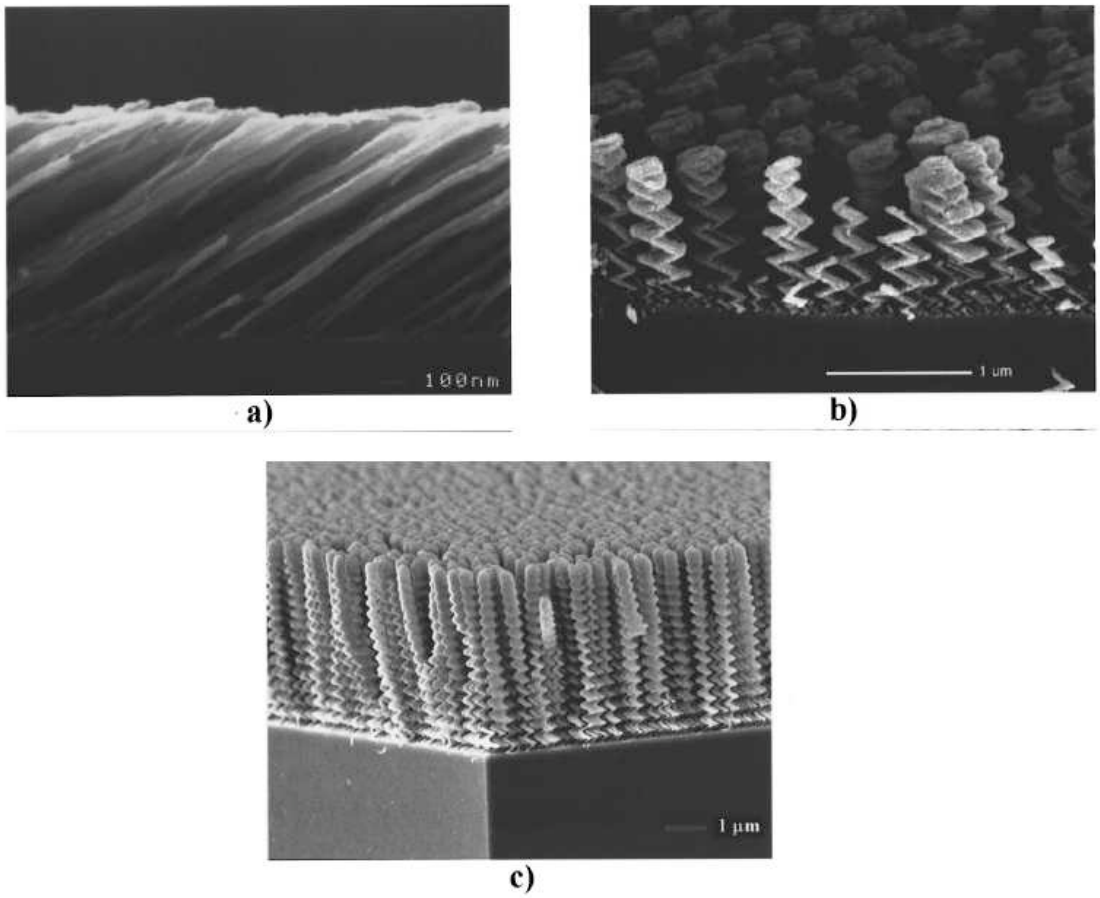

Figure 7.9. Mechanics of GLAD technique. Oblique flux at 85° from one side produces a slanted microstructure (a), alternating oblique flux at 85 produces a zigzag (b), and rotory substrate motion produces helices (c).[138]

The 'oblique angle deposition' (Figure 7.9a) resembles the 'low angle deposition' in my study with further lower deposition angles. By using the current sputtering set up, I wanted to try to make the 'chevron' structure by rotating the substrate holder. However, since the target did not rotate, I was not able to synthesize the 'helices' structure.

The purposes of studying 'GLAD' were to: 1) Explore the relationship of the photo-activity with the unique structure created by GLAD; and 2) Explore the possibility to calculate the surface areas (especially the inner surface areas) for the more open 'GLAD'

films and thus, may help to estimate the surface areas of the low angle deposited films which showed high reactivities from previous chapters.

7.2.2. Experiment

7.2.2.1 Synthesize 'chevron' structures by DC magnetron sputtering

Figure 7.10 shows the sample positions by rotating sample holders to make 'chevron' structures. I alternated the deposition position 5 times per sample and sputtered about 7 minutes at each position. Since the incident angle was much less compared to the previous low angle deposition, I had to increase target power and substrate bias in order to achieve the original phase compositions. The oxygen partial pressure was set at 0.07 pa with minimum nitrogen addition to stabilize. However, although I was able to get mixed phase titania (70% anatase) by 'GLAD', the crystalline domains of the films were very low and I had to anneal the samples after deposition at 400°C for 1 hour to obtain good crystallinity.

7.2.2.2 Structural and functional characterizations

The characterization includes: XRD (Rigaku, using Cu-Kα radiation operated at 40 kV-200 mA),and SEM (LEO Gemini 1525). The activity test was carried out for CO_2 reduction under visible illumination. All the details about the methods and the process can be found in the previous chapters.

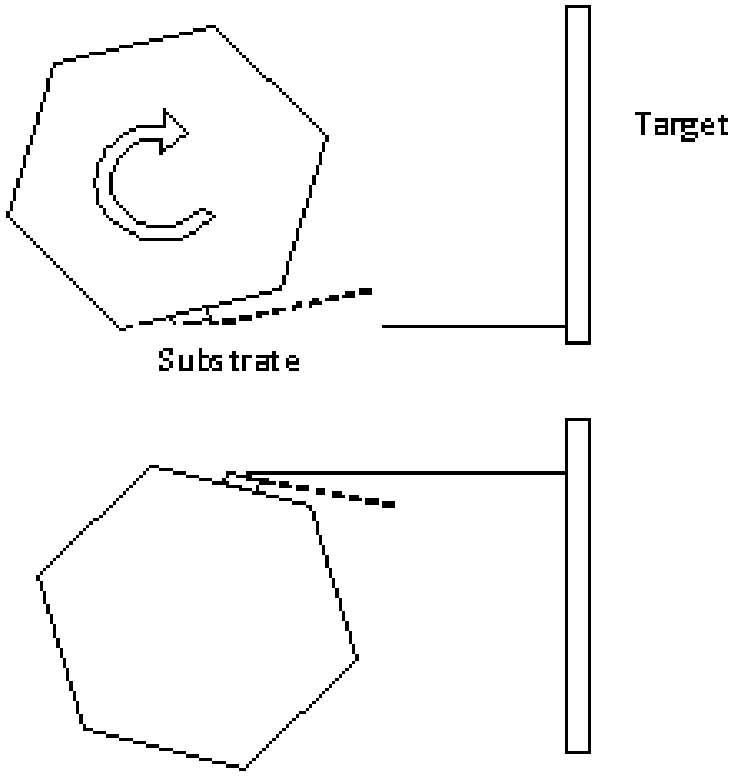

Figure 7.10. Sample positions in making 'chevron' structure

7.2.3. Results and Discussions

Figure 7.11 and 7.12 show the SEM plan-view and cross section images for the 'GLAD' film (after annealing). The 'GLAD' film shares similar columnar structures with a regular low angle deposited film. But due to deposition angle's difference, the 'shadowing effect' is more obvious for the 'GLAD' film than the regular low angle deposited one. Figure 7.12 shows a zig-zag 'chevron' structure. Although the structure is not as organized as the one from the literature, it shows the possibility of synthesizing 'chevron' structure by simply alternating deposition positions in our existing sputtering equipment. However, we still need a more organized structure to calculate and estimate the surface areas.

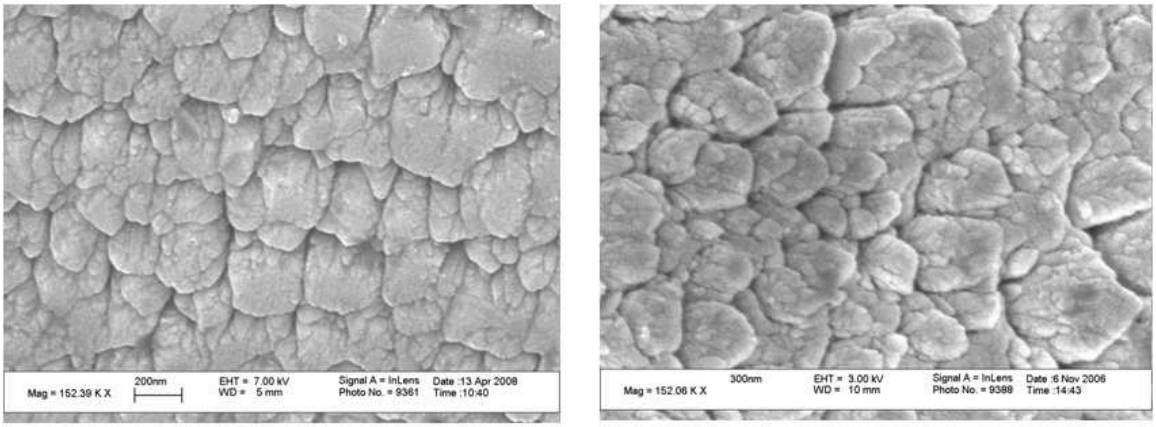

Figure 7.11. Plan-view SEM images for a 'GLAD' film (a) and a regular low angle deposited film (b).

Figure 7.13 compares the CO_2 reduction result under visible condition among the non-stoichiometric titania (a), the 'GLAD' film (b) as well as the nitrogen doped film (c). The 'GLAD' film and the non-stoichiometric titania were both deposited at the same oxygen partial pressure with trace nitrogen addition. However, the 'GLAD' film only displayed half of the photo-activity of the non-stoichiometric film. Since the two films have the similar phase composition and stoichiometry, the major suspected reason for the reactivity difference is a structural difference. Since the 'GLAD' generates a more open structure may be associated with the elimination of the reactive solid-solid interfaces among columns, reduced photo-activity. However, more study needs to carried out to provide explanations with more certainty.

7.3. Conclusions

This chapter describes the other attempts I have made to explore the relationships of synthesis-structure-function.

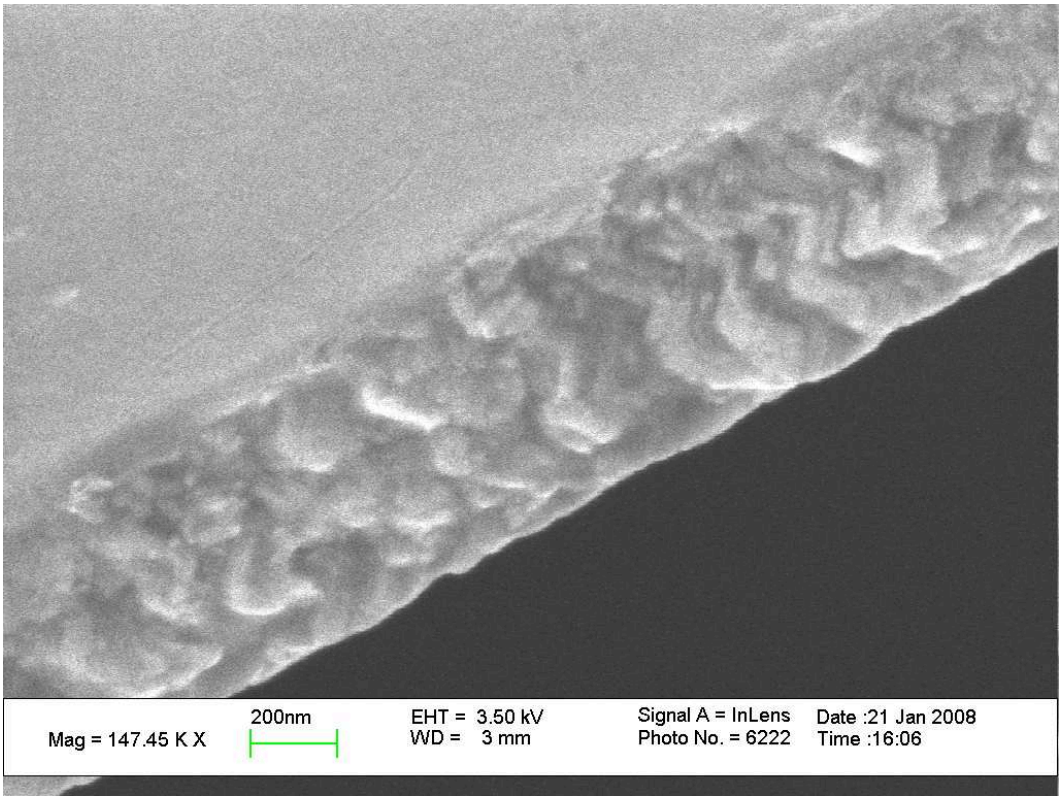

Figure 7.12. cross-section SEM images for a 'GLAD' film.

The biggest challenge of these two tasks lies in the synthesis part. Sputtering with 2 reactive gases (nitrogen and oxygen; hydrogen and oxygen) by using partial pressure control requires knowledge about the properties of the different gases and how they interact with each other, the substrate, as well as the target. The 'chevron' glancing angle deposition, on the other hand, requires a proper process design. In addition, all of the synthesis processes require modification of the sputtering parameters to obtain the desirable phase compositions.

For the films deposited by two reactive gasses, not only did the phase composition and chemical composition change, but the surface morphology and photo-reactivity were

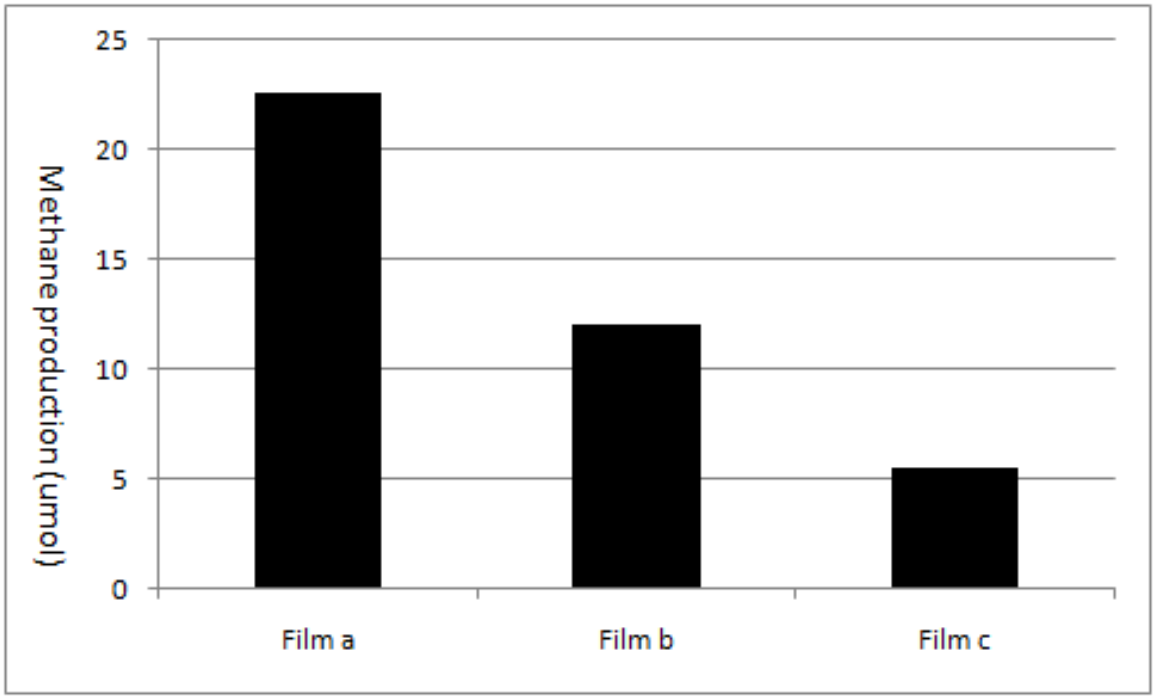

Figure 7.13. CO_2 photoreduction results after 4 hours' visible light illumination for film (a) a non-stoichiometric titania film prepared at 0.07 pa oxygen partial pressure with minimum nitrogen addition, film (b) the 'GLAD' titania film also prepared at 0.07 pa oxygen partial pressure with minimum nitrogen addition, and film (c) a nitrogen doped film described in the previous section.

influenced as well. The nitrogen doped film showed the shift between the two phases (anatase and rutile) as the nitrogen partial pressure increased. Big crystals (columns) could be observed from the nitrogen doped titania and the hydrogen influenced titania tended to have more organized and uniform columns. The nitrogen doped titania showed a photoresponse redshifted in the visible range with some photoactivity under visible illumination. However, its photoactivity under UV illumination was relatively low compared to the other sputtered titania films. Hydrogen addition had a mixed influence on the photo-activity of the deposited films: reduced photoactivity for anatase and enhanced

photoactivity for mixed phase similar to that of the non-stoichiometric titania. The further study is needed to identify the influence and explain it.

The 'chevron' structured 'GLAD' films had a more open structure compared to the regular low angle deposited films. However, its photoactivity was much lower than the low angle deposited titania films and this may be explained by a decrease in the reactive solid-solid interface among the more isolated columns.

CHAPTER 8

Conclusions

The relationships among synthesis-structure-function of TiO_2 based nanocomposites have been studied in this thesis. I was able to deposit titania thin films with various compositions and structures by reactive DC magnetron sputtering. They showed enhanced photoreactivity of both oxidative and reductive chemistry. The sputtered films also displayed a photo-response shifted into the visible light range, which has significant potential for targeted solar utilization and storage as well as environmental treatment.

The key findings of my researches are:

- **Mixed phase titania films with a high density of solid-solid interfaces are prepared by reactive DC magnetron sputtering.** Films having different phase compositions and structures were achieved by determining combinations of the process parameters such as sputtering power and substrate bias, total pressure, deposition angles etc. In conclusion, the target power, substrate bias, total pressure and deposition angles affect the phase composition of anatase and rutile most during the sputtering. High power and bias input, low total pressure as well as high angle deposition, tended to grow rutile. In contrast, a low level of power and bias input, high total pressure as well as lower angle deposition, tends to grow anatase. Thus, I determined the intermediate levels of

the sputtering conditions to generate mixed phase with different phase compositions. Post-deposition annealing and substrate type provided additional tuning on the phase composition. Oxygen partial pressure during the sputtering process, however, was not critical to the phase composition according to our characterization results but determined the stoichiometry of the films. For a sputtered mixed phase TiO_2, anatase had larger crystal size (around 20-40 nm) than rutile (10-15 nm), in contrast to the hydro-thermally synthesized mixed phase TiO_2. SEM images showed columnar structures of the low angle sputtered mixed phase titania films with visible interfaces among columns and crystals. TEM confirmed the uniform distribution of mixed anatase and rutile indicating high density of interfaces between two phases.

- **The sputtered mixed phase titania photocatalysts showed enhanced photoactivity for both oxidation and reduction reactions compared to mixed phase sol-gel and P25 samples.** The low angle sputtered mixed phase tiania films displayed the highest photoactivity in terms of acetaldehyde oxidation and CO_2 reduction. This is likely due to the high density of solid-solid interfaces in the sputtered mixed phase titania (promotes charge separation resulting in enhanced photocatalytic efficiency). Both optical measurement and EPR characterization revealed oxygen vacancies, that were found to be located at the interfaces by EELS characterization and correlated with reactive interfacial sites. Non-stoichiometry gives rise to the redshifted photoresponse and may

also serve as adsorption sites or recombination centers depending on the concentration to influence the photoactivity.

- **Oxygen vacancies gave rise to the red-shifted photoresponse and had trade-off effects on the photoactivity.** Varied degrees of non-stoichiometric titania films were sputtered by monitoring oxygen partial pressure in the transition mode during deposition process. These non-stoichiometric catalyst films successfully oxidized acetaldehyde under UV conditions and reduced CO_2 to fuel (methane) with the addition of water as a hole scavenger under both UV and visible illumination. In contrast, the P25 coated films showed no reactivity under these conditions. There is an optimal oxygen partial pressure of 0.07 pa at the turning point of transition mode and metal mode to synthesize non-stoichometric titania in terms of CO_2 reduction. The oxygen vacancies likely serve at least three roles: 1)adsorption, 2)trapping active sites and 3)recombination centers. The trade-off effect between these three roles determines an optimal degree of non-stoichiometry of the titania in terms of photocatalytic reactivity. The non-stoichiometric titania films displayed different structure. SEM showed the decreased column size and crystallinity ascribed to restricted atomic mobility and a lack of sufficient oxygen to form crystalline phase for non-stoichiometric films.

- **Modifications of the sputtering process and functional tests were also carried out in my research**. For example, trace nitrogen was added to stabilize the process when I tried to control the oxygen partial pressure at the turning

region of the transition mode and the metal mode. The influence of nitrogen addition to the film surface structure and photoactivity, from low to high concentration was also studied. Trace nitrogen addition increased the mobility and the columns size. The non-stoichiometric titania film synthesized with minimum nitrogen addition for stabilizing the sputtering showed the optimal balance between crystallinity and total interfacial surface areas reflected by the column size resulting in the highest methane production from photoreducing CO_2. Optimization of CO_2 reduction reactor system was studied by monitoring temperature, CO_2 concentration and reactor volume. About 22% CO_2 conversion under UV conditions was achieved for the most reative, mixed phase, non-stoichiometric sputtered tiania under optmized reactor conditions.

Future work will be focused on 1) clarifying the role of oxygen vacancies as reactive interfacial sites; 2) continue searching accurate ways to measure or calculate the surface areas of the sputtered and dip-coated films; 3) further optimize the reaction conditions (light source, water to CO_2 ratio etc.) to increase the CO_2 conversion and try to tailor the reaction for different products other than methane; and 4) identify the visible light range the non-stoichiometric sputtered titania films respond to.

References

[1] *Surface analysis method in materials science*. Springer-Verlag, Heidelberg, 1992.

[2] D. R. Acosta, A. I. Martinez, A. A. Lopez, and C. R. Magana. Titanium dioxide thin films: the effect of the preparation method in their photocatalytic properties. *Journal of Molecular Catalysis A-Chemical*, 228(1-2):183–188, 2005.

[3] Dwight R. Acosta, Arturo Martnez, Carlos R. Magaa, and Jess M. Ortega. Electron and atomic force microscopy studies of photocatalytic titanium dioxide thin films deposited by dc magnetron sputtering. *Thin Solid Films*, 490(2):112–117, 2005.

[4] Kenji Adachi, Kiyohisa Ohta, and Takayuki Mizuno. Photocatalytic reduction of carbon dioxide to hydrocarbon using copper-loaded titanium dioxide. *Solar Energy*, 53(2):187–90, 1994.

[5] D. M. Adams, L. Brus, C. E. D. Chidsey, S. Creager, C. Creutz, C. R. Kagan, P. V. Kamat, M. Lieberman, S. Lindsay, R. A. Marcus, R. M. Metzger, M. E. Michel-Beyerle, J. R. Miller, M. D. Newton, D. R. Rolison, O. Sankey, K. S. Schanze, J. Yardley, and X. Y. Zhu. Charge transfer on the nanoscale: Current status. *Journal of Physical Chemistry B*, 107(28):6668–6697, 2003.

[6] A. G. Agrios, K. A. Gray, and E. Weitz. Narrow-band irradiation of a homologous series of chlorophenols on tio_2: Charge-transfer complex formation and reactivity. *Langmuir*, 20(14):5911–5917, 2004.

[7] Alexander G. Agrios and Kimberly A. Gray. Beyond photocatalytic environmental remediation: Novel TiO_2 materials and applications. *Environmental Catalysis*, pages 369–390, 2005.

[8] Norman S. Allen, Michele Edge, Amaya Ortega, Christopher M. Liauw, John Stratton, and Robert B. McIntyre. Factors affecting the interfacial adsorption of stabilisers on to titanium dioxide particles (flow microcalorimetry, modelling, oxidation and FTIR studies): Nano versus pigmentary grades. *Dyes and Pigments*, 70(3):192–203, 2006.

[9] H. Alouach and G. J. Mankey. Texture orientation of glancing angle deposited copper nanowire arrays. *Journal of Vacuum Science & Technology A*, 22(4):1379–1382, 2004.

[10] S. C. Ameta, R. Chaudhary, R. Ameta, and J. Vardia. Photocatalysis: a promising technology for wastewater treatment. *Journal of the Indian Chemical Society*, 80(4):257–265, 2003.

[11] M. Anpo. Preparation, characterization, and reactivities of highly functional titanium oxide-based photocatalysts able to operate under UV-visible light irradiation: Approaches in realizing high efficiency in the use of visible light. *Bulletin of the Chemical Society of Japan*, 77(8):1427–1442, 2004.

[12] M. Anpo and M. Takeuchi. The design and development of highly reactive titanium oxide photocatalysts operating under visible light irradiation. *Journal of Catalysis*, 216(1-2):505–516, 2003.

[13] Masakazu Anpo, Hiromi Yamashita, Yuichi Ichihashi, and Shaw Ehara. Photocatalytic reduction of CO_2 with H_2O on various titanium oxide catalysts. *Journal of*

Electroanalytical Chemistry, 396(1-2):21–6, 1995.

[14] Lidia Armelao, Davide Barreca, Gregorio Bottaro, Alberto Gasparotto, Silvia Gross, Cinzia Maragno, and Eugenio Tondello. Recent trends on nanocomposites based on cu, ag and au clusters: A closer look. *Coordination Chemistry Reviews*, 250(11+12):1294–1314, 2006.

[15] R. D. Arnell and P. J. Kelly. Recent advances in magnetron sputtering. *Surface & Coatings Technology*, 112(1-3):170–176, 1999.

[16] R. Asahi, T. Morikawa, T. Ohwaki, K. Aoki, and Y. Taga. Visible-light photocatalysis in nitrogen-doped titanium oxides. *Science*, 293(5528):269–271, 2001.

[17] T. Asanuma, T. Matsutani, C. Liu, T. Mihara, and M. Kiuchi. Structural and optical properties of titanium dioxide films deposited by reactive magnetron sputtering in pure oxygen plasma. *Journal of Applied Physics*, 95(11):6011–6016, 2004. Part 1.

[18] J. Augustynski. The role of the surface intermediates in the photoelectrochemical behavior of anatase and rutile TiO_2. *Electrochimica Acta*, 38(1):43–46, 1993.

[19] S. Azad, M. H. Engelhard, and L. Q. Wang. Adsorption and reaction of co and CO_2 on oxidized and reduced $SrTiO_3(100)$ surfaces. *Journal of Physical Chemistry B*, 109(20):10327–10331, 2005.

[20] K. Baba and R. Hatada. Synthesis and properties of TiO_2 thin films by plasma source ion implantation. *Surface & Coatings Technology*, 136(1-3):241–243, 2001.

[21] H. Barankova, S. Berg, P. Carlsson, and C. Nender. Hysteresis effects in the sputtering process using 2 reactive gases. *Thin Solid Films*, 260(2):181–186, 1995.

[22] Y. Bessekhouad, D. Robert, and J. V. Weber. Photocatalytic activity of Cu_2O/TiO_2, Bi_2O_3/TiO_2 and $ZnMn_2O_4/TiO_2$ heterojunctions. *Catalysis Today*, 101(3-4):315–321, 2005.

[23] S. Bhaumik, P. Mondal, and A. K. Barua. The influence of hydrogen gas in the ambient gas mixture on the properties of indium tin oxide films deposited on glass and acrylic substrates by dc magnetron sputtering. *Journal of Physics D-Applied Physics*, 39(17):3838–3843, 2006.

[24] G. Binnig, C. F. Quate, and C. Gerber. Atomic force microscope. *Physical Review Letters*, 56(9):930–933, 1986.

[25] R. Brahimi, Y. Bessekhouad, A. Bouguelia, and M. Trari. Improvement of eosin visible light degradation using pbS-sensititized TiO_2. *Journal of Photochemistry and Photobiology a-Chemistry*, 194(2-3):173–180, 2008.

[26] D. Brinkley and T. Engel. Evidence for structure sensitivity in the thermally activated and photocatalytic dehydrogenation of 2-propanol on TiO_2. *Journal of Physical Chemistry B*, 104(42):9836–9841, 2000.

[27] J. Chen, D. F. Ollis, W. H. Rulkens, and H. Bruning. Photocatalyzed oxidation of alcohols and organochlorides in the presence of native TiO_2 and metallized TiO_2 suspensions. part (i): Photocatalytic activity and ph influence. *Water Research*, 33(3):661–668, 1999.

[28] L. Chen, M. E. Graham, G. Li, D. R. Gentner, and K. A. Gray. Photoreduction of CO_2 by TiO_2 nanocomposties synthesized through reactive dc magnetron sputter deposition. *Thin Solid Films*, in review, 2008.

[29] Le Chen, Michael E. Graham, Gonghu Li, and Kimberly A. Gray. Fabricating highly active mixed-phase TiO_2 photocatalysts by reactive DC magnetron sputter deposition. *Thin Solid Films*, 515(3):1176–1181, 2006.

[30] S. Z. Chen, P. Y. Zhang, D. M. Zhuang, and W. P. Zhu. Investigation of nitrogen doped TiO_2 photocatalytic films prepared by reactive magnetron sputtering. *Catalysis Communications*, 5(11):677–680, 2004.

[31] Y. Chihara, K. Fujimoto, H. Kondo, Y. Moriwaka, T. Sasahira, Y. Hirao, and H. Kuniyasu. Anti-tumor effects of liposome-encapsulated titanium dioxide in nude mice. *Pathobiology*, 74(6):353–358, 2007.

[32] Y. L. Choi, S. H. Kim, Y. S. Song, and D. Y. Lee. Photodecomposition and bactericidal effects of TiO_2 thin films prepared by a magnetron sputtering. *Journal of Materials Science*, 39(18):5695–5699, 2004.

[33] C. Colbeau-Justin, M. Kunst, and D. Huguenin. Structural influence on charge-carrier lifetimes in TiO_2 powders studied by microwave absorption. *Journal of Materials Science*, 38(11):2429–2437, 2003.

[34] B. Dick, M. J. Brett, T. J. Smy, M. R. Freeman, M. Malac, and R. F. Egerton. Periodic magnetic microstructures by glancing angle deposition. *Journal of Vacuum Science & Technology a-Vacuum Surfaces and Films*, 18(4):1838–1844, 2000.

[35] D. Dimova-Malinovska, H. Nichev, O. Angelov, V. Grigorov, and A. Kamenova. Electrical and optical properties of zno thin films prepared by magnetron rf sputtering - influence of al, er and h. *Superlattices and Microstructures*, 42(1-6):123–128, 2007.

[36] DOE. "basic research needs for solar energy utilization", report of the 2005 basic energy sciences workshop on solar energy utilization. 2005.

[37] C. F Doodeve and J. A Kitchener. *Trans. Faraday Soc.*, 34:902, 1938.

[38] Ray F. Egerton. *Physical Principles of Electron Microscopy: An Introduction to TEM, SEM, and AEM.* Springer, 2008.

[39] R.F. Egerton. *Electron Energy-Loss Spectroscopy in the Electron Microscope.* Springer, 2nd edition, 1996.

[40] A. V. Emeline, V. K. Ryabchuk, and N. Serpone. Photoreactions occurring on metal-oxide surfaces are not all photocatalytic. *Catalysis Today*, 122(1-2):91–100, 2007.

[41] A. V. Emeline, N. V. Sheremetyeva, N. V. Khomchenko, V. K. Ryabchuk, and N. Serpone. Photoinduced formation of defects and nitrogen stabilization of color centers in n-doped titanium dioxide. *Journal of Physical Chemistry C*, 111(30):11456–11462, 2007.

[42] E. Finazzi, C. Di Valentin, A. Selloni, and G. Pacchioni. First principles study of nitrogen doping at the anatase TiO_2(101) surface. *Journal of Physical Chemistry C*, 111(26):9275–9282, 2007.

[43] M. A. Fox and M. T. Dulay. Heterogeneous photocatalysis. *Chemical Reviews*, 93(1):341–357, 1993.

[44] P. Frach, U. Heisig, C. Gottfried, and H. Walde. Aspects and results of long-term stable deposition of Al_2O_3 with high-rate pulsed reactive magnetron sputtering. *Surface & Coatings Technology*, 59(1-3):177–182, 1993.

[45] X. Fu, W. A. Zeltner, and M. A. Anderson. Applications in photocatalytic purification of air. In *Semiconductor Nanoclusters- Physical, Chemical, and Catalytic Aspects*, volume 103 of *Studies in Surface Science and Catalysis*, pages 445–461. 1997.

[46] A Fujishima and K. Honda. Electrochemical photolysis of water at a semiconductor electrode. *Nature*, 238(5358):37–38, 1972.

[47] S. Fukahori, Y. Iguchi, H. Ichiura, T. Kitaoka, H. Tanaka, and H. Wariishi. Effect of void structure of photocatalyst paper on voc decomposition. *Chemosphere*, 66(11):2136–2141, 2007.

[48] A. R. Gandhe and J. B. Fernandes. A simple method to synthezise N-doped rutile titania with enhanced photocatalytic activity in sunlight. *Journal of Solid State Chemistry*, 178(9):2953–2957, 2005.

[49] M. Vernica Ganduglia-Pirovano, Alexander Hofmann, and Joachim Sauer. Oxygen vacancies in transition metal and rare earth oxides: Current state of understanding and remaining challenges. *Surface Science Reports*, 62(6):219–270, 2007.

[50] L. Ge, M. X. Xu, and H. B. Fang. Photo-catalytic degradation of methyl orange and formaldehyde by Ag/InVO4-TiO2 thin films under visible-light irradiation. *Journal of Molecular Catalysis a-Chemical*, 258(1-2):68–76, 2006.

[51] P. R. Gogate and A. B. Pandit. A review of imperative technologies for wastewater treatment I: oxidation technologies at ambient conditions. *Advances in Environmental Research*, 8(3-4):501–551, 2004.

[52] P. R. Gogate and A. B. Pandit. Sonophotocatalytic reactors for wastewater treatment: A critical review. *Aiche Journal*, 50(5):1051–1079, 2004.

[53] M. Gopal, W. J. M. Chan, and L. C. DeJonghe. Room temperature synthesis of crystalline metal oxides. *Journal of Materials Science*, 32(22):6001–6008, 1997.

[54] D. Y. Goswami. A review of engineering developments of aqueous phase solar photocatalytic detoxification and disinfection processes. *Journal of Solar Energy Engineering-Transactions of the Asme*, 119(2):101–107, 1997.

[55] M. Gratzel. Mesoporous oxide junctions and nanostructured solar cells. *Current Opinion in Colloid & Interface Science*, 4(4):314–321, 1999.

[56] Michael Gratzel. Photoelectrochemical cells. *Nature*, 414(6861):338–344, 2001.

[57] G. R. Gu, Y. A. Li, Y. C. Tao, Z. He, J. J. Li, H. Yin, W. Q. Li, and Y. N. Zhao. Investigation on the structure of TiO_2 films sputtered on alloy substrates. *Vacuum*, 71(4):487–490, 2003.

[58] C. Guillard, J. Disdier, J. M. Herrmann, C. Lehaut, T. Chopin, S. Malato, and J. Blanco. Comparison of various titania samples of industrial origin in the solar photocatalytic detoxification of water containing 4-chlorophenol. *Catalysis Today*, 54(2-3):217–228, 1999.

[59] G. L. Haller. New catalytic concepts from new materials: understanding catalysis from a fundamental perspective, past, present, and future. *Journal of Catalysis*, 216(1-2):12–22, 2003.

[60] G. He, L. D. Zhang, G. H. Li, M. Liu, and X. J. Wang. Structure, composition and evolution of dispersive optical constants of sputtered TiO_2 thin films: effects of nitrogen doping. *Journal of Physics D-Applied Physics*, 41(4), 2008.

[61] J. M. Herrmann. Heterogeneous photocatalysis: fundamentals and applications to the removal of various types of aqueous pollutants. *Catalysis Today*, 53(1):115–129,

1999.

[62] M. Higuchi, S. Uekusa, R. Nakano, and K. Yokogawa. Micrograin structure influence on electrical characteristics of sputtered indium tin oxide-films. *Journal of Applied Physics*, 74(11):6710–6713, 1993.

[63] M. R. Hoffmann, S. T. Martin, W. Y. Choi, and D. W. Bahnemann. Environmental applications of semiconductor photocatalysis. *Chemical Reviews*, 95(1):69–96, 1995.

[64] N. Y. Hong, J. Sakai, and A. Hassini. Ferromagnetism at room temperature with a large magnetic moment in anatase V-doped TiO_2 thin films. *Applied Physics Letters*, 84(14):2602–2604, 2004.

[65] D. C. Hurum, A. G. Agrios, S. E. Crist, K. A. Gray, T. Rajh, and M. C. Thurnauer. Probing reaction mechanisms in mixed phase TiO_2 by EPR. *Journal of Electron Spectroscopy and Related Phenomena*, 150:155–163, 2006.

[66] D. C. Hurum, A. G. Agrios, K. A. Gray, T. Rajh, and M. C. Thurnauer. Explaining the enhanced photocatalytic activity of degussa P25 mixed-phase TiO_2 using EPR. *Journal of Physical Chemistry B*, 107(19):4545–4549, 2003.

[67] D. C. Hurum, K. A. Gray, T. Rajh, and M. C. Thurnauer. Photoinitiated reactions of 2,4,6 TCP on degussa P25 formulation TiO_2: Wavelength-sensitive decomposition. *Journal of Physical Chemistry B*, 108(42):16483–16487, 2004.

[68] D. C. Hurum, K. A. Gray, T. Rajh, and M. C. Thurnauer. Recombination pathways in the degussa P25 formulation of TiO_2: Surface versus lattice mechanisms. *Journal of Physical Chemistry B*, 109(2):977–980, 2005.

[69] Jin-Soo Hwang, Jong-San Chang, Sang-Eon Park, Keita Ikeue, and Masakazu Anpo. Photoreduction of carbondioxide on surface functionalized nanoporous catalysts.

Topics in Catalysis, 35(3-4):311–319, 2005.

[70] K. Iijima, M. Goto, S. Enomoto, H. Kunugita, K. Ema, M. Tsukamoto, N. Ichikawa, and H. Sakama. Influence of oxygen vacancies on optical properties of anatase TiO_2 thin films. *Journal of Luminescence*, 128(5-6):911–913, 2008.

[71] S. In, A. Orlov, F. Garcia, M. Tikhov, D. S. Wright, and R. M. Lambert. Efficient visible light-active N-doped TiO_2 photocatalysts by a reproducible and controllable synthetic route. *Chemical Communications*, (40):4236–4238, 2006.

[72] T. Inoue, A. Fujishima, S. Konishi, and K. Honda. Photoelectrocatalytic reduction of carbon-dioxide in aqueous suspensions of semiconductor powders. *Nature*, 277(5698):637–638, 1979.

[73] H. Irie, Y. Watanabe, and K. Hashimoto. Carbon-doped anatase TiO_2 powders as a visible-light sensitive photocatalyst. *Chemistry Letters*, 32(8):772–773, 2003.

[74] H. Irie, Y. Watanabe, and K. Hashimoto. Nitrogen-concentration dependence on photocatalytic activity of $TiO_{2-x}N_x$ powders. *Journal of Physical Chemistry B*, 107(23):5483–5486, 2003.

[75] I. Justicia, G. Garcia, G. A. Battiston, R. Gerbasi, F. Ager, M. Guerra, J. Caixach, J. A. Pardo, J. Rivera, and A. Figueras. Photocatalysis in the visible range of sub-stoichiometric anatase films prepared by MOCVD. *Electrochimica Acta*, 50(23):4605–4608, 2005.

[76] K. Kabra, R. Chaudhary, and R. L. Sawhney. Treatment of hazardous organic and inorganic compounds through aqueous-phase photocatalysis: A review. *Industrial & Engineering Chemistry Research*, 43(24):7683–7696, 2004.

[77] P. V. Kamat. Photoinduced transformations in semiconductor-metal nanocomposite assemblies. *Pure and Applied Chemistry*, 74(9):1693–1706, 2002.

[78] N. Kanai, T. Nuida, K. Ueta, K. Hashimoto, T. Watanabe, and H. Ohsaki. Photocatalytic efficiency of TiO_2/snO2 thin film stacks prepared by DC magnetron sputtering. *Vacuum*, 74(3-4):723–727, 2004.

[79] Satoshi Kaneco, Hidekazu Kurimoto, Kiyohisa Ohta, Takayuki Mizumo, and Akira Saji. Photocatalytic reduction of CO_2 using TiO_2 powders in liquid CO_2 medium. *Journal of Photochemistry and Photobiology, A: Chemistry*, 109(1):59–63, 1997.

[80] M. Kanna and S. Wongnawa. Mixed amorphous and nanocrystalline TiO_2 powders prepared by sol-gel method: Characterization and photocatalytic study. *Materials Chemistry and Physics*, 110(1):166–175, 2008.

[81] H. R. Kaufman, J. J. Cuomo, and J. M. E. Harper. Technology and applications of broad-beam ion sources used in sputtering. part i. ion source technology. *J. Vac. Sci. Technol.*, 21:725–736, 1982.

[82] T. Kawahara, Y. Konishi, H. Tada, N. Tohge, J. Nishii, and S. Ito. A patterned TiO_2(anatase)/TiO_2(rutile) bilayer-type photocatalyst: Effect of the anatase/rutile junction on the photocatalytic activity. *Angewandte Chemie-International Edition*, 41(15):2811–2813, 2002.

[83] E. Keidel. Die beeinflussung der lichtechtheit von teerfarblacken durch titanweiss [influence of titanium white on the fastness to light of coal-tar days]. *Farben-Zeitung*, 34:1242–1243, 1929.

[84] V. Keller, P. Bernhardt, and F. Garin. Photocatalytic oxidation of butyl acetate in vapor phase on TiO_2, pt/TiO_2 and WO_3/TiO_2 catalysts. *Journal of Catalysis*,

215(1):129–138, 2003.

[85] J. M. Kesselman, O. Weres, N. S. Lewis, and M. R. Hoffmann. Electrochemical production of hydroxyl radical at polycrystalline nb-doped TiO_2 electrodes and estimation of the partitioning between hydroxyl radical and direct hole oxidation pathways. *Journal of Physical Chemistry B*, 101(14):2637–2643, 1997.

[86] Hisashi Kikuchi, Masaaki Kitano, Masato Takeuchi, Masaya Matsuoka, Masakazu Anpo, and Prashant V. Kamat. Extending the photoresponse of TiO_2 to the visible light region: Photoelectrochemical behavior of TiO_2 thin films prepared by the radio frequency magnetron sputtering deposition method. *Journal of Physical Chemistry B*, 110(11):5537–5541, 2006.

[87] J. H. Kim, S. Lee, and H. S. Im. The effect of different ambient gases, pressures, and substrate temperatures on tio2 thin films grown on Si(100) by laser ablation technique. *Applied Physics a-Materials Science & Processing*, 69:S629–S632, 1999. Suppl. S.

[88] M. Kitano, K. Funatsu, M. Matsuoka, M. Ueshima, and M. Anpo. Preparation of nitrogen-substituted TiO_2 thin film photocatalysts by the radio frequency magnetron sputtering deposition method and their photocatalytic reactivity under visible light irradiation. *Journal of Physical Chemistry B*, 110(50):25266–25272, 2006.

[89] H. Kloepfer and patent 762723 AG. Degussa, 1942.

[90] S. Klosek and D. Raftery. Visible light driven V-doped TiO_2 photocatalyst and its photooxidation of ethanol. *Journal of Physical Chemistry B*, 105(14):2815–2819, 2001.

[91] H. Kominami, M. Kohno, and Y. Kera. Synthesis of brookite-type titanium oxide nano-crystals in organic media. *Journal of Materials Chemistry*, 10(5):1151–1156, 2000.

[92] M. Komiyama and Y. J. Li. Photoresponse of surface oxygen defects on TiO_2(110). *Applied Surface Science*, 244(1-4):550–553, 2005.

[93] G. W. Kriechbaum and P. Kleinschmit. Superfine oxide powders -flame hydrolysis and hydrothermal synthesis. *Angewandte Chemie-International Edition in English*, 28(10):1416–1423, 1989.

[94] Y. Ku, R. M. Leu, and K. C. Lee. Decomposition of 2-chlorophenol in aqueous solution by UV irradiation with the presence of titanium dioxide. *Water Research*, 30(11):2569–2578, 1996.

[95] C. C. Lee, H. C. Chen, and C. C. Jaing. Effect of thermal annealing on the optical properties and residual stress of TiO_2 films produced by ion-assisted deposition. *Applied Optics*, 44(15):2996–3000, 2005.

[96] B. Levy. Photochemistry of nanostructured materials for energy applications. *Journal of Electroceramics*, 1(3):239–272, 1997.

[97] Nathan S. Lewis. Photochemistry: Light work with water. *Nature (London, United Kingdom)*, 414(6864):589–590, 2001.

[98] P. Lőbl, M. Huppertz, and D. Mergel. Nucleation and growth in TiO_2 films prepared by sputtering and evaporation. *Thin Solid Films*, 251(1):72–79, 1994.

[99] D. Li, H. Haneda, S. Hishita, N. Ohashi, and N. K. Labhsetwar. Fluorine-doped TiO_2 powders prepared by spray pyrolysis and their improved photocatalytic activity for decomposition of gas-phase acetaldehyde. *Journal of Fluorine Chemistry*,

126(1):69–77, 2005.

[100] G. Li, N.M. Dimitrijevic, L. Chen, T. Rajh, and K.A. Gray. Role of surface/interfacial Cu_2^+ sites in the photocatalytic activity of coupled CuO−TiO_2 nanocomposites. *Journal of Physical Chemistry C*, 2008.

[101] Gonghu Li, Le Chen, Michael E. Graham, and Kimberly A. Gray. A comparison of mixed phase titania photocatalysts prepared by physical and chemical methods: The importance of the solid-solid interface. *Journal of Molecular Catalysis A: Chemical*, 275:30–35, 2007.

[102] Gonghu Li, Shannon Ciston, Le Chen, Nada Dimitrijevic, Tijana Rajh, and Kimberly A. Gray. Synthesizing mixed phase TiO_2 nanocomposites using a hydrothermal method for photooxidation and photoreduction applications. *Journal of Catalysis*, 253:105–110, 2008.

[103] Gonghu. Li and Kimberly A. Gray. Photochemical properties of anion-doped TiO_2 photocatalysts prepared from a molecular nitrogen-containing titanium precursor. *Applied Catalysis B: Environmental*, page Under review, 2007.

[104] Gonghu. Li and Kimberly A. Gray. The solid-solid interface: Explaining the high and unique photocatalytic reactivity of TiO_2-based nanocomposite materials. *Chemical Physics*, 339:173–187, 2007.

[105] Y. Li, T. J. White, and S. H. Lim. Low-temperature synthesis and microstructural control of titania nano-particles. *Journal of Solid State Chemistry*, 177(4-5):1372–1381, 2004.

[106] Y. Li, T. J. White, and S. H. Lim. Low-temperature synthesis and microstructural control of titania nano-particles. *Journal of Solid State Chemistry*, 177(4-5):1372–1381, 2004.

[107] Y. Z. Li, D. S. Hwang, N. H. Lee, and S. J. Kim. Synthesis and characterization of carbon-doped titania as an artificial solar light sensitive photocatalyst. *Chemical Physics Letters*, 404(1-3):25–29, 2005.

[108] T. Lindgren, J. M. Mwabora, E. Avendano, J. Jonsson, A. Hoel, C. G. Granqvist, and S. E. Lindquist. Photoelectrochemical and optical properties of nitrogen doped titanium dioxide films prepared by reactive DC magnetron sputtering. *Journal of Physical Chemistry B*, 107(24):5709–5716, 2003.

[109] A. L. Linsebigler, G. Q. Lu, and J. T. Yates. Photocatalysis on TiO_2 surfaces - principles, mechanisms, and selected results. *Chemical Reviews*, 95(3):735–758, 1995.

[110] B. S. Liu, L. P. Wen, and X. J. Zhao. The structure and photocatalytic studies of N-doped TiO_2 films prepared by radio frequency reactive magnetron sputtering. *Solar Energy Materials and Solar Cells*, 92(1):1–10, 2008.

[111] Bi-Jin Liu, Tsukasa Torimoto, and Hiroshi Yoneyama. Photocatalytic reduction of carbon dioxide in the presence of nitrate using TiO_2 nanocrystal photocatalyst embedded in SiO2 matrixes. *Journal of Photochemistry and Photobiology, A: Chemistry*, 115(3):227–230, 1998.

[112] Stefano Livraghi, Maria Cristina Paganini, Elio Giamello, Annabella Selloni, Cristiana Di Valentin, and Gianfranco Pacchioni. Origin of photoactivity of nitrogen-doped titanium dioxide under visible light. *Journal of the American Chemical Society*, 128(49):15666–15671, 2006.

[113] H. M. Luo, C. Wang, and Y. S. Yan. Synthesis of mesostructured titania with controlled crystalline framework. *Chemistry of Materials*, 15(20):3841–3846, 2003.

[114] W. Ma, Z. Lu, and M. Zhang. Investigation of structural transformations in nanophase titanium dioxide by raman spectroscopy. *Applied Physics a-Materials Science & Processing*, 66(6):621–627, 1998.

[115] M. A. Malati and W. K. Wong. Doping titanium dioxide for solar energy applications. *Surface Technology*, 22(4):305–22, 1984.

[116] A. Markovits, B. Mguig, M. Calatayud, and C. Minot. Spin localization for NO adsorption on surface O atoms of metal oxides. *Catalysis Today*, 113(3-4):201–207, 2006.

[117] N. Martin, C. Rousselot, D. Rondot, F. Palmino, and R. Mercier. Microstructure modification of amorphous titanium oxide thin films during annealing treatment. *Thin Solid Films*, 300(1-2):113–121, 1997.

[118] P. J. Martin. Ion-based methods for optical thin-film deposition. *Journal of Materials Science*, 21(1):1–25, 1986.

[119] M. Matsuoka, M. Kitano, M. Takeuchi, M. Anpo, and J. M. Thomas. Photocatalytic water splitting on visible light-responsive TiO_2 thin films prepared by a RF magnetron sputtering deposition method. *Topics in Catalysis*, 35(3-4):305–310, 2005.

[120] M. Matsuoka, M. Kitano, M. Takeuchi, K. Tsujimaru, M. Anpo, and J. M. Thomas. Photocatalysis for new energy production - recent advances in photocatalytic water splitting reactions for hydrogen production. *Catalysis Today*, 122(1-2):51–61, 2007.

[121] R. W. Matthews. Photooxidation of organic impurities in water using thin-films of titanium-dioxide. *Journal of Physical Chemistry*, 91(12):3328–3333, 1987.

[122] T. Miyata, S. Tsukada, and T. Minami. Preparation of anatase TiO_2 thin films by vacuum are plasma evaporation. *Thin Solid Films*, 496(1):136–140, 2006.

[123] P. T. Moseley. Materials selection for semiconductor gas sensors. *Sensors and Actuators B-Chemical*, 6(1-3):149–156, 1992.

[124] J. A. Navio, G. Colon, M. Trillas, J. Peral, X. Domenech, J. J. Testa, J. Padron, D. Rodriguez, and M. I. Litter. Heterogeneous photocatalytic reactions of nitrite oxidation and Cr(VI) reduction on iron-doped titania prepared by the wet impregnation method. *Applied Catalysis B-Environmental*, 16(2):187–196, 1998.

[125] J. A. Navio, J. J. Testa, P. Djedjeian, J. R. Padron, D. Rodriguez, and M. I. Litter. Iron-doped titania powders prepared by a sol-gel method. part II: Photocatalytic properties. *Applied Catalysis a-General*, 178(2):191–203, 1999.

[126] D. Noguchi, Y. Kawamata, and T. Nagatomo. Relationship between the photocatalytic characteristics and the oxygen partial pressure of TiO_2 thin films prepared by a DC reactive sputtering method. *Japanese Journal of Applied Physics Part 1-Regular Papers Short Notes & Review Papers*, 43(4A):1581–1585, 2004.

[127] C. Nouvellon, J. P. Dauchot, M. Hecq, and H. Cornil. Chromium reactive sputtering in argon-oxygen and argon-water vapor mixtures. *Surface & Coatings Technology*, 200(1-4):425–430, 2005.

[128] E. Obuchi, T. Sakamoto, K. Nakano, and F. Shiraishi. Photocatalytic decomposition of acetaldehyde over $TiO_{2/}SiO_2$ catalyst. *Chemical Engineering Science*, 54(10):1525–1530, 1999.

[129] B. Oregan and M. Gratzel. A low-cost, high-efficiency solar-cell based on dye-sensitized colloidal TiO_2 films. *Nature*, 353(6346):737–740, 1991.

[130] James Ovenstone and Kazumichi Yanagisawa. Effect of hydrothermal treatment of amorphous titania on the phase change from anatase to rutile during calcination. *Chemistry of Materials*, 11(10):2770–2774, 1999.

[131] I. P. Parkin and R. G. Palgrave. Self-cleaning coatings. *Journal of Materials Chemistry*, 15(17):1689–1695, 2005.

[132] F. Peng and Y. Q. Ren. Preparation of nano-TiO_2-SnO_2 composite film and its photocatalytic activity for toluene degradation. *Chinese Journal of Catalysis*, 24(4):243–247, 2003.

[133] V. Pore, M. Heikkila, M. Ritala, M. Leskela, and S. Areva. Atomic layer deposition of $TiO_2{-}xN_x$ thin films for photocatalytic applications. *Journal of Photochemistry and Photobiology a-Chemistry*, 177(1):68–75, 2006.

[134] K. Prabakar, T. Takahashi, T. Nezuka, T. Nakashima, Y. Kubota, and A. Fujishima. Effect of nitrogen on the photocatalytic activity of TiO_xN_y thin films. *Journal of Vacuum Science & Technology A*, 24(4):1156–1160, 2006.

[135] V. Randle and Olaf Engler. *Introduction to Texture Analysis*. CRC Press, 2008.

[136] K. S. Rane, R. Mhalsiker, S. Yin, T. Sato, K. Cho, E. Dunbar, and P. Biswas. Visible light-sensitive yellow $TiO_{2-x}N_x$ and Fe-N co-doped $Ti_{1-y}Fe_yO_{2-x}N_x$ anatase photocatalysts. *Journal of Solid State Chemistry*, 179(10):3033–3044, 2006.

[137] G. Riegel and J. R. Bolton. Photocatalytic efficiency variability in TiO_2 particles. *Journal of Physical Chemistry*, 99(12):4215–4224, 1995.

[138] K. Robbie and M. J. Brett. Sculptured thin films and glancing angle deposition: Growth mechanics and applications. *Journal of Vacuum Science & Technology a-Vacuum Surfaces and Films*, 15(3):1460–1465, 1997.

[139] A. I. Rogozin, M. V. Vinnichenko, A. Kolitsch, and W. Moller. Effect of deposition parameters on properties of ito films prepared by reactive middle frequency pulsed dual magnetron sputtering. *Journal of Vacuum Science & Technology A*, 22(2):349–355, 2004.

[140] A. M. Ruiz, G. Dezanneau, J. Arbiol, A. Cornet, and J. R. Morante. Insights into the structural and chemical modifications of Nb additive on TiO_2 nanoparticles. *Chemistry of Materials*, 16(5):862–871, 2004.

[141] H. Sadiki, J. F. Pierson, C. Rousselot, N. Martin, and G. Terwagne. Properties and electrochromic performances of reactively sputtered tungsten oxide films with water as reactive gas. *Surface & Coatings Technology*, 200(1-4):232–235, 2005.

[142] Y. Sakai and S. Ehara. Scanning tunneling microscopy/spectroscopy study of point defects on TiO_2(110)-(1 x 1) surface. *Japanese Journal of Applied Physics Part 2-Letters*, 40(7B):L773–L775, 2001.

[143] T. Sakata and T. Kawai. Heterogeneous photocatalytic production of hydrogen and methane from ethanol and water. *Chemical Physics Letters*, 80(2):341–344, 1981.

[144] Franz Saladin and Ivo Alxneit. Temperature dependence of the photochemical reduction of CO_2 in the presence of H_2O at the solid/gas interface of TiO_2. *Journal of the Chemical Society, Faraday Transactions*, 93(23):4159–4163, 1997.

[145] T. Sano, N. Negishi, K. Uchino, J. Tanaka, S. Matsuzawa, and K. Takeuchi. Photocatalytic degradation of gaseous acetaldehyde on TiO_2 with photodeposited metals and metal oxides. *Journal of Photochemistry and Photobiology a-Chemistry*, 160(1-2):93–98, 2003.

[146] P. A. Sant and P. V. Kamat. Interparticle electron transfer between size-quantized cdS and TiO_2 semiconductor nanoclusters. *Physical Chemistry Chemical Physics*, 4(2):198–203, 2002.

[147] Natarajan Sasirekha, Sheikh John Sardhar Basha, and Kannan Shanthi. Photocatalytic performance of ru doped anatase mounted on silica for reduction of carbon dioxide. *Applied Catalysis, B: Environmental*, 62(1-2):169–180, 2006.

[148] S. Satapathy and K. B. R. Varma. Orientated nano grain growth and effect of annealing on grain size in $LiTaO_3$ thin films deposited by sol-gel technique. *Journal of Crystal Growth*, 291(1):232–238, 2006.

[149] C. M. Schmidt, E. Weitz, and F. M. Geiger. Interaction of the indoor air pollutant acetone with Degussa P25 TiO2 studied by chemical ionization mass spectrometry. *Langmuir*, 22(23):9642–9650, 2006.

[150] R. A. Scholl. In *37th Annual Technical Conference Proceedings, Society of Vacuum Coaters*, page 312, Albuquerque, NM, 1994.

[151] Klaus K. Schuegraf. *Handbook of Thin-film Deposition Processes and Techniques*. Noyes Publications, New Jersey, 1988.

[152] N. Serpone. Is the band gap of pristine TiO_2 narrowed by anion- and cation-doping of titanium dioxide in second-generation photocatalysts? *J. Phys. Chem. B*, 110(48):24287–24293, 2006.

[153] N. Serpone, P. Maruthamuthu, P. Pichat, E. Pelizzetti, and H. Hidaka. Exploiting the interparticle electron-transfer process in the photocatalyzed oxidation of phenol, 2-chlorophenol and pentachlorophenol - chemical evidence for electron and hole transfer between coupled semiconductors. *Journal of Photochemistry and Photobiology a-Chemistry*, 85(3):247–255, 1995.

[154] D. Severin, O. Kappertz, T. Kubart, T. Nyberg, S. Berg, A. Pflug, M. Siemers, and M. Wuttig. Process stabilization and increase of the deposition rate in reactive sputtering of metal oxides and oxynitrides. *Applied Physics Letters*, 88(16), 2006.

[155] A. Shiga, A. Tsujiko, S. Yae, and Y. Nakato. High photocurrent quantum yields in short wavelengths for nanocrystalline anatase-type TiO_2 film electrodes compared with those for rutile-type. *Bulletin of the Chemical Society of Japan*, 71(9):2119–2125, 1998.

[156] M. Shui, L. H. Yue, and Z. D. Xu. Photocatalytic activity of iron doping TiO_2 prepared by several methods. *Acta Physico-Chimica Sinica*, 17(3):282–285, 2001.

[157] V. P. Solntsev and E. G. Tsvetkov. Absorption and EPR spectra of $KTiOPO_4$ crystals. *Inorganic Materials*, 33(10):1055–1057, 1997.

[158] G. A. Somorjai. The catalytic nanodiode. its role in catalytic reaction mechanisms in a historical perspective. *Catalysis Letters*, 101(1-2):1–3, 2005.

[159] Iis Sopyan. Kinetic analysis on photocatalytic degradation of gaseous acetaldehyde, ammonia and hydrogen sulfide on nanosized porous TiO_2 films. *Science and Technology of Advanced Materials*, 8(1-2):33–39, 2007.

[160] W. D. Sproul, D. J. Christie, and D. C. Carter. Control of reactive sputtering processes. *Thin Solid Films*, 491(1-2):1–17, 2005.

[161] W. D. Sproul, M. E. Graham, M. S. Wong, S. Lopez, D. Li, and R. A. Scholl. Reactive direct-current magnetron sputtering of aluminum-oxide coatings. *Journal of Vacuum Science & Technology a-Vacuum Surfaces and Films*, 13(3):1188–1191, 1995.

[162] W. D. Sproul, M. E. Graham, M. S. Wong, and P. J. Rudnik. Reactive dc magnetron sputtering of the oxides of Ti, Zr, and Hf . *Surface & Coatings Technology*, 89(1-2):10–15, 1997.

[163] R. A. Spurr and H. Myers. Quantitative analysis of anatase-rutile mixtures with an x-ray diffractometer. *Analytical Chemistry*, 29(5):760–762, 1957.

[164] U Stafford, KA Gray, PV Kamat, and A. Varma. An insitu diffuse reflectance FTIR investigation of photocatalytic degradation of 4-chlorophenol on a TiO_2 power surface. *Chem. Phys.Lett.*, 205, 1993.

[165] T. Sumita, T. Yamaki, S. Yamamoto, and A. Miyashita. Photo-induced surface charge separation of highly oriented TiO_2 anatase and rutile thin films. *Applied Surface Science*, 200(1-4):21–26, 2002.

[166] B. Sun, A. V. Vorontsov, and P. G. Smirniotis. Role of platinum deposited on TiO_2 in phenol photocatalytic oxidation. *Langmuir*, 19(8):3151–3156, 2003.

[167] K. Sunada, Y. Kikuchi, K. Hashimoto, and A. Fujishima. Bactericidal and detoxification effects of TiO_2 thin film photocatalysts. *Environmental Science & Technology*, 32(5):726–728, 1998.

[168] S. Takeda, S. Suzuki, H. Odaka, and H. Hosono. Photocatalytic TiO_2 thin film deposited onto glass by DC magnetron sputtering. *Thin Solid Films*, 392(2):338–344, 2001.

[169] Qi Tang, Kazuo Kikuchi, Shigetaro Ogura, and Angus Macleod. Mechanism of columnar microstructure growth in titanium oxide thin films deposited by ion-beam assisted deposition. *Journal of Vacuum Science & Technology A: Vacuum, Surfaces, and Films*, 17(6):3379–3384, 1999.

[170] Tracy L. Thompson and Jr. Yates, John T. TiO_2-based photocatalysis: Surface defects, oxygen and charge transfer. *Topics in Catalysis*, 35(3-4):197–210, 2005.

[171] H. Tomaszewski, K. Eufinger, H. Poelman, D. Poelman, R. De Gryse, P. F. Smet, and G. B. Marin. Effect of substrate sodium content on crystallization and photocatalytic activity of TiO_2 films prepared by dc magnetron sputtering. *International Journal of Photoenergy*, 2007.

[172] T. Torimoto, R. J. Fox, and M. A. Fox. Photoelectrochemical doping of TiO_2 particles and the effect of charge carrier density on the photocatalytic activity of microporous semiconductor electrode films. *Journal of the Electrochemical Society*, 143(11):3712–3717, 1996.

[173] G. R. Torres, T. Lindgren, J. Lu, C. G. Granqvist, and S. E. Lindquist. Photoelectrochemical study of nitrogen-doped titanium dioxide for water oxidation. *Journal of Physical Chemistry B*, 108(19):5995–6003, 2004.

[174] I. Hsiang Tseng and Jeffrey C. S. Wu. Chemical states of metal-loaded titania in the photoreduction of CO_2. *Catalysis Today*, 97(2-3):113–119, 2004.

[175] T. Umebayashi, T. Yamaki, H. Itoh, and K. Asai. Band gap narrowing of titanium dioxide by sulfur doping. *Applied Physics Letters*, 81(3):454–456, 2002.

[176] T. Umebayashi, T. Yamaki, T. Sumita, S. Yamamoto, S. Tanaka, and K. Asai. UV-ray photoelectron and ab initio band calculation studies on electronic structures

of cr- or nb-ion implanted titanium dioxide. *Nuclear Instruments & Methods in Physics Research Section B-Beam Interactions with Materials and Atoms*, 206:264–267, 2003.

[177] Phairat Usubharatana, Dena McMartin, Amornvadee Veawab, and Paitoon Tontiwachwuthikul. Photocatalytic process for CO_2 emission reduction from industrial flue gas streams. *Industrial & Engineering Chemistry Research*, 45(8):2558–2568, 2006.

[178] C. Di Valentin, G. Pacchioni, A. Selloni, S. Livraghi, and E. Giamello. Characterization of paramagnetic species in N-doped TiO_2 powders by EPR spectroscopy and DFT calculations. *Journal of Physical Chemistry B*, 109(23):11414–11419, 2005.

[179] John C. Vickerman and David Briggs. *ToF-SIMS:Surface Analysis by Mass Spectrometry*. IM Publications, 2001.

[180] V.Ondok and J. Musil. Effect of hydrogen on reactive sputtering of transparent oxide films. *Plasma Processes and Polymers*, 4(S1):S319–S324, 2007.

[181] E. Wallin, J. M. Andersson, M. Lattemann, and U. Helmersson. Influence of residual water on magnetron sputter deposited crystalline al2o3 thin films. *Thin Solid Films*, 516(12):3877–3883, 2008.

[182] C. Wang, Z. X. Deng, and Y. D. Li. The synthesis of nanocrystalline anatase and rutile titania in mixed organic media. *Inorganic Chemistry*, 40(20):5210–5214, 2001.

[183] C. C. Wang and J. Y. Ying. Sol-gel synthesis and hydrothermal processing of anatase and rutile titania nanocrystals. *Chemistry of Materials*, 11(11):3113–3120, 1999.

[184] C. Y. Wang, C. Bottcher, D. W. Bahnemann, and J. K. Dohrmann. A comparative study of nanometer sized Fe(III)-doped TiO_2 photocatalysts: synthesis, characterization and activity. *Journal of Materials Chemistry*, 13(9):2322–2329, 2003.

[185] John A. Weil and James R. Bolton. *Electron Paramagnetic Resonance: Elementary Theory and Practical Applications*. WileyBlackwell, 2nd edition, 2007.

[186] D. Wicaksana, A. Kobayashi, and A. Kinbara. Process effects on structural-properties of TiO_2 thin films by reactive sputtering. *Journal of Vacuum Science & Technology a-Vacuum Surfaces and Films*, 10(4):1479–1482, 1992. Part 2.

[187] MS Wong, HP Chou, and TS Yang. Reactively sputtered N-doped titanium oxide films as visible-light photocatalyst. *Thin Solid Films*, 494:244, 2006.

[188] M. M. Wu, G. Lin, D. H. Chen, G. G. Wang, D. He, S. H. Feng, and R. R. Xu. Sol-hydrothermal synthesis and hydrothermally structural evolution of nanocrystal titanium dioxide. *Chemistry of Materials*, 14(5):1974–1980, 2002.

[189] A. H. Yahaya, M. A. Gondal, and A. Hameed. Selective laser enhanced photocatalytic conversion of CO_2 into methanol. *Chemical Physics Letters*, 400(1-3):206–212, 2004.

[190] T. Yamaki, T. Umebayashi, T. Sumita, S. Yamamoto, M. Maekawa, A. Kawasuso, and H. Itoh. Fluorine-doping in titanium dioxide by ion implantation technique. *Nuclear Instruments & Methods in Physics Research Section B-Beam Interactions with Materials and Atoms*, 206:254–258, 2003.

[191] H. Yamashita, H. Nishiguchi, N. Kamada, M. Anpo, Y. Teraoka, H. Hatano, S. Ehara, K. Kikui, L. Palmisano, and et al. Photocatalytic reduction of CO_2 with H_2O on TiO_2 and Cu/TiO_2 catalysts. *Research on Chemical Intermediates*,

20(8):815–23, 1994.

[192] Hiroshi Yoneyama. Photoreduction of carbon dioxide on quantized semiconductor nanoparticles in solution. *Catalysis Today*, 39:169–175, 1997.

[193] P. Zeman and S. Takabayashi. Effect of total and oxygen partial pressures on structure of photocatalytic TiO_2 films sputtered on unheated substrate. *Surface & Coatings Technology*, 153(1):93–99, 2002.

[194] H. Z. Zhang and J. F. Banfield. Phase transformation of nanocrystalline anatase-to-rutile via combined interface and surface nucleation. *Journal of Materials Research*, 15(2):437–448, 2000.

[195] J. Zhao and X. D. Yang. Photocatalytic oxidation for indoor air purification: a literature review. *Building and Environment*, 38(5):645–654, 2003.

APPENDIX

The full spectrum for the UV light and Solar lamp

The UV lamp I used for the activity tests is a Mercury vapor UV lamp (100W), providing an energy density of around 21.7 mW/cm^2.

The visible light source I used for the activity tests is a commercial solar light lamp (SVLVANIA, 20W) (full solar spectra). A UV cutoff (filter) of 400nm wavelength was applied to the reaction with visible illumination

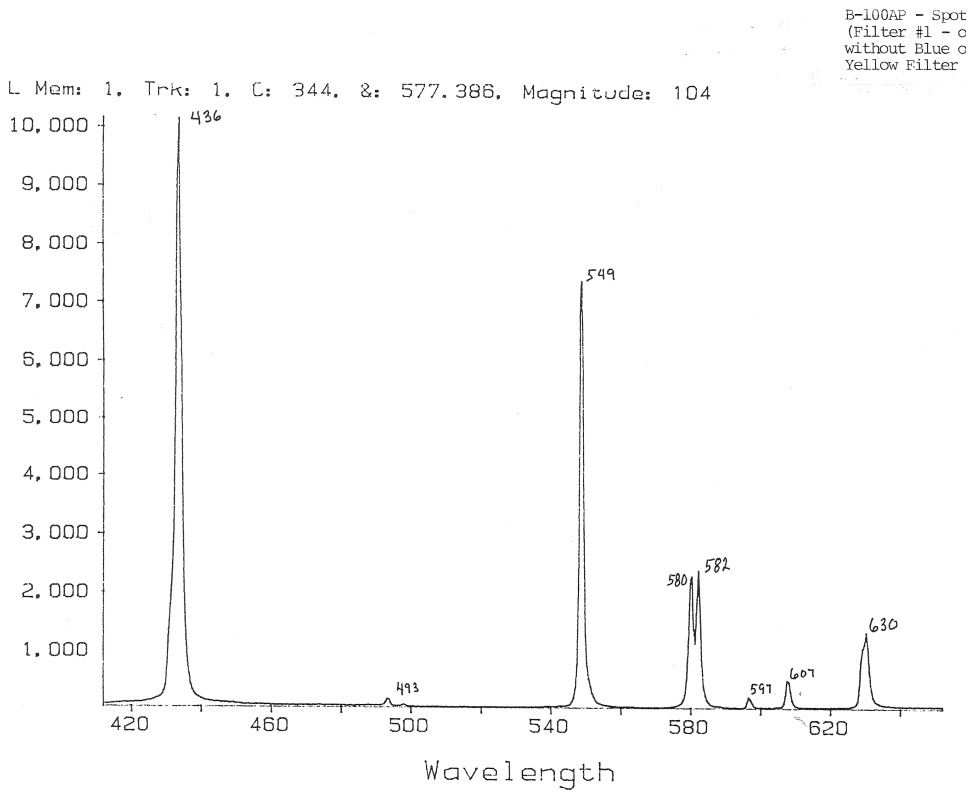

(a)

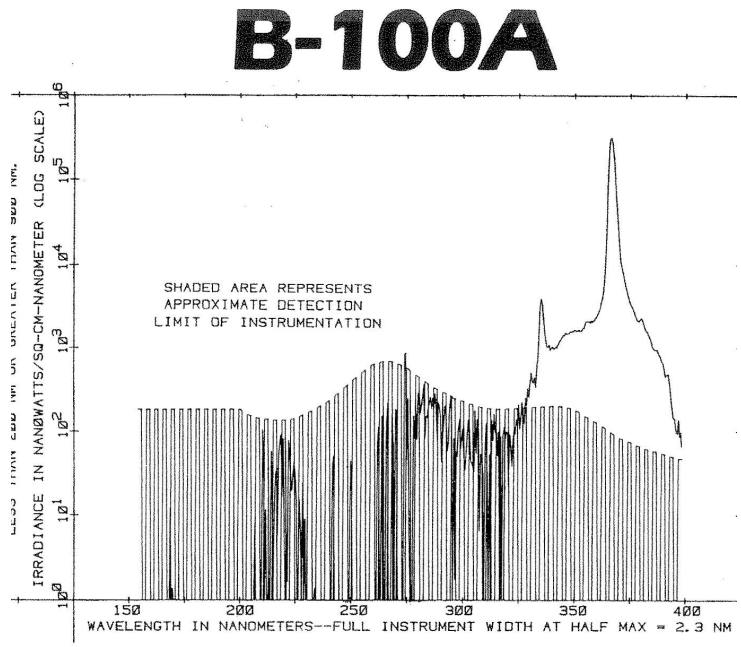

(b)

Figure .1. Light spectrum for UV lamp B-100 AP

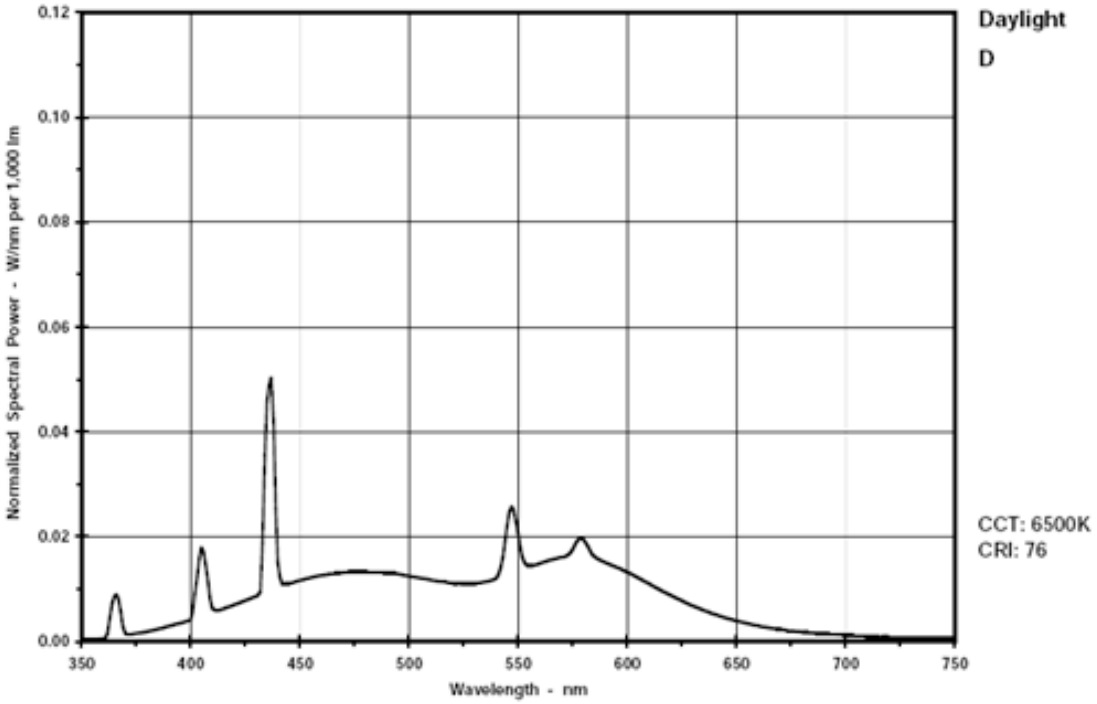

Figure .2. Light spectrum for the solar lamp